Productivity Along the California Margin During Early Pliocene Warmth

AS
36
2014
GEOL
.S39

A thesis submitted to the faculty of
San Francisco State University
In partial fulfillment of
The requirements for
The Degree

Master of Science

In

Geosciences

by

Valerie Evelyn Schwartz

San Francisco, California

August 2014

CERTIFICATION OF APPROVAL

I certify that I have read Productivity Along the California Margin During Early Pliocene Warmth by Valerie Evelyn Schwartz , and that in my opinion this work meets the criteria for approving a thesis submitted in partial fulfillment of the requirement for the degree: Master of Science in Geoscience at San Francisco State University.

Petra S. Dekens, Ph.D.
Associate Professor of Oceanography

Lisa D. White, Ph.D.
Adjunct Professor of Geology

Ivano W. Aiello, Ph.D.
Associate Professor of
Geology and Oceanography

PRODUCTIVITY ALONG THE CALIFORNIA MARGIN DURING EARLY PLIOCENE WARMTH

Valerie Evelyn Schwartz
San Francisco, California
2014

The early Pliocene is the most recent time in Earth history when average global temperatures were warmer than today. This study presents smear slide derived phytoplankton MAR from ODP Sites 1016 and 1022 along the California margin from 2.5-4.5 Ma. At ODP site 1016 a 2 to 10 $g/cm^2/ky$ increase in bulk sedimentation and a 0.30 to 1.00 $g/cm^2/ky$ increase in diatom MAR from the early to late Pliocene, split at at 3.5 Ma, is likely the result of tectonic movement from within an upwelling shadow zone to a location more directly influenced by the California Current. Significant increases in coccolith MAR at both sites and a decrease in diatom MAR from the early to late Pliocene at ODP Site 1022 suggests a decrease in surface nutrient availability as SST cooled. Existing SST and paleo-productivity records suggest sustained upwelling from 2.5-4.5 Ma, and changes in diatom and coccolith productivity can be explained by a deepening nutricline from 4.5 to 2.5 Ma.

I certify that the abstract is a correct representation of the content of this thesis

______________________________	7/11/14
Chair, Thesis Committee	Date

ACKNOWLEGEMENTS

I would like to thank my primary advisor, Dr. Petra Dekens for selecting me to take on this project and the immeasurable hours spent on draft revisions and providing me support. I would also like to thank Dr. Ivano Aiello for letting me into his lab and teaching me how to use the NSF-funded laser Beckman Coulter Laser Particle Sizer LS1230, Michelle Drake for showing me how to do the smear slide analysis, and Jenny Miles for preforming the preliminary smear slide analysis for ODP site 1022. Thank you to Dr. Lisa White for your encouragement and optimism throughout this project. I am appreciative to Mitch Lyle and the ODP for the age models and additional site data used in this project, and to the NASA GES-DISC-DAAC for SST and Chlorophyll-a data usd in this project. I acknowledge use of the NSF-MRI-funded Carl Zeiss Ultra 55 FE-SEM and supporting equipment at SF State. I am grateful for all of the scholarships and funding I have received from the ACS-PRF, ARCS foundation, and Pestrong grant.

Lastly, I would like to thank my mom-Sherry and grandparents–Doris and Sy for their support in allowing me to pursue my educational goals. I could not have accomplished any of this without you.

TABLE OF CONTENTS

LIST OF TABLES

LIST OF FIGURES

Figure Page

LIST OF APPENDICES

Appendix Page

1. **Introduction**

The modern California Current System (CCS) is an eastern boundary current that supports a diverse ecosystem and provides important feedbacks to both the climate and the economy through the fishing industry. Alongshore equatorward winds result in upwelling, which sustains high rates of primary productivity fueled by cold and nutrient rich upwelled waters. The cool sea surface temperatures (SST) along upwelling regions trigger important air-sea feedbacks that influence both regional and global climate (Seager et al., 2003). The primary productivity sustained through upwelling is important in the global carbon cycle and greenhouse gas concentrations through the biological pump (Behrenfeld et al., 2006; Kahru et al., 2009). Modern oceanic primary productivity accounts for half of global photosynthetic carbon fixation, and coastal upwelling regions account for half of total oceanic primary productivity (Falkowski, 2012). The response of modern upwelling systems and primary productivity to the anticipated warmer global conditions of the future is still largely unknown.

The early Pliocene (3-5 Ma) is the most recent time in Earth's history when average global temperatures were warmer than today (by 3-4°C) (Brierley et al., 2009; Haywood et al., 2009). Pliocene conditions such as continent locations, ocean currents, and atmospheric CO_2 levels were all similar to today (Ravelo et al., 2006; Pagani et al., 2009). Although atmospheric CO_2 concentrations in the early Pliocene were similar to today (from 350~450ppm), average global temperatures were 3-4˚C warmer, and questions remain about what climate feedbacks may have played a role in sustaining Pliocene global warmth. Current modeling studies can not simulate all the known conditions of the warm Pliocene (Fedorov et al., 2013). This indicates that the climate feedbacks that sustained Pliocene warmth may not be well accounted for in climate models, and implies possible uncertainties of future climate projections. Warmer SST in upwelling regions is one possibly important feedback in sustaining Pliocene warmth, as this would lead to a reduction of highly reflective stratus clouds and reduced albedo (Fedorov et al., 2013).

The SST patterns in the early Pliocene was different than today. The tropical Pacific resembled permanent El Niño-like conditions, with an eastward expansion of the Pacific warm pool (Wara et al., 2005) and a symmetrically deep thermocline from east to west across the equatorial Pacific (Ravelo et al., 2006). The early Pliocene was a time of high-latitude warmth (Haywood et al., 2009), and reduced equator-to-pole SST gradients (Dowsett & Robinson, 2009) due to a broader meridional extent of the Pacific warm pool compared to today (Fedorov et al., 2013). The reduced meridional gradients along the eastern Pacific California margin are evident in SST reconstructions, particularly in the more northern sites (Dekens et al., 2007; Reed-Sterrett et al., 2010). Given the connection between primary productivity and cold SSTs today, lower levels of productivity would be expected during the Pliocene when SSTs were warmer. Yet there appears to have been productivity along the California margin during the Pliocene (Dekens et al., 2007; Ravelo et al., 1997; Reed-Sterrett et al., 2010), and organic carbon mass accumulation rates (MAR) remain fairly constant throughout Pliocene aged sediments along the California margin (Lyle et al., 1997). This project investigates how productivity could take place in the Pliocene when SST was warmer, where the nutrients in the water column were, and the mechanisms bringing nutrients to the surface. Various phytoplankton groups thrive within particular SST and nutrient availability ranges, therefore a record of the dominant groups can help reconstruct the SST and nutrient conditions in the water column were, and if it experienced any changes during the Pliocene as SST was cooling. Aside from the ODP identifications and sediment descriptions that partly rely on microfossil groups, the relative distribution of various phytoplankton groups along the California margin during the Pliocene is largely unknown.

California margin ODP sites 1016 and 1022 (Figure 1) both recorded warmer SST during the Pliocene, and currently represent two faunally distinguishable zones primarily influenced by the California Current. Both ODP sites 1022 and 1016 have relatively high organic carbon mass accumulation rates (MAR) throughout the cores (~1.5% and ~1%, respectively) (Lyle et al., 1997), which makes them good candidates for biogenic smear slide analysis. This project generates and cautiously interprets smear slide phytoplankton fossil abundance records as a proxy for primary productivity (Appendix I) to better characterize upwelling and surface nutrient availability along the California margin during the Pliocene, from 2.5-4.5 Ma. Comparison of a northern and southern site will shed light on how water column structure shifted under the SST regimes experienced in the northern and southern California margin and what, if any, latitudinal changes took place in the strength or location of the California Current during the Pliocene These results are compared with the litho- and biostratigraphic columns of ODP sites 1016 and 1022 recorded in the ODP Initial Results (IR) volumes for the cruise (Lyle et al.,1997). Additionally, this project will test the applicability of laser particle size analysis as an additional method for documenting changes within these sediments, which should correspond to the smear slide data at ODP Sites 1016 and 1022 through the Pliocene. Understanding how various phytoplankton groups responded to early Pliocene warmth can help us diagnose surface nutrient availability and consequently, the physical water mass properties in the water column during a time of global warmth. This data can help us better predict what we may expect from upwelling systems and productivity in the future.

1.1 *Modern Oceanographic Setting*

The CCS is the eastern boundary current system of the North Pacific Gyre and consists of the southward flowing eastern boundary California Current (CC), the northward flowing Southern California Current, Davidson Current, and the Southern California Countercurrent (Figure 2) (Batteen et al., 2003; Yamamoto et al., 2007). The predominant flow is the CC, which is a broad (~1000 km offshore), shallow (surface down to ~500 m), relatively slow (~10 cm/s), year-round southward current (Batteen et al., 2003) that is derived from the North Pacific Current, coastal jet, and subarctic west wind drift (Checkley & Barth, 2009; Hickey, 1979). The CC extends from the North Pacific Current (~50°N) to off Baja California (~15°-25°N) and includes a major discontinuity at Point Conception (~34.5°N) (Checkley & Barth, 2009). The CC is the strongest and most geographically influential ~250-350 km from the coast of Oregon as far south as Point Conception (Lyle, et al., 2000). The Southern California Current is a relatively narrow (~10-40 km), weak (~2-10 cm/s), subsurface northward flow strongest at ~100-300 m depth and varies seasonally (Batteen et al., 2003). The Davidson Current is a weak, inshore, surface flow north of Point Conception which flows northward during fall and winter (Batteen et al., 2003). Other northward flows include the Southern California Countercurrent south of Point Conception and the Southern California Eddy within the Southern California Bight (Batteen et al., 2003). The dominant mechanisms for the large scale structure of the CCS include seasonal variations in alongshore wind stress, coastline irregularities, bottom topography, and can be recorded by variations in temperature and salinity (Batteen et al., 2003). The main atmospheric driver of the CCS is the winds of the North Pacific High pressure system, the Aleutian Low, and the thermal low-pressure system from central California to northern Mexico (Figure 3; Checkley & Barth, 2009).

Upwelling along coastal California is driven by equatorward winds that roughly parallel the coast, generated by the North Pacific High pressure system, which can be enhanced by the atmospheric pressure gradient between the land and ocean (Figure 3; Huyer, 1983). The winds drive surface water offshore due to the Coriolis effect and Ekman transport, which draws water up from below to replace it (Huyer, 1983). In the summer, a low pressure cell develops over the continental US (continental low), while a high pressure system develops in the North Pacific (North Pacific High) (Figure 3; Checkley & Barth, 2009; Huyer, 1983). The increased pressure gradient strengthens equatorward winds, increase wind stress curl, and driving Ekman pumping and increasing the volume of upwelled waters (Checkley & Barth, 2009). Wind forces vary from moderately strong and seasonally varying along the northern California coast, to strong and persistently equatorward along the central coast, to relatively weak and persistently equatorward along the southern California coast (Checkley & Barth, 2009). Alongshore upwelling variability is also driven by interactions of along-shelf coastal upwelling jets, fronts, and eddies that are related to the shape of the shelf and coastline (Checkley & Barth, 2009; Jacox & Edwards, 2011). Today, upwelling along the coast of Northern California occurs mainly in the summer, from May to June, when upwelling favorable winds occur from days to weeks (Lassiter et al., 2006).

Coastal upwelling along the California margin currently penetrates deep enough to draw up water from beneath the relatively shallow thermocline (Checkley & Barth, 2009), and the lowest SST are observed in the spring months, when upwelling from beneath the thermocline is reignited (Huyer, 1983; Figure 4). Variability in weather within the seasonal cycle affects mixing and water column stratification, and the systems alternates between upwelling, relaxation, and downwelling (Checkley & Barth, 2009). Because wind-driven coastal upwelling brings cold nutrient-rich water to the surface, cold SST has been linked to higher rates of primary productivity (Huyer, 1983). Cyclonic eddies form west of the upwelling jet and are often areas of high productivity (Checkley & Barth, 2009).

Phytoplankton are microscopic organisms that are extremely diverse, and typically respire using photosynthesis. Phytoplankton growth is limited by light and nutrient (nitrate and phosphate) availability, and they therefore thrive in areas where a mechanism, such as upwelling, brings nutrients to the photic zone (from 0 to 50-150m water depth). Diatoms, one of the most common types of phytoplankton, have silica shells and are most abundant in cold, nutrient-rich regions, such as those that experience upwelling (Crosta & Koc, 2007). Coccolithophores are another common type of phytoplankton, but are found in subtropical and tropical oceans, which are typically warm, stratified, and oligotrophic (Baumann et al., 2005). In areas that experience upwelling, coccolithophores usually appear off shore during relaxation events and during seasonal cycles of reduced upwelling (Giraudeau & Beaufort, 2007). The coccolithophore skeleton is comprised of many coccolith plates, made out of calcium carbonate, and release gaseous emissions of dimethyl sulfide (Giraudeau & Beaufort, 2007), which help form the sulfate aerosols that act as cloud condensation nuclei and aids in the creation of highly reflective stratus cloud that increase albedo (Seager et al., 2003), helping reduce incoming solar radiation.

Modern studies of upwelling systems and productivity are limited by the short time period (1-15 years) represented in the in situ data, satellite data from SeaWiFS began in 1997 (Behrenfeld et al., 2006), but even longer term observationally based studies of ~40-50 years are relatively short. Paleoceanographic studies covering longer timescales are needed to see how these systems respond to differing climate conditions. Worldwide, observed primary production biomass shows, on average, trends toward decreasing productivity, particularly in the typically warm, stratified parts of the oceans (Demarcq, 2009). Today, the cool SST in eastern boundary upwelling systems are associated with increased productivity (Demarcq, 2009). However, in all four main eastern boundary upwelling systems (California, Canary, Hunboldt, Benguela), average SST increases of ~0.42°C/decade are accompanied by trends of increasing biomass from 1998-2007 (Demarcq, 2009). The main exception to this is the southern portion of the Canary system, where there are trends of decreasing biomass (Demarcq, 2009). While it is generally true that upwelled waters need to be cold and nutrient-rich to sustain productivity, recent studies are showing that the relationship between SST and productivity is not always clear (Demarcq, 2009).

Upwelling along northern California with high primary productivity rates are typically dominated by large phytoplankton such as diatoms. Smaller phytoplankton, such as coccolithophorids and small flagellated phytoplankton species occur when nutrient concentrations are low during reduced upwelling and increased stratification (Lassiter et al., 2006). Phytoplankton biomass at Pt. Conception displays significant spatial heterogeneity largely affected by the Southern California Eddy (Mantyla et al., 2008). Point Conception is a latitudinal transition zone for physical and biological variations that differ to the north and south (Mantyla et al., 2008; Venrick, 1998). There is a separation between inshore and offshore flora based on chlorophyll concentration and phytoplankton group and species data (Venrick, 1998). There is also a reduction in biomass moving away from the inshore environments that are dominated by diatoms to the offshore regions where coccolithophores and other flagellate species become dominant (Venrick, 1998).

The California Current System, coastal upwelling, and productivity are greatly altered during El Niño events. Under normal conditions the atmospheric circulation above the equatorial Pacific consists of easterly trade winds, rising air in the western equatorial Pacific, westerly flow aloft, and sinking air over the high sea level pressure region in the eastern equatorial Pacific, and is called Walker circulation (Ravelo et al., 2006). During an El Niño event, Walker circulation breaks down and in the eastern tropical Pacific SST warms, the pycnocline deepens, and productivity is greatly reduced (Checkley & Barth, 2009). Coastally trapped waves propagate the El Niño signal from the tropics poleward and cause a deepening of the thermocline along the California and Peru margins (Checkley & Barth, 2009). The deeper thermocline prevents winds from reaching cooler nutrient rich waters, which results in reduced productivity along both upwelling margins (Checkley & Barth, 2009). El Niño events occur irregularly approximately every two to seven years, and effects can be felt around the globe for a year before recovering back to normal conditions (Checkley & Barth, 2009).

1.2 *Possible Affects of Global Warming on Upwelling and Productivity*

Atmospheric CO_2 levels have increased by ~40% since the start of the industrial revolution (Falkowski, 2012). The Earth has not experienced CO_2 levels as high as today for at least the last 650,000 years, and likely not for the last 4-5 million years (Haywood et al., 2009; Pagani et al., 2009; Siegenthaler et al., 2005). Currently, atmospheric CO_2 is approaching 400 ppm (NOAA-ESRL). Climate models have considerable uncertainty in predictions for future climate (Jansen et al., 2007), largely due to variations in how climate feedbacks are incorporated into models (Haywood et al., 2009). When models keep CO_2 levels at year 2000 values (370 ppm), they predict a 0.6°C warming with a likely range of 0.3-0.9°C for the year 2100 (Jansen et al., 2007). The model predicted warming for CO_2 levels similar to today does not match the early Pliocene, which was 3-4°C warmer, even though CO_2 concentrations do not appear to have been much higher.

How upwelling strength and productivity along eastern boundaries will respond to global warming is not well known. It is possible that global warming will increase upwelling favorable winds, due to an increase in temperature driven atmospheric pressure gradients(García-Reyes & Largier, 2010). Upwelling favorable winds are due the gradient fields between the high-pressure system over the ocean and the thermal low-pressure system over the landmass (Figure 3) (García-Reyes & Largier, 2010). Simulations for the CCS show that increased atmospheric CO_2 levels leads to a stronger low-pressure system over land due to the differences in heat capacity of land and water, which leads to an intensification of upwelling favorable winds which has been observed along the California margin over the last few decades (García-Reyes & Largier, 2010). However, surface heating associated with global warming is expected to lead to warmer SST, a deeper thermocline, and higher stratification, which may counteract the effect of stronger upwelling favorable winds (García-Reyes & Largier, 2010). Warmer oceanic conditions are expected to result in decreased productivity in upwelling regions, because the warmer surface waters imply an increase in stratification, suppressing nutrient exchange to the surface (Behrenfeld et al., 2006). Recent observations have shown increases in biomass corresponding to increases in offshore wind in the California, whereas variable but increasing SST do not appear to be related to changes in biomass (Demarcq, 2009; Kahru et al., 2009).

Global warming induced SST increases essentially deepens the thermocline. However, if enough nutrients are supplied to the surface ocean for productivity to continue, the warm upwelling water can remain nutrient-rich. This scenario would imply the nutricline may remain unchanged and is not always coupled to the thermocline. The apparent decoupling between winds and upwelling SST in the California upwelling system demonstrates the need for studies to explore the roles and responses of the California upwelling system during times of global warmth.

1.3 *The Early Pliocene*

The early Pliocene is considered to be a possible analog for future warming because it is the most recent time in earth history when temperatures were warmer than today (Brierley et al., 2009; Haywood et al., 2009) and the geologic and oceanographic conditions were similar to today (Ravelo et al., 2006; Pagani et al., 2009). However, it also presents a paradox because despite the similarities in climate forcings (such as atmospheric CO_2 and orbital parameters), global temperatures were 3-4°C warmer (Brierley et al., 2009; Haywood et al., 2009). In addition, there was little ice in the Northern Hemisphere, and sea level was ~25m higher then today (Dowsett & Robinson, 2009). The Pliocene was marked by reduced meridional SST gradients, weak zonal SST gradients, and SST stability in the tropical warm pools (Brierley et al., 2009; Dowsett & Robinson, 2009; Fedorov et al., 2013; Ravelo et al., 2006). These trends imply there was a large structural change in climate with major global and regional implications (Fedorov et al., 2013). Because these changes occur with only moderate differences in atmospheric CO_2, the Pliocene was a time of high structural climate sensitivity (Fedorov et al., 2013). Modeling studies of proposed mechanisms for early Pliocene warmth are currently unable to simulate the observed data (Fedorov et al., 2013; Haywood et al., 2009). Therefore it is possible that these models are underestimating some essential climate feedback mechanisms.

Pliocene SST and productivity records in the eastern and western equatorial Pacific indicate that the modern zonal SST gradient did not exist during the early

Pliocene (Dowsett & Robinson, 2009; Wara et al., 2005) and the thermocline was either deeper or warmer in the eastern tropical Pacific (Brierley et al., 2009; Haywood et al., 2009), reflecting an El Niño-like pattern (Ravelo et al., 2006). It should be noted that this interpretation is challenged in a very recent publication that suggests ENSO-type interannual climate variability existed during the Pliocene (Zhang et al., 2014).

Pliocene SST records from the southern California bight and off the coast of Mendocino were 9°C and 3°C warmer in the early Pliocene compared to today, respectively (Dekens et al., 2007; Reed-Sterrett et al., 2010; Figures 4 & 5). The larger, northern meridional SST gradient between ODP Sites 1014 (33°N, 119°W) and 1022 along the California margin (~6-8°C in the early Pliocene compared to ~ 3°C in the modern ocean) could be due to the influence of the tropical warm pool expansion on the more southern sites (Figure 5) (Dekens et al., 2007; Reed-Sterrett et al., 2010). Additionally, SST data from the equator, ODP Site 846 (3°S, 91°W) and subtropics, OSP Site 1012 (32°N, 118°W) show the equitorial meridional SST gradient increased from 2°C in the Pliocene to 8°C today (Brierley et al., 2009), also likely due to the expanded warm pool influence on the subtropics. Warmer Pliocene SST along the California margin could have resulted from either a decrease in the strength of wind driven upwelling, or from a deeper thermocline, which would not have allowed winds to access the cooler deep water (Dekens et al., 2007). SST reconstructions alone cannot differentiate between a decrease in upwelling and a deeper thermocline, but these records of primary productivity (Appendix I) could help differentiate between these two scenarios.

2. **Methods**

2.1 *ODP Sites*

ODP site 1016 (34.3°N, 122.16°W, 3846 m water depth) is located ~150 km west of Point Conception, and ~70 km west of the toe of the continental slope (Figure 1). The site is located on a northeast trending abyssal hill and rises 50-100 m above the surrounding sea floor (Lyle et al., 1997). ODP site 1016 sits on Pacific Plate ocean crust and has been carried seaward (toward the Northwest) since the late Pliocene based on both hotspot and fixed North American reference frames (Lyle et al., 1997). ODP site 1016 is within the central region and primarily influenced by the core of the California current (Lyle et al., 1997). ODP site 1016 is located in an important transitional zone between modern subtropical and subarctic flora and fauna and should therefore be sensitive to changes in the California Current (Lyle et al., 1997).

ODP site is 1022 (40.0°N, 125.5°W, 1925 m water depth) is located on the continental slope off the northern California coast, ~90 km from Cape Mendocino (Lyle et al., 1997) (Figure 1). ODP site 1022 is in a tectonically active region, sitting near the Mendocino Triple Junction of the Pacific, North American, and Gorda Plates (Lyle et al., 1997). It sits on a sliver of continental crust and has been carried seaward (toward the Northwest) since the late Miocene based on both hotspot and fixed North American reference frames (Lyle et al., 1997). ODP site 1022 is primarily influenced by the California current, and should provide a good record of upwelling and preservational affects (Lyle et al., 1997).

2.2 *Age Model, Sedimentation Rate, and Sampling*

The age models for ODP sites 1016 and 1022 are based on a best-fit polynomial for 9 and 7 shipboard biostratigraphic points, respectively (Lyle et al., 1997). The age model was also used to to calculate sedimentation rates using the samples whose ages were identified by biostratigraphic points. For each ODP site 1016 and 1022, 23 samples with known $U^{K'}_{37}$ temperature estimates were selected for smear slide and laser particle size analysis. We sampled ODP site 1016 every ~1-3m from 133 to 185.6 mcd, corresponding to 2.6-4.4 Ma, giving an average resolution of ~50 kyr. There is one large gap in the available samples for ODP site 1016, creating a gap in the data from 3.3-4 Ma. The lack of available samples during that time is likely a function of the corresponding reduction in the sedimentation rate, making fewer samples available. We sampled ODP site 1022 every ~2-5m (with a few samples between 10-15m apart) from 80-223 mcd, corresponding to 2.8-4.2 Ma, giving an average resolution of ~60 kyr. This resolution allows us to reconstruct long-term trends, but not to resolve orbital-scale variability.

2.3 *Scanning Electron Microscope Imaging*

Four samples, two from each ODP site of an early and late Pliocene sample were selected for Scanning Electron Microscope (SEM) imaging using a Carl Zeiss ultra 55 Field Emission Scanning Electron Microscope (SEM) equipped with an Everheart-Thornley detector. For each sample, dry sediment was adhered to the SEM stub using carbon paint and let dry for no less then 24 hours. Samples were coated with iridium prior to SEM imaging to make the sample conductive for the electron beam. Several images were taken of dominating biogenic components visible in each sample. The images were used to confirm the correct identifications of the components in the sediment samples.

2.4 *Smear Slide Methods*

Smear slides were made by placing a small amount of sediment on a glass slide using a clean toothpick, adding Millipore water to evenly distribute a thin film of sample on the slide, and setting to dry on a hot plate. Once the slide was dry, optical adhesive glue and a coverslip was placed on top of the sample, taking care to minimize the presence of air bubbles. The slides were placed under a UV light box for at least 30 minutes for the adhesive to set prior to being examined.

After the slides were set, they were viewed using a transmitted-light petrographic microscope equipped with a standard eyepiece micrometer. Biogenic and mineral components were identified within both normal and cross-polarized light, and their percentage abundance was visually estimated, based on the guide by Rothwell, 1989, under the 40x magnification lens. The components that were counted include pennate diatoms, whole centric diatoms, centric diatom fragments (all added together to get total diatoms), sponge spicules, radiolarian, silicoflagelates, foraminifera, coccoliths, volcanic glass, clay minerals, opaques, and siliclastics.

Each field of view was randomly selected to contain between the required 10 and 30% total coverage based on the Rothwell visual estimates (Rothwell, 1989), this range ensures that there is enough material present to contain a proper distribution of sediment, but not so much sediment that individual particles cannot be seen. The sediment covered portion of the slide is visually divided into six sections, counts of each slide were preformed for 10 different fields of view in the six sections; section were chosen randomly by a number generator. The final slide data is the average of the 10 counts for each slide, normalized to 100% using the average total coverage (Tables 1-4). The individual counts for each slide for ODP Site 1016 are listed in Appendix II and for ODP Site 1022 are listed in Appendix III. Two slides representing different sediment types were chosen and recounted an additional two times (Appendix IV) to ensure there was consistency in the smear slide visual quantifications. For each slide, the averages of each category for the three ten-counts were used to calculate a standard deviation of the three averages for each category, and all the values were under ~5.

2.5 *Mass Accumulation Rate Calculations*

The bulk Mass Accumulation Rate (MAR) for each sample was calculated using the calculated sedimentation rate and dry bulk density (Tables 5 and 6). The percent abundance of each smear slide component was converted to a density specific percent abundance, and used to calculate the MAR of each component (Tables 5-8). First, the relative density of each component was calculated by multiplying the normalized smear slide percent with the standard mineral density for that component. The mineral density representative of diatoms, sponge spicules, silicoflagellates, radiolarian, and volcanic glass is primarily opal, which has a density of ~2 g/cm^3 (AmMin). The mineral density representative of coccoliths and foraminifera is calcite, which has a density of ~2.6 g/cm^3 (AmMin). The mineral density representative of clay minerals, opaques, and siliciclastics is illite, magnetite, and quartz, which has densities of ~2.7, 5, and 2 g/cm^3, respectively (AmMin). Components listed in the ODP IR smear slides also included dolomite and pyrite, which have densities of ~2.8 and 5 g/cm^3, respectively (AmMin). Next, the relative to bulk density of each component was calculated by generating a ratio of the relative density of each component to the sum of all the component relative densities of the sample, multiplied by the corresponding ODP IR dry bulk density. Lastly, the percent relative to the bulk density of each component was calculated by generating a ratio of the relative to bulk density value of each component to the sum of all the component relative to bulk densities of the sample (equivalent to the sample ODP IR dry bulk density). The final value is a revised smear slide percent abundance that takes account of the specific density of each component. The MAR of each component is calculated by multiplying the density specific percent abundance by the bulk MAR of each sample. The density specific MAR of the ODP IR smear slide counts covering the same timespan of this study at both ODP Sites 1016 and 1022 was also calculated (Tables 9 and 10).

The calculated density specific MAR for each component is a good way to quantify the various components of the sediments through time because it takes into account the total amount of material that makes it into the sediments for a given time, in addition to the actual input of each component based on their density normalized contribution to the bulk density. For example, a decrease in the relative percent of a component of the sediment may actually be reflecting an increase in the MAR of that component if it remains present with a decreased bulk MAR. Additionally, small changes in relative percent of a very dense component, like opaques, can be balanced by large changes in the lower-density components, in samples with little differences in dry bulk density and MAR.

2.6 *Particle Size Methods*

Particle size analysis (PSA) was done at Moss Landing Marine Laboratories under the supervision of Dr. Ivano Aiello. The Beckman Coulter Laser Particle Sizer LS 13-320, equipped with an aqueous module with a pump and ultrasound unit, captures and records IR laser light backscattering off the individual grains through multiple detectors. The instrument correlates the pattern of scattered light via laser diffraction to the particle size distribution of the sample using the Mie principal of light diffraction (Figure 6). The assumptions used to convert from optical light scattering to size is based on the sample being made up of spherical particles of quartz. The particles from the samples in this project are not necessarily spherical, nor are they primarily quartz, which needs to be taken into consideration when examining the results. Because the calibration of the instrument is determined by the optical design, no actual calibration is necessary, measuring the electrical offsets and aligning the laser beam makes all the necessary adjustments.

Scrapings, of no more than 0.25 grams from the sample were slowly added into the water-bath of the instrument until detectors indicated that enough sample was present to perform the analysis. Because the bulk sediments for this project were freeze dried and break into aggregates of multiple grains prior to analysis, sample sonication, which gently breaks these up, was necessary. Multiple runs under various sonication times of 10, 15, 20, and 30 seconds were carried out for the oldest (4.2 Ma) and youngest (2.6 Ma) sediment samples in the ODP site 1016 record to determine the appropriate time to sonicate the sample (Figure 7). No sonication resulted in a very narrow range of sediments sizes and larger mean grain sizes, indicating aggregates were still present. More than 20 seconds appeared to break up the larger particles; various peaks in the grain size distribution were smoothed or lost entirely, indicating a general deterioration of grain sizes due to over-sonication (Figure 8). A sonication time of between 15 and 20 seconds was deemed appropriate to break up the aggregates, without overly disrupting the truly larger particle sizes. Therefore, once enough of each sample was placed in the water-bath, it was sonicated for between 15-20 seconds prior to instrumental analysis.

For each day the instrument was used, the alignment procedure was conducted before the first sample run, and then between every 2-3 samples, as well as prior to any duplicate sample run if the results did not seem appropriate. Before each sample run the instrument measures the background noise of the deionized water-bath, which is later subtracted from the data signal. Additionally, at least two runs were preformed for each sample to ensure confidence in the results. If there were significant differences in the visualization of the grain size distributions, or interpolation points (differences over 15% between the bin sizes) between the runs, the instrument was realigned before rerunning the sample another two times.

Particle size data analysis was done using the laser particle size proprietary software, and subsequently exported into Microsoft Excel and JMP software programs. Particle size data include mean, mode, and standard deviations of particle surface area, diameter, and percent volume for any size fractions desired. Using the proprietary software, initial particle size fractions were divided based on the standard grain size categories of clay (<4 μm), very fine silt (4-8 μm), fine silt (8-16 μm), medium silt (16-31 μm), course silt (31-62 μm), and very fine sand (62-125 μm).

3. **Results**

3.1 *Smear Slide Analysis*

Diatoms and coccoliths are the dominant biogenic components of the sediments at both ODP Sites 1016 and 1022; important minor components include clay minerals, siliclastics, opaques and sponge spicules (Figure 9; Tables 1 and 2; Appendix II and III). The twice counted smear slide experiment used to establish consistency shows that the standard deviation of all the components percents are > 5% (Appendix IV). The age division of 3.5 Ma was chosen by and used in this study to separate the early and late Pliocene, because the data separated at that age displays the largest statistical differences in coccolith and diatom populations. When dividing the samples at 3.5 Ma at both ODP Sites 1016 and 1022 the percent coccoliths increase (29 to 60%, and 33 to 80%, respectively) and the percent diatoms decrease (20 to 13%, and 30 to 10%, respectively) from the early to late Pliocene. The percent of minor components also decrease from the early to late Pliocene at both ODP Sites 1016 and 1022. The various diatom components counted in the smear slides for ODP Sites 1016 and 1022 include pennate, whole centric, centric fragments, total centric, and total diatoms and are listed in Tables 3 and 4. At both ODP Sites 1016 and 1022 pennate diatoms contribute slightly over 50% of the total diatoms, and centric diatom fragments are the primary component (< 90%) of total centric diatoms (Figure 10).

3.2 *Mass Accumulation Rates*

The bulk MAR is most strongly influenced by sedimentation rate, which experiences a drastic change at ODP Site 1016 from low MAR in the early Pliocene (<2 g/cm^2/ky) to almost an order of magnitude higher in the late Pliocene (~10 g/cm^2/ky) (Figure 11). ODP Site 1022 has more constant, albeit slightly increasing, MAR through the Pliocene, with values just above the highest values for ODP Site 1016 (~11-13 g/cm^2/ky). All of the smear slide component percent abundances were converted to density specific percent abundances and MAR for both ODP Sites 1016 and 1022 (Tables 5 and 6, respectively). Just as with the percent abundance data, when dividing the samples at 3.5 Ma, coccolith MAR are larger in the late Pliocene then in the Early Pliocene at both ODP Sites 1016 and 1022 (Figure 12). At ODP Site 1016 the non-coccolith components MAR increase slightly from <~1 g/cm^2/ky the early Pliocene to <~2 g/cm^2/ky in the late Pliocene. At ODP Site 1022 the non-coccolith components MAR decrease from <~4 g/cm^2/ky in the early Pliocene to <~2 g/cm^2/ky in the Late Pliocene. At ODP Site 1016 all of the diatom components MAR are slightly increased (by ~0.5-1 g/cm^2/ky) in the late Pliocene compared to the early Pliocene, and at ODP Site 1022 all of the diatom components MAR are decreased (by ~2-2.5 g/cm^2/ky) in the late Pliocene compared to the early Pliocene (Figure 13; Tables 7 and 8). At both ODP Sites 1016 and 1022, normalizing the diatom component MAR to the total diatom MAR shows that pennate diatoms contribute to ~ 60% of the total diatoms, and centric diatom fragments are the primary component (< 90%) of total centric diatoms and contribute to ~40 % of the total diatoms (Figure 14).

3.3 *ODP Initial Results Smear Slides and Mass Accumulation Rates*

The ODP shipboard scientific party uses smear slide analysis as one of several methods to determine sediment lithology down each drill core. The calculated MAR of the available smear slide data for ODP Sites 1016 and 1022 generated by the ODP for the same drill core and depth (age) of this study display large variations and few trends, differing from the results of this study (Tables 9 and 10). At ODP Site 1016 the diatom MAR remains relatively low, ~1 g/cm^2/ky throughout the record, whereas the coccolith MAR increases from < 1 g/cm^2/ky in the early Pliocene to ~ 4 g/cm^2/ky in the late Pliocene (Figure 15). There are three slides with high volcanic glass MAR, that likely correspond to ODP IR identified volcanic ash layers in the core, and are also characterized by the ODP IR as being from a minor lithology (Lyle et al., 1997; Table 9). The only components identified in both this study and the ODP IR for the ODP Site 1022 samples are diatoms, coccoliths, and clay (Figure 15). At ODP site 1022 there is no smear slide data available for the same core younger then ~3 Ma (Lyle et al., 1997). The early Pliocene coccolith MAR fluctuates between 0-4 g/cm^2/ky until ~3.5 Ma, then increases to ~7 g/cm^2/ky until the end of the available record, diatom MAR fluctuates between ~0.5-4 g/cm^2/ky, and clay MAR fluctuates between ~0.5-7.5 g/cm^2/ky.

3.4 *Combined Diatom and Coccolith Mass Accumulation Rates and Statistics*

Analysis of variance (ANOVA) is used to test if any shifts in the density specific MAR of the coccolioth and diatom sediment populations during the Pliocene are statistically significant for both this study and the ODP IR slide data, using two specific age divisions at each ODP Site (Tables 11 and 12). The first age division used is based on the lithologic unit and subunit separations identified in the ODP Site 1016 and 1022 IR site chapters, and are 2.8 Ma and 3.58 Ma, respectively (Lyle et al., 1997). The second age division was chosen at the age that when divided by, displayed the largest statistical differences in diatom and coccolith populations, and at both ODP Sites 1016 and 1022 is 3.5 Ma.

At ODP Site 1016 the only populations that significantly differs statistically between the early and late Pliocene using the ODP IR lithologic unit age division is the coccolith MAR from this study (Table 11A). However, using the 3.5 Ma age division chosen in this study at ODP Site 1016 the only populations that do not significantly differ statistically between the early and late Pliocene is the diatom MAR from the ODP IR dataset (Table 11B). At ODP Site 1022 the only populations that significantly differs statistically between the early and late Pliocene using the ODP IR lithologic unit age division is the diatom MAR from the ODP IR dataset (Table 12A), whereas all the diatom and coccolith populations for this study and the ODP IR dataset significantly differs statistically for both age divisions of the early and late Pliocene (Table 12B).

The diatom MAR for this study and the ODP IR data are compared at both ODP Sites 1016 and 1022 (Figure 16). At ODP Site 1016 diatom MAR show similar average values for this study and the ODP IR volume, generally <2 g/cm^2/ky, with slightly increased diatom MAR in the late Pliocene then the early Pliocene. At ODP Site 1022 diatom MAR in the early Pliocene are slightly larger for this study, ~3 g/cm^2/ky than for the IR volume, ~2 g/cm^2/ky, but both this study and the IR volumes have low diatom MAR in the late Pliocene compared to the early Pliocene, <1.5 g/cm^2/ky (Figure 16). Unlike this study, the ODP IR diatom MAR displays more variability at site 1016 in the late Pliocene and at site 1022 for the early Pliocene.

The coccolith MAR for this study and the ODP IR data are compared at both ODP Sites 1016 and 1022 (Figure 17). At ODP Site 1016 coccolith MAR show similar values for this study and the ODP IR dataset in the early Pliocene, >1 g/cm^2/ky, with increasing MAR from the early Pliocene to the late Pliocene, however the site 1016 ODP IR dataset coccolith MAR on the late Pliocene displays more variability, ~0-8 g/cm^2/ky than this study, ~5-8 g/cm^2/ky. At ODP Site 1022 coccolith MAR increase from the early Pliocene toward the late Pliocene in both this study and the ODP IR data, although the maximum coccolith MAR values are slightly higher for this study ~10 g/cm^2/ky than for the ODP IR data ~8 g/cm^2/ky. The site 1022 IR volume ends at ~3 Ma, and coccolith MAR at that point is ~8 g/cm^2/ky, this study has samples through 2.8 Ma, and coccolith MAR reach ~10 g/cm^2/ky.

ANOVA was also used to compare the diatom and coccolith MAR between this study and the ODP IR data at both ODP Sites 1016 and 1022 for both the lithologic unit and statistically identified age divisions (Table 13). At ODP Site 1016 the only populations that are statistically distinguishable between this study and the ODP IR data are the coccolith MAR of the late Pliocene for the age division chosen in this study. At ODP Site 1022 the diatom MAR populations of this study and the ODP IR data are statistically distinguishable for the early Pliocene in both the lithologic unit and chosen age divisions. At ODP Site 1022 the only coccolith MAR populations not statistically distinguishable between this study and the ODP IR data is for the ODP IR lithologic age unit of the early Pliocene.

3.5 *Particle Size Analysis*

Particle size analysis (PSA) was carried out on all the same samples where smear slide data was collected. When particle size was divided into the standard Wentworth grain size categories of clay (<4 μm), very fine silt (4-8 μm), fine silt (8-16 μm), medium silt (16-31 μm), course silt (31-62 μm), and very fine sand (62-125 μm) there was no statistically significant trend through time for either ODP Site 1016 or 1022 (Figure 18). Clay and course silt size particles dominate the majority of the samples, however between ~3.1-3.5 Ma the course silt sized component is decreased. At both ODP sites 1016 and 1022 there is no significant trend between mean grain size with age or SST, using linear regression or ANOVA (Figures 19 and 20). At ODP site 1016 there is no significant trend (within a 95% confidence level) between mean particle size and smear slide generated percent abundance of coccoliths or diatoms (Figure 21). At ODP site 1022 there is a slight linear trend between mean grain size and coccolith and diatom abundance (R^2 = 0.16 and 0.17 respectively), however these trends are just outside of the 95% confidence level and thus can not be considered significant (Figure 21). There are also no significant trends between mean particle size and density specific coccolith or diatom MAR at either ODP Sites 1016 and 1022 (Figure 22).

3.6 *SEM Imaging*

The two samples older then 3.3 Ma at ODP sites 1016 (4.26 Ma) and 1022 (3.96 Ma) contained virtually no visible coccolith fragments when viewed under the SEM. The older samples did contain centric and pennate diatoms, sponge spicules, and clay-sized minerals (Figure 23). The two samples younger then 3.3 Ma at both ODP sites 1016 (2.73 Ma) and 1022 (2.95 Ma) contained abundant coccolith fragments when viewed under the SEM. Only the younger site at ODP site 1022 sample had visible diatoms and spicules, whereas the biogenic component of the younger ODP site 1016 sediment is primarily coccolith fragments (Figure 24).

4. Discussion

4.1 *Particle Size Analysis*

PSA of marine sediments have been successfully used as a paleoenviornmental tool to detect and quantify compositional and textural changes of fine grained pelagic sediments, such as carbonate oozes in sediment cores from the Walvis Ridge in the southeast Atlantic Ocean, which has been correlated with downcore variations of magnetic susceptibility (Aiello & Kellett, 2006). Shifts in the particle size distributions in a sediment column can shed light on changes in the environmental and depositional setting (Aiello & Ravelo, 2012). Between ~3.1-3.4 Ma there is a decrease in the abundance of course silt-sized particles, and a corresponding increase in the clay-sized particles at both ODP Sites 1016 and 1022, indicating that they may be responding to the same forcing (Figure 18). Because the particle size analyses were carried out over several days and samples were not run in the order they appear in the core, this slight shift in particle sizes is likely a true feature in the cores, and not an analytical artifact. Even though both sites experience this grain size shift simultaneously, the bulk MAR appears vastly different at each site; bulk MAR at ODP Site 1016 increases by ~50m/Ma from the early to late Pliocene, split at 3.5 Ma, whereas bulk MAR remain nearly constant at ODP Site 1022 during that time (Figure 11). It is possible that there was a weakening or slackening of the California Current System, which was unable to carry the larger course silt-sized particles all the way to ODP site 1016, and allowed for more suspended clay sized particles to be deposited.

Overall, the PSA at ODP Sites 1016 and 1022 show very little variability in all of the standard sediment grain size categories during the Pliocene (Figure 18). At both ODP Sites 1016 and 1022 PSA clay (<4μm) and course silt-sized (31-62μm) particles are most abundant (~20-35%). Very fine silt (4-8μm), fine silt (8-16μm), and medium silt-sized (16-31μm) particles are slightly less abundant (~15-20%), and very fine sand- sized (62-125μm) particles are the least abundant (~<5%) in the samples (Figure 18). Based on the changes observed in the smear slide and MAR records, we would have expected the PSA of those same samples to display a corresponding shift, yet there is not. The lack of any statistical correlation between mean grain size and sample age at both ODP Sites 1016 and 1022 (Figure 19) is unexpected given the observable trends in the smear slide analysis and MAR, and may partly be a function of the small range (12 μm) of the mean particle sizes. The lack of any statistical correlation between mean grain size and SST at both ODP Sites 1016 and 1022 (Figure 20) is less surprising given the relatively small SST changes during this time period.

PSA has been used on Pliocene sediments from the Bering Sea, where up to 40% of the variance in mean particle size was attributed to diatom abundances (Aiello & Ravelo, 2012). The mean particle sizes in the Bering Sea bulk sediments ranged from 5-45μm (Aiello & Ravelo, 2012), whereas the mean particle sizes at ODP Sites 1016 and 1022 are smaller (4-16 μm). At both ODP Sites 1016 and 1022 there were no statistically significant correlations between mean grain size with either the percent normalized (Figure 21) or density specific normalized MAR (Figure 22) smear slide coccolith and diatom data. The lack of any correlation between mean grain size and diatoms in this study could be because the majority of observed diatoms were pennate or fragmented centric pieces, which can vary greatly in size and shape. Additionally, the observed differences in diatom abundances in the early and late Pliocene, split at 3.5 Ma, 2.43 to 0.90 g/cm^2/ky at ODP Site 1022, and 0.30 to 1.00 g/cm^2/ky at ODP Site 1016, is relatively small compared to the observed increase in coccolith abundances, 3.63 to 9.07 $g/cm^2/ky$ at ODP Site 1022, and 0.55 to 6.07 $g/cm^2/ky$ at ODP Site 1016 (Tables 11 and 12).

The significant increases observed in smear slide coccolith abundances through the Pliocene would be expected to correspond to either a decrease in mean grain sizes, or an increase in the clay-sized component of the sediments through the Pliocene. The fact that there is no correlation between mean grain size and coccoliths abundance is surprising, given that the observed coccoliths were unbroken and generally uniform in size. One possible explanation for this is that there was a decrease in clay accumulation through the Pliocene so that the increase in coccolith accumulation was accompanied by a decrease in clay accumulation, and thus the total abundance of clay sized material does not change. This is supported by the smear slide percent normalized data that shows clay-sized material is between ~10-20% more abundant in the early Pliocene then in the late Pliocene (Figure 9). However, the density specific MAR in clay-sized material at ODP site 1016 shows a slight increase, while the ODP Site 1022 clay-sized material shows a decrease through the Pliocene (Figure 12). The inconsistency in the ODP Site 1016 MAR data can be explained by the understanding that in the early Pliocene, the proportion of clay size material accumulating increased and the total MAR was significantly reduced. In the late Pliocene when there was in increase in coccolith accumulation, there was also an increase in the total MAR including all particle sizes, so that the distribution, or contribution of various particle sizes to the bulk sediment, remained the same.

There are a few sources of uncertainty in PSA. The particle size instrument assumes a spherical shape when determining particle diameter; therefore the size for both coccoliths and centric diatoms, which are flat and circular, could be underestimated if not directly facing the optical system while being measured. Similarly, pennate diatoms and sponge spicules could cause overestimation of particle sizes if their length is measured as a representative of diameter. Most of the diatoms and spicules observed in the smear slides were fragmented, which could have lead to underestimates of particle sizes. Other factors that could affect PSA include the dissolution of coccoliths by the deionized water (Giraudeau & Beaufort, 2007), which would result in an overestimation of the larger particle sizes, and air bubbles in the solution of the particle sizer instrument (Aiello & Kellett, 2006).

Even though the majority of the larger material in this study was fragmented, the lack of any correlation between particle size analysis and smear slide analysis (Figures 18-22) is unsatisfying. The smear slides appeared to be primarily biogenic and displayed distinct abundance trends that should have been recorded within some particle size category. Future PSA work should focus on particle size analysis method development. Experiments with various methods for pretreatment of the sediment to remove either the siliceous and/or the carbonate fractions of the sediment can be used to examine trends that might otherwise be hidden in the bulk sediment sample. Various pretreatment protocols can remove the organic, carbonate, and silicate components of the sediment (Aiello & Ravelo, 2012). Because there is no correlation between the PSA data and age, SST, or the smear slide data, it will not be further interpreted in the context of productivity, and this paper will focus in the results from the smear slide analysis.

4.2 *Smear Slide Analysis*

Smear slides are a widely used tool to characterize marine sediments (Rothwell, 1989). Smear slide analysis has been successfully used in paleoceanographic studies as a productivity proxy, as they offer a reasonably quick and straightforward measure of the relative abundances of sedimentary components through a stratigraphic section. The ODP prepares and examines smear slides onboard expeditions to classify sediments, identify biostratigraphic zonations, and date the sediment (Lyle et al., 1997). A study of paleoproductivity patterns at the Eocene-Oligocene boundary in southern high latitudes and equatorial oceans used smear slides as part of their multi-proxy approach (Schumacher & Lazarus, 2004). Smear slide analysis has also been used for the Bering

Sea and Eastern Equatorial Pacific to characterize sediment types and distributions through the Pliocene (Aiello & Kellett, 2006; Aiello & Ravelo, 2012).

The methods for smear slide visualizations and analysis outlined in Rothwell (1989) has become standard procedure. Errors in smear slide visual estimation can be increased by factors related to the preparation of the smear slide. Smear slides of poorly sorted sediment can segregate coarse from fine grain sizes, which is why the methodology includes counting ten fields of view of each slide to reduce any biased view of the composition, which is a function of texture, in the sample. The thickness of the smear can also have an affect by either being too thin and having too much void space, or being too thick and having grains stacked one upon the other; both cases cause errors in abundance estimations. This is why the methodology requires each counted field of view to have a total percent coverage between 10-30%. There can also be human error reading the slides, including misidentifications of the particles, or having a bias toward over or under estimating the various components identified.

Interpretation of the sediments is complex given that both productivity and preservation play a role in sediment composition (Appendix I). Bearing in mind the possible limitations, including that the sediment composition is a reflection of both productivity and preservation, this project will cautiously interpret smear slide data as primarily being a proxy record for productivity.

4.3 *Comparisons of This Study to the ODP IR Smear Slide Dataset*

There are several differences between the data from this study and the data from the ODP generated slides. The ODP smear slide data appears highly variable through the sediment record (Figure 15), and the clay accumulation, particularly at ODP Site 1022 (Figures 12 and 15), is quite different. Both data sets display a decrease in clay MAR from the early to late Pliocene, but the clay MAR from this study are nearly an order of magnitude lower, 0.2 g/cm^2/ky, than from the ODP data, 2 g/cm^2/ky. Clay-sized material can be hard to quantify because of its small size and tendency to remain in aggregates in the smear slide. There is certainly a possibility for bias in either data set, however the fact that the both datasets display a similar shift in abundances from the early to late Pliocene implies this is a true shift in lithology taking place at ~3.5 Ma (Figure 15; Table 10).

Two versions of age divisions were used to separate the early and late Pliocene for statistical analysis of the data from the study and the data from the ODP generated slides. The first age division is based on the ODP lithologic unit age divisions in the site chapters, 2.8 Ma at ODP Site 1016 and 3.58 Ma at ODP Site 1022, and the second age division is based on the time separating the largest observed abundance shifts, 3.5 Ma at both sites. An interesting feature of the ODP smear slide data is that that the coccolith and diatom abundances are only statistically significantly distinguishable between the early and late Pliocene using the observed 3.5 Ma age division chosen in this study, not the ODP IR lithological unit age division (Tables 11 and 12). This is the case for the coccolith abundances at ODP Site 1016 and the diatom abundances at ODP Site 1022. It is particularly interesting because the ODP uses the smear slides to help generate the lithological units and age divisions. The age divisions made by this study and the ODP IR at ODP Site 1022 are similar, the ODP has the split at 3.58 Ma and this study at 3.5 Ma, however this slight difference in age is enough to make the ODP smear slide diatom populations between the early and late Pliocene not statistically distinguishable. While ODP divides the lithology at ODP Site 1016 at 2.8 Ma, this study sets the split at 3.5 Ma. Splitting the data at 2.8 Ma makes the ODP smear slide early and late Pliocene coccolith populations indistinguishable. The ODP IR also takes into account other physical property data when choosing the lithological unit divisions, however the particularly long difference in age divisions for ODP Site 1016 is particularly confusing given the large shift in bulk MAR (Figure 11) around 3.5 Ma. The similarity of the coccolith and diatom population abundances between this study and the ODP smear slides data for both age divisions separating the early and late Pliocene was tested using ANOVA (Table 13). If the populations were not statistically distinguishable, they can be combined to form a larger, more robust dataset. Unfortunately, there was no time division that resulted in no statistical difference in the diatom and coccolith populations for either ODP Site 1016 or 1022 (Table 13).

Core sample selection may play a role in the differences between data from this study and from the ODP. This study aimed to select samples as evenly distributed by age as possible. The onboard smear slides are typically made from all representative lithologies, and from special or unique layers of interest, thus the number of smear slides produced is a function of the homogeneity of the sedimentary section. In addition to a more uneven distribution of samples, some of the ODP smear slides are listed as being from a minor lithology (Tables 9 and 10).

4.4 *Productivity*

In the modern ocean, coccolithophorid production is highest in stratified, warm, tropical and subtropical environments with low nutrient availability (Giraudeau & Beaufort, 2007). Coccolithophores use dissolved calcium and carbonate to make up their skeleton, which is readily available in most surface water (Baumann et al., 2005). In nutrient-rich enviornments, like the California upwelling system, coccolithophores are often outcompeted by diatoms and other phytoplankton groups for available nutrients (Baumann et al., 2005). Coccolithophorid growth typically takes place during relaxation events after upwelling or in the non-upwelling season, and are further offshore (Anderson et al., 2008; Lassiter et al., 2006; Venrick, 1998). Given our understanding of modern coccolithophorid growth and distribution patterns, high coccolith abundances in past climates would indicate more stratified conditions. Therefore, when SST decreases and implies increased upwelling, we would expect to see a lower abundance of coccoliths. However, at both ODP sites 1016 and 1022 there is a large and statistically significant increase in the average coccolith MAR (Tables 11 and 12) as SST decreases from the early to late Pliocene (Figure 5). The increases in the average coccolith MAR at both

ODP Sites through the Pliocene imply that even though SST was cooling, nutrient supply decreased such that coccoliths became the dominant signal in the sediment.

In the modern ocean, diatoms flourish in upwelling systems with adequate nutrient concentrations and cold SSTs (Crosta & Koc, 2007). Diatoms use hydrated silicon dioxide to make their skeletons, and therefore silica concentration is another important factor governing diatom growth (Crosta & Koc, 2007). Diatoms are well adapted to the high-energy, nutrient-rich conditions in the California Current System and are the dominant phytoplankton during the upwelling season along the California margin (Lassiter et al., 2006; Venrick, 1998). Given our understanding of modern diatom growth and distribution patterns, we would expect diatom abundances in past climates to correlate with SST and nutrient rich upwelling conditions. For example, when SST is relatively warm, implying reduced upwelling, we would expect to see a lower abundance of diatoms. This appears to be the case at ODP Site 1016, where there is a slight but statistically significant increase in the average diatom MAR from 0.30± 0.09 before 3.5 Ma to 1.00± 0.07 g/cm^2/ky after 3.5 Ma (Table 11; Figures 12 and 13) as SST decreases from 18°C to 16°C (Figure 5). This does not appear to be the case at ODP Site 1022, where there is a decrease in the average diatom MAR from 2.43± 0.22 before 3.5 Ma to 0.90± 0.21 g/cm^2/ky after 3.5 Ma (Table 12; Figures 12 and 13) as SST decreases from 17°C to 14°C (Figure 5). The data at ODP Site 1022 suggest that as SST was decreasing, nutrient supply was also decreasing through the Pliocene, whereas the data at ODP Site 1016 suggest that nutrient supply increased slightly.

A decrease in nutrient supply at both ODP Sites 1016 and 1022 from the late to early Pliocene is supported by the increase in coccolith MAR, but the diatom MAR tells a different story. Because productivity is so closely linked with geographical location, tectonic movenemt of the ODP sites can certainly affect their sediment records. Both ODP Sites moved Northwest, nearly parrellel to the California margin, and were transported by ~1° North during the time period of this study (Figure 1). The consistancy in bulk MAR (Figure 11) at ODP Site 1022 suggests the sediment recorded comparable

CCS conditions through the Pliocene. ODP Site 1016 is currently located on a major biogeographic boundary between the central and southern CCS, near the discontinuity in the Caifornia Current which begins near Point Conception (Checkley & Barth, 2009). This transition is caused by moving from within relatively weak wind driven upwelling south of Point Conception in the southern California Bight, referred to as a shaddow zone (Checkley & Barth, 2009), to an area of strong offshore upwelling jets containing significant amounts of nutrients and productivity adjacent to point Conception (Checkley & Barth, 2009). The tectonic movement of ODP Site 1016 from within the southern California Bight northwards to a location more closely adjacent to Point Conception (Figure 1) likely had a more significant affect on the diatom accumulation than for ODP Site 1022.

Although diatom accumulation at ODP Sites 1016 and 1022 display opposing trends, with diatom MAR increasing at ODP Site 1016 and decreasing at ODP Site 1022 from the early to late Pliocene, the late Pliocene total diatom values at both sites are quite similar (1.00± 0.07 and 0.90± 0.21, respectively; Tables 11 and 12; Figure 13). ODP Site 1022 was likely influenced by the California Current throughout the Pliocene, as it appears to be today (Lyle, et al., 1997). The similarity of the late Pliocene diatom MAR at both sites suggests that by the late Pliocene, ODP Site 1016 had moved to a location more strongly influenced by the California Current. In addition to the extremly low diatom accumulation at ODP Site 1016 in sediment older then 3.5 Ma, bulk sediment accumulation was nearly an order of magnitude lower in the early Pliocene (Figure 11). This indicates the site transitioned a more plagic to a more hemiplagic zone as the rate of particles settling to the seafloor increased toward the late Pliocene. Therefore, the slight increase in diatom accumulation from the early to late Pliocene at ODP Site 1016 is likely a function of a change in geography rather than being a representation of a larger trend of a decrease in nutrient supply along the majority of the California margin.

This is one of few studies suggesting that there was a decrease in productivity along the California margin during the late Pliocene. The ODP Site 1022 diatom assemblage study concluded that there was sustained productivity through the Pliocene (Reed-Sterrett et al., 2010). Other proxies used to document productivity in various California margin studdies include calcite, organic carbon, C_{37} (alkenones), and % nitrogen (Lyle et al., 2000; Ravelo et al., 1997; Yasuda, 1997) find the coccolith derrived proxies, calcite and C_{37}, to show increased or sustained productivity, and attribute decreases in other proxies, including organic carbon and silica, to an opal crash. While in many cases alkenone concentrations can provide a rough guide to total paleoproduction (Lawrence et al., 2006), care should be taken that it is not only reflecting coccolith production, as it appears to be along the California margin during the late Pliocene.

Productivity along the California margin during the Pliocene could have been affected by physical and chemical properties of the water column. There are two possible explanations for the decreased nutrient supply to the photic zone along the California margin during the late Pliocene. The first option is that despite the cooling SST, upwelling was actually decreasing and stratification was increasing through time, leading to the decreased diatom and increased coccolith abundances in the late Pliocene. The second possibility is that upwelling did not change through time, and that instead there was a change in the nutrient concentrations of the upwelled water, so that even in the presence of upwelling, the upwelled water may not have been as nutrient-rich as it is today.

4.5 *Possible Changes in Upwelling Through the Pliocene*

One possible explanation for the observed diatom and coccolith trends is that upwellling of nutrient-rich water decreased through the Pliocene. If the cooling SST along the California margin (Figure 5) was due to increased upwelling through the Pliocene, diatom productivity should have also increased through this time, which is not the case at ODP Site 1022. However, a reduction in upwelling through the Pliocene could lead to both the decrease in nutrient supply and diatom abundances, as well as increased stratification, which would favor higher abundances of coccolithophores, which is observed at both ODP Sites 1016 and 1022 (Figure 12). While diatom accumulation at ODP Site 1016 does increase through the Pliocene, it is most likely due to tectonic movement of the site location, as discussed in the previous section. There are several paleoproductivity studies along the California margin during the Pliocene that have somewhat conflicting implications for changes in upwelling.

Diatom assemblage and stratigraphy data for all the California Margin drill sites show that the late Miocene and Pliocene was an interval of particularly low diatom abundances at almost all the California margin sites (Maruyama, 2000), which was contributed to a decline in diatom productivity in the surface waters due to slackening of the southward flow of the California Current and reduced coastal upwelling (Maruyama, 2000). Diatoms persisted at ODP sites 1016 and 1022 during the Pliocene, and those sites appear to have been less effected by the proposed reduction in upwelling, although possible reasons for this were not discussed (Barron, 2000; Maruyama, 2000). The data presented here is in agreement with the ODP data that these sites were slightly less affected, but ODP Site 1022 did experience a reduction in diatom abundance through the Pliocene.

A diatom assemblages study at ODP site 1022 attempted to constrain changes in oceanographic conditions along the California margin during the early to middle Pliocene (Reed-Sterrett et al., 2010). The relative abundance of a diatom species indicative of upwelling strenth did not display a long term trend from 4.2 to 3 Ma, although variability did exist (Reed-Sterrett et al., 2010). The diatom taxa used to represent upwelling (*Thalassionema nitzschiodes* and *Thalassiothrix longissima*) are both pennate diatoms and were the most abundant of all the diatom species counted (Reed-Sterrett et al., 2010). This is in agreement with the data from this study in that pennate diatoms are the most abundant diatom form at ODP Site 1022 (Figure 14). The abundant and persistent record of the pennate diatoms from 4.2 to 3 Ma was interpreted as indication that there was no change in upwelling strength, and the decrease in SST through that time is attributed to a shoaling thermocline (Reed-Sterrett et al., 2010).

The decrease in diatom accumulation at ODP Site 1022 from the early to late Pliocene in this study does not necessarily contradict the diatom assemblage study. The diatoms in this study are counted as a relative percent of the total material in the sediment, while the assemblage study dissolved the sample of other material prior to making the diatom counts, and counted the same number of diatoms, regardless of species (Reed-Sterrett et al., 2010). This means that while the total diatom productivity was decreasing, the relative contribution of the upwelling indicator species remained the same (Figure 14), suggesting that upwelling strength did not vary much through this time period. The decreasing diatom abundances through time in this study suggests that, while upwelling strength may not have changed, there was a decrease in nutrient supply to the surface along the entire California margin.

4.6 *Evidence for Decreased Surface Nutrient Supply Through the Pliocene*

A second possible explanation for the increase in coccoliths at both ODP Sites 1016 and 1022, and decrease in diatoms at ODP Site 1022, and overall low levels of diatoms at both ODP Sites 1016 and 1022, is that the nutrient content of upwelled water changed through time. If upwelling or vertical mixing did not change much through this time period, the late Pliocene increase in coccolith accumulation and similarly low diatom accumulation at both ODP Sites 1016 and 1022 implies that after ~3.5 Ma there was a decrease in nutrient supply to the surface. A deeper location of nutrient-rich water so that nutrients can not be transferred to the photic zone could explain the apparent changes in productivity. Decreased nutrient supply, rather then reduced upwelling, could also explain cooling SST, because a shoaling thermocline can be supplying the cooler, even if still nutrient-poor, upwelling water (Kwiek & Ravelo, 1999; Liu et al., 2008; Reed-Sterrett et al., 2010).

Benthic stable isotope data suggest that while the general structure of large scale north Pacific circulation was similar during the Pliocene, however from 5 to 1.4 Ma the core of the nutrient enriched return flow became deeper than it is today (~2500 m, compared to ~1500 m today) (Kwiek & Ravelo, 1999; Figure 25). This deepening has been attributed to the enhancment of North Pacific Intermediate Water (NPIW), becoming a larger water mass layer, which sits directly on top of the nutrient-rich Pacific Deep Water return flow (Kwiek & Ravelo, 1999). Today, new NPIW forms from winter icing in the Sea of Okhotsk and enters the Pacific from the northwest corner of the subtropical gyre via the Bussol Strait (Yasuda, 1997). Therefore the transition toward a cooler climate and the appearance of northern hemisphere ice out of the late Pliocene may be partially responsible for enhanced NPIW. Higher carbon isotope values in the north Pacific during the Pliocene suggests it was also possible that there was additional evaporation-supported production of intermediate water in the Bering Sea Basin (Kwiek & Ravelo, 1999). Future work should aim to more thouroughly examine the mechanisms or feedbacks that led to the enhancment of NPIW, so that early warning signs of history repeating itself can be identified and prepared for.

The downward displacment and subsequent isolation of nutrient-rich water starting ~5 Ma was apparently stable on a long timescale, before becoming shallower after 1.4 Ma, like in the modern north Pacific (Kwiek & Ravelo, 1999; Figure 25). It is possible that as the nutrient rich return flow was deepening in the early Pliocene, that until ~3.5 Ma the depth of nutrient-rich waters had not reached a critical depth so that some nutrients could still be brought into the photic zone by upwelling and/or vertical mixing. The smear slide data suggests that by ~3.5 Ma, very few nutrients made it to the surface, and this might represent the point at which nutrient-rich waters had reached some critical depth that neither vertical mixing or upwelling could bring it to the surface. This coincides with records showing that the slope of the northern Pacific vertical nutrient profile became more steep from the early to late Pliocene (Kwiek & Ravelo, 1999; Figure 25). Additional records extending the time period covered by this study through the

Pleistocene would help determine if the end members of the nutrient displacment coincided with the phytoplankton abundance records.

It is apparent in the accumulation data presented here, and from the diatom assembage study for ODP site 1022 (Reed-Sterrett et al., 2010), that productivity along the California margin did not change with SST, and certainly did not show a gradual increase as would be expected if the gradual decrease in SST were caused by an increase in upwelling alone (Reed-Sterrett et al., 2010 & Dekens et al., 2007). The diatom assemblage study also concluded that the main difference between modern and Pliocene upwelling is the apparent decoupling of the nutricline (fueling productivity) and the thermocline during the Pliocene (Reed-Sterrett et al., 2010).

It could be argued that the decrease in surface nutrient supply could be due to an overall decrease in nutrients throughout the water column, rather then a downward displacement of nutrient rich waters. High latitude nutrient availability forcing appears to be a primary control on long-tern productivity changes on the California margin (Liu et al., 2008). Nitrogen can be a limiting factor for phytoplankton growth, thus high levels of microbial denitrification, which removes nitrogen from the water, can lead to reduced productivity. However, a 4 Ma-long nitrogen isotope record, representing denitrification intensity, from ODP Site 1012 shows that denitrification was relatively week through much of the Pliocene (Liu et al., 2008). This indicates that there were nutrients available in the water column during the late Pliocene, and suggests that a downward displacement of nutrients is the most likely scenario to explain the diatom abundances.

In the modern ocean coccolithophorids generally dominate the middle of oligotrophic gyres, whereas other calcifying organisms dominate in the more mesotrophic areas like equatorial divergence zones and continental margins (Baumann et al., 2005). The higher coccolith accumulation at ODP sites 1022 and 1016 after 3.5 Ma indicate the California margin turned into a more nutrient-poor regime during the late Pliocene. The timing of the observed increase in coccolith accumulation corresponds to increases in carbonate MAR from ~4 to 2 Ma at ODP site 1016 and from 3.5 to 2.2 Ma at ODP site

1022 (Lyle, et al., 1997; Figure 26), and other sites along the California margin during the Pliocene (Ravelo et al., 1997). This calcite event had previously been attributed to enhanced foraminifera production (Ravelo et al., 1997), in part because it is rare for coccolith based calcite to accumulate in the productive active upwelling margins of today. At ODP site 1016 the intensity and duration of the increased calcite MAR are much higher compared to ODP site 1022 (Figure 26). This suggests that ODP site 1016 may have been more strongly influenced by the decrease in nutrient supply than ODP site 1022. The organic carbon MAR record for ODP site 1016 is the inverse of the calcite trend for the same time interval; organic carbon MAR decreases as calcite MAR increases (Figure 27) (Lyle et al., 1997). Unfortunatly there is only a short record of calcite and organic carbon MAR available for ODP site 1022, and while it appears to show a drop for the short interval that calcite MAR is increased it is diffricult to make any kind of correlation. The decreased organic carbon (Figure 27) and low diatom accumulation (Figures 12 and 13) that are coincident with increases in calcite (Figure 26) and coccolith accumulation (Figure 12) in the late Pliocene at both ODP Sites 1016 and 1022, more strongly suggests that there was a decreased nutrient supply in the source waters, rather than reduced upwelling, as upwelling likely supported the cooling SST trend through the Pliocene (Figure 5).

4.7 *Evidence for Global Oceanic and Atmospheric Reorginization and Restructuring*

At around 3.5 Ma, the same time that there are significant changes in the coccolith and diatom MAR at both ODP Sites 1016 and 1022, there are several ongoing large-scale changes in global oceanic and atmospheric circulation and orginization. The early Pliocene tropical Pacific Ocean resembled a permanent El Niño-like state ~3.2-4.6 Ma, where the thermocline was deep and equally distributed and SST more uniformly warm across the equatorial Pacific (Ravelo et al., 2006; Reed-Sterrett et al., 2010; Wara et al., 2005). Within 500 kyr the Pacific transitioned from its El Niño like state to the general structure observed today (Dowsett & Robinson, 2009; Haywood et al., 2009). The thermocline shoaled along the California margin during this time as well (Reed-Sterrett et al., 2010).

The Pliocene climate can be split into two stages, the first is a relatively warm and stable climate (Brierley et al., 2009; Dowsett & Robinson, 2009), and the second is a transition to a globally cooler time leading to northern hemisphere glaciation ~2.7 Ma (Haug et al., 2005). The transition to a world with northern hemisphere ice was not completely linear; global high latitude benthic oxygen isotope records suggest there were small fluctuations between intervals of more and less ice (De Schepper et al., 2013). The intervals of more ice volume are viewed as a premature attempt of the climate system to establish an ice age world. One of the earliest identified premature global glaciation periods, marine isotope stage (MIS) M2, which interrupted Pliocene warmth took place ~3.3 Ma and lasted <100 kyr (De Schepper et al., 2013). The initiation of the event has been partly attributed to the weakening of the Pacific to Atlantic flow via the Central American Seaway, which caused a cooling of the high latitude oceans (De Schepper et al., 2013). It has also been suggested that in increase in the stratification of the subarctic Pacific Ocean combined with increases in summer SST provided the water vapor content to northern North America which allowed the initiation of Northern Hemisphere glaciation (Haug et al., 2005).

While each of these events can not directly explain the observed shifts in the various phytoplankton group MAR at ODP Sites 1016 and 1022, similarities in the timing of these events strongly supports the notion that a large scale restructuring of the global oceans through the Pliocene was a key factor in all of these events. It is possible that the ongoing fluctuations of ice buildup and melting led to the enhancement of north pacific intermediate water. In addition to this water mass being responsible for the downward displacement and isolation of nutrients in the water column through the Pliocene, it was also cooler than the typical SST along the California margin during the Pliocene. This scenario explains both the SST trends and the late Pliocene coccolith and diatom MAR shifts at ODP Sites 1016 and 1022.

5. **Conclusions**

Primary productivity in upwelling systems has important impacts on both regional and global scales (Behrenfeld et al., 2006; Falkowski, 2012; Seager et al., 2003). It is important to understand how these areas may respond to future global warmth. Modern sattelite and observtion-based productivity studdies are limited in that they have only been collecting data for a short amount of time. While not a perfect analog for future global warming, the Pliocene presents an opportunity to examine the equilibrium response of productivity in upwelling regions to conditions of global warmth. This study presented a Pliocene aged, 2.5-4.5 Ma, record of smear slide generated phytoplankton assemblage data at two sites along the California upwelling margin, ODP Sites 1016 and 1022, to document the evolution of phytoplankton species abundances through the Pliocene.

The similarity of the late Pliocene diatom MAR, and the increase in coccolith MAR through the Pliocene at both ODP Sites 1016 and 1022 suggests that there was a decrease in surface nutrient availability, particularly in areas strongly influenced by the California Current. There are two possible causes for decreased nutrient availability along the California margin: a decrease in upwelling strength or a deepening of nutrient rich waters so that they became impenetrable by upwelling. The productivity trends cannot be explained by a decrease in upwelling because diatom assemblage data indicates there was no change in upwelling strength during the Pliocene (Reed-Sterrett et al., 2010). In addition, a decrease in upwelling would not support the cooling SST trends along the entire California margin (Dekens et al., 2007; Liu et al., 2008; Reed-Sterrett et al., 2010). A relatively low and constant denitrification record at nearby ODP Site 1012 (Liu et al., 2008) provides evidence that nutrients remained in the water column, however a deepening nutricline is supported by a study suggesting enhanced NPIW formation and expansion during the Pliocene, causing a nearly 1000 m downward displacement of the nutrient rich return flow (Kwiek & Ravelo, 1999). The enhancement of NPIW could have been caused by the cooling climate generating the winter ice in the Sea of Okhotsk, which is currently responsible for new NPIW formation (Yasuda, 1997). It is also possible that Pliocene warmth increased evaporation and produced intermediate waters in the Bering Sea (Kwiek & Ravelo, 1999). The productivity record in conjunction with the cooling SST trends through the Pliocene is consistent with the idea of a decoupled thermocline and nutricline, where upwelling penetrated waters closer to the shoaling thermocline, but above the deepening nutricline.

This study also tested the applicability of using particle size analysis, to correlate with the smear slide data, as an additional method for characterizing and quantifying the sediment. While there are several sources of uncertainty, PSA has previously been successfully correlated with diatom abundances in the Bering Sea (Aiello & Ravelo, 2012) and should continue to be tested as an additional method to help characterize biogenic ocean sediments. Unfortunately, the sediments used in this study displayed no significant correlations between any of the particle size categories with the smear slide data. Future work should aim to test various pretreatments of the sediment to remove the siliceous or carbonate components prior to analysis. The relative ease and speed at which PSA can be preformed makes it a very useful tool in paleoceanographic studies examining long timespans.

6. **References**

American Mineralogist: Mineralogical Society of America, Washington, DC

Aiello, I. W., & Kellett, K. (2006). Sedimentology of open-ocean biogenic sediments from ODP Leg 201, Eastern Equatorial Pacific (Sites 1225 and 1226). *In Jorgensen, B.B., D'Hondt, S.L., Miller, D.J. (Eds.), Proceedings of ODP, Scientific Results, 201*, 1–25.

Aiello, I. W., & Ravelo, A. C. (2012). Evolution of marine sedimentation in the Bering Sea since the Pliocene. *Geosphere*, *8*(6), 1231–1253. doi:10.1130/GES00710.1

Anderson, C. R., Siegel, D. a., Brzezinski, M. a., & Guillocheau, N. (2008). Controls on temporal patterns in phytoplankton community structure in the Santa Barbara Channel, California. *Journal of Geophysical Research*, *113*(C4), 1–16. doi:10.1029/2007JC004321

Barron, J. A. (2000). Data report: mid-Pliocene diatom assemblages at Sites 1016, 1021, and 1022. *In Lyle, M., Koizumi, I., Richter, C., and Moore, T.C., Jr. (Eds.), Proc. ODP, Sci. Results, 167: College Station, TX (Ocean Drilling Program),* 111-113. doi:10.2973/odp.proc.sr.167.201.2000

Batteen, M., Cipriano, N., & Monroe, J. (2003). A Large-Scale Seasonal Modeling Study of the California Current System. *Journal of Oceanography*, *59*(1997), 545–562.

Baumann, K., Andruleit, H., & Böckel, B. (2005). The significance of extant coccolithophores as indicators of ocean water masses, surface water temperature, and palaeoproductivity: a review. *Paläontologische Zeitschrift*, *79*(1), 93–112.

Behrenfeld, M. J., O'Malley, R. T., Siegel, D. A., McClain, C. R., Sarmiento, J. L., Feldman, G. C., Milligan, A.J., Falowski, P.G., Letelier, R.M., & Boss, E. S. (2006). Climate-driven trends in contemporary ocean productivity. *Nature*, *444*(7120), 752–5. doi:10.1038/nature05317

Brierley, C. M., Fedorov, A. V., Liu, Z., Herbert, T. D., Lawrence, K. T., & LaRiviere, J. P. (2009). Greatly expanded tropical warm pool and weakened Hadley circulation in the early Pliocene. *Science*, *323*(5922), 1714.

Checkley, D. M., & Barth, J. A. (2009). Patterns and processes in the California Current System. *Progress in Oceanography*, *83*(1-4), 49–64. doi:10.1016/j.pocean.2009.07.028

Crosta, Ã. X., & Koc, N. (2007). Diatoms : From Micropaleontology to Isotope Geochemistry. In C. Hillaire-Marcell & A. De Vernal (Eds.), *Proxies in Late Cenozoic Paleoceanography* (1st ed., Vol. 1, pp. 327–369). Amsterdam: Elsevier Ltd. doi:10.1016/S1572-5480(07)01013-5

De Schepper, S., Groeneveld, J., Naafs, B. D. A., Van Renterghem, C., Hennissen, J., Head, M. J., Louwye, S., & Fabian, K. (2013). Northern Hemisphere Glaciation during the Globally Warm Early Late Pliocene. *PLoS ONE*, *8*(12), e81508. doi:10.1371/journal.pone.0081508

Dekens, P. S., Ravelo, A. C., & McCarthy, M. D. (2007). Warm upwelling regions in the Pliocene warm period. *Paleoceanography*, *22*(3), PA3211. doi:10.1029/2006PA001394

Demarcq, H. (2009). Trends in primary production, sea surface temperature and wind in upwelling systems (1998–2007). *Progress In Oceanography*, *83*(1-4), 376–385. doi:10.1016/j.pocean.2009.07.022

Dowsett, H. J., & Robinson, M. M. (2009). Mid-Pliocene equatorial Pacific sea surface temperature reconstruction: a multi-proxy perspective. *Philosophical Transactions. Series A, Mathematical, Physical, and Engineering Sciences*, *367*(1886), 109–25. doi:10.1098/rsta.2008.0206

Falkowski, P. (2012). Ocean science: the power of plankton. *Nature*, *483*(7387), 17–20.

Fedorov, a V, Brierley, C. M., Lawrence, K. T., Liu, Z., Dekens, P. S., & Ravelo, A. C. (2013). Patterns and mechanisms of early Pliocene warmth. *Nature*, *496*(7443), 43–9. doi:10.1038/nature12003

Giraudeau, J., & Beaufort, L. (2007). Coccolithophores: from extant populations to fossil assemblages. In C. Hillaire-Marcell & A. De Vernal (Eds.), *Proxies in Late Cenozoic Paleoceanography* (1st ed., Vol. 1, pp. 409–443). Amsterdam: Elsevier Ltd. doi:10.1016/S1572-5480(07)01015-9

Haug, G. H., Ganopolski, A., Sigman, D. M., Rosell-Mele, A., Swann, G. E., Tiedemann, R., Jaccard, S.L., Bollmann, J., Maslin, M. A., Leng, M. J., & Eglinton, G. (2005). North Pacific seasonality and the glaciation of North America 2.7 million years ago. *Nature*, *433*(7028), 821–5. doi:10.1038/nature03332

Haywood, A. M., Dowsett, H. J., Valdes, P. J., Lunt, D. J., Francis, J. E., & Sellwood, B. W. (2009). Introduction. Pliocene climate, processes and problems. *Philosophical*

Transactions. Series A, Mathematical, Physical, and Engineering Sciences, *367*(1886), 3–17. doi:10.1098/rsta.2008.0205

Hedges, J. I., & Keil, R. G. (1995). Sedimentary organic matter preservation: an assessment and speculative synthesis. *Marine Chemistry*, *49*(2-3), 81–115. doi:10.1016/0304-4203(95)00008-F

Henrichs, S. M. (1992). Early diagenesis of organic matter in marine sediments: progress and perplexity. *Marine Chemistry*, *39*, 119–149.

Hickey, B. M. (1979). The California Current System-hypotheses and facts. *Progress In Oceanography*, *8*, 191–279.

Huyer, A. (1983). Coastal upwelling in the California Current system. *Progress in Oceanography*, *12*, 259–284.

Jacox, M. G., & Edwards, C. A. (2011). Effects of stratification and shelf slope on nutrient supply in coastal upwelling regions. *Journal of Geophysical Research*, *116*(C3), C03019. doi:10.1029/2010JC006547

Jansen, E., J. Overpeck, K.R. Briffa, J.-C. Duplessy, F. Joos, V. Masson-Delmotte, D. Olago, B. Otto-Bliesner, W.R. Peltier, S. Rahmstorf, R. Ramesh, D. Raynaud, D. Rind, O. Solomina, R. V. & D. Z. (2007). Paleoclimate. *Fourth Assessment Report of the Intergovernmental Panel on Climate Change, Climate Change: The Physical Science Basis*.

Kahru, M., Kudela, R., Manzano-Sarabia, M., & Mitchell, B. G. (2009). Trends in primary production in the California Current detected with satellite data. *Journal of Geophysical Research*, *114*(C2), 1–7. doi:10.1029/2008JC004979

Kwiek, P. B., & Ravelo, A. C. (1999). Pacific Ocean intermediate and deep water circulation during the Pliocene. *Palaeogeography, Palaeoclimatology, Palaeoecology*, *154*(3), 191–217. doi:10.1016/S0031-0182(99)00111-X

Lassiter, A. M., Wilkerson, F. P., Dugdale, R. C., & Hogue, V. E. (2006). Phytoplankton assemblages in the CoOP-WEST coastal upwelling area. *Deep Sea Research Part II: Topical Studies in Oceanography*, *53*(25-26), 3063–3077. doi:10.1016/j.dsr2.2006.07.013

Lawrence, K., Liu, Z., & Herbert, T. (2006). Evolution of the eastern tropical Pacific through Plio-Pleistocene glaciation. *Science*, *312*, 79–83. doi:10.1126/science.1120395

Liu, Z., Altabet, M. A., & Herbert, T. D. (2008). Plio-Pleistocene denitrification in the eastern tropical North Pacific: Intensification at 2.1 Ma. *Geochemistry, Geophysics, Geosystems*, *9*(11), 14p. doi:10.1029/2008GC002044

Lyle, M., Koizumi, I., Delaney, M. L., & Barron, J. A. (2000). Sedimentary Record of the California Current System, Middle Miocene to Holocene: A Synthesis of Leg 167 Results. *In Lyle, M., Koizumi, I., Richter, C., and Moore, T.C., Jr. (Eds.), Proc. ODP, Sci. Results, 167: College Station, TX (Ocean Drilling Program)*, 341–376. doi:10.2793/odp.proc.sr.167.238.2000

Lyle, M., Koizumi, I., Richter, C., et al. (1997). Proc. ODP, Init. Repts., 167: College Station, TX (Ocean Drilling Program). doi:10.2973/odp.proc.ir.167.1997

Mantyla, A. W., Bograd, S. J., & Venrick, E. L. (2008). Patterns and controls of chlorophyll-a and primary productivity cycles in the Southern California Bight. *Journal of Marine Systems*, *73*(1-2), 48–60. doi:10.1016/j.jmarsys.2007.08.001

Maruyama, T. (2000). Middle Miocene to Pleistocene Diatom Stratigraphy of Leg 167. *In Lyle, M., Koizumi, I., Richter, C., and Moore, T.C., Jr. (Eds.), Proc. ODP, Sci. Results, 167: College Station, TX (Ocean Drilling Program)*, 63–110. doi:10.2973/odp.proc.sr.167.217.2000

NASA, Goddard Earth Sciences (GES) and Data Information Services Center (DISC) Distributes Active Archive Center (DAAC)

Nelson, D., Tréguer, P., & Brzezinski, M. (1995). Production and dissolution of biogenic silica in the ocean: revised global estimates, comparison with regional data and relationship to biogenic sedimentation. *Global Biogeochemical Cycles*, *9*(3), 359–372.

Pagani, M., Liu, Z., LaRiviere, J., & Ravelo, A. C. (2009). High Earth-system climate sensitivity determined from Pliocene carbon dioxide concentrations. *Nature Geoscience*, *3*(1), 27–30. doi:10.1038/NGEO724

Ravelo, A. C., Lyle, M., Koizumi, I., Caulet, J. P., Fornaciari, E., Hayashida, A., Heider, F., Hood, J., Hovan, S., Janecek, T., Janik, A., Stax, R., & Yamamoto, M. (1997). Pliocene carbonate accumulation along the California Margin. *Paleoceanography*, *12*(6), 729. doi:10.1029/97PA02525

Ravelo, A. C., Dekens, P. S., & McCarthy, M. (2006). Evidence for El Niño-like conditions during the Pliocene. *Gsa Today*, *16*(3), 4–11. doi:10.1130/1052-5173(2006)016<4

Reed-Sterrett, C., Dekens, P., & White, L. (2010). Cooling upwelling regions along the California margin during the early Pliocene: Evidence for a shoaling thermocline. *Stratigraphy*, 141–150.

Rothwell, R. G. (1989). *Minerals and mineraloids in marine sediments: An optical identification guide* (p. 279). London: Elsevier.

Schumacher, S., & Lazarus, D. (2004). Regional differences in pelagic productivity in the late Eocene to early Oligocene—a comparison of southern high latitudes and lower latitudes. *Palaeogeography, Palaeoclimatology, Palaeoecology*, *214*(3), 243–263. doi:10.1016/j.palaeo.2004.06.018

Seager, R., Murtugudde, R., Naik, N., Clement, A., Gordon, N., & Miller, J. (2003). Air-Sea Interaction and the Seasonal Cycle of the Subtropical Anticyclones. *Journal of Climate*, *16*, 1948–1967.

Siegenthaler, U., Stocker, T. F., Monnin, E., Lüthi, D., Schwander, J., Stauffer, B., Raynaud, D., Barnola, J., Fischer, H., Masson-Delmontte, V., & Jouzel, J. (2005). Stable carbon cycle-climate relationship during the Late Pleistocene. *Science (New York, N.Y.)*, *310*(5752), 1313–7. doi:10.1126/science.1120130

Venrick, E. (1998). Spring in the California Current:the distribution of phytoplankton species, April 1993 and April 1995. *Marine Ecology Progress Series*, *167*, 73–88. doi:10.3354/meps167073

Wara, M. W., Ravelo, A. C., & Delaney, M. L. (2005). Permanent El Niño-like conditions during the Pliocene warm period. *Science (New York, N.Y.)*, *309*(5735), 758–61. doi:10.1126/science.1112596

White, L. D., & Alexandrovich, J. M. (1992). Pliocene and Pleistocene Abundance and Preservation of Siliceous Micro-Fossil Assemblages from Sites 794, 795, and 797: Implications for Circulation and Productivity in the Japan Sea. *Proceedings of the Ocean Drilling Program, Scientific Results*, *127, 128*, 341–357.

Yamamoto, M., Yamamuro, M., & Tanaka, Y. (2007). The California current system during the last 136,000 years: response of the North Pacific High to precessional forcing. *Quaternary Science Reviews*, *26*(3-4), 405–414. doi:10.1016/j.quascirev.2006.07.014

Yasuda, I. (1997). The origin of the North Pacific Intermediate Water. *Journal of Geophysical Research*, *102*(C1), 893–909.

Zhang, Y. G., Pagani, M., & Liu, Z. (2014). A 12-million-year temperature history of the tropical Pacific Ocean. *Science*, *344*(6179), 84–7. doi:10.1126/science.1246172

Zonneveld, K. A. F., Versteegh, G. J. M., Kasten, S., Eglinton, T. I., Emeis, K. C., Huguet, C., Koch, B. P., de Lange, G. J., Middleburg, J. J., Mollenhauer, G., Prahl, F. G., Rethemever, J., & Wakeham, S. G. (2010). Selective preservation of organic matter in marine environments; processes and impact on the sedimentary record. *Biogeosciences*, *7*(2), 483–511.

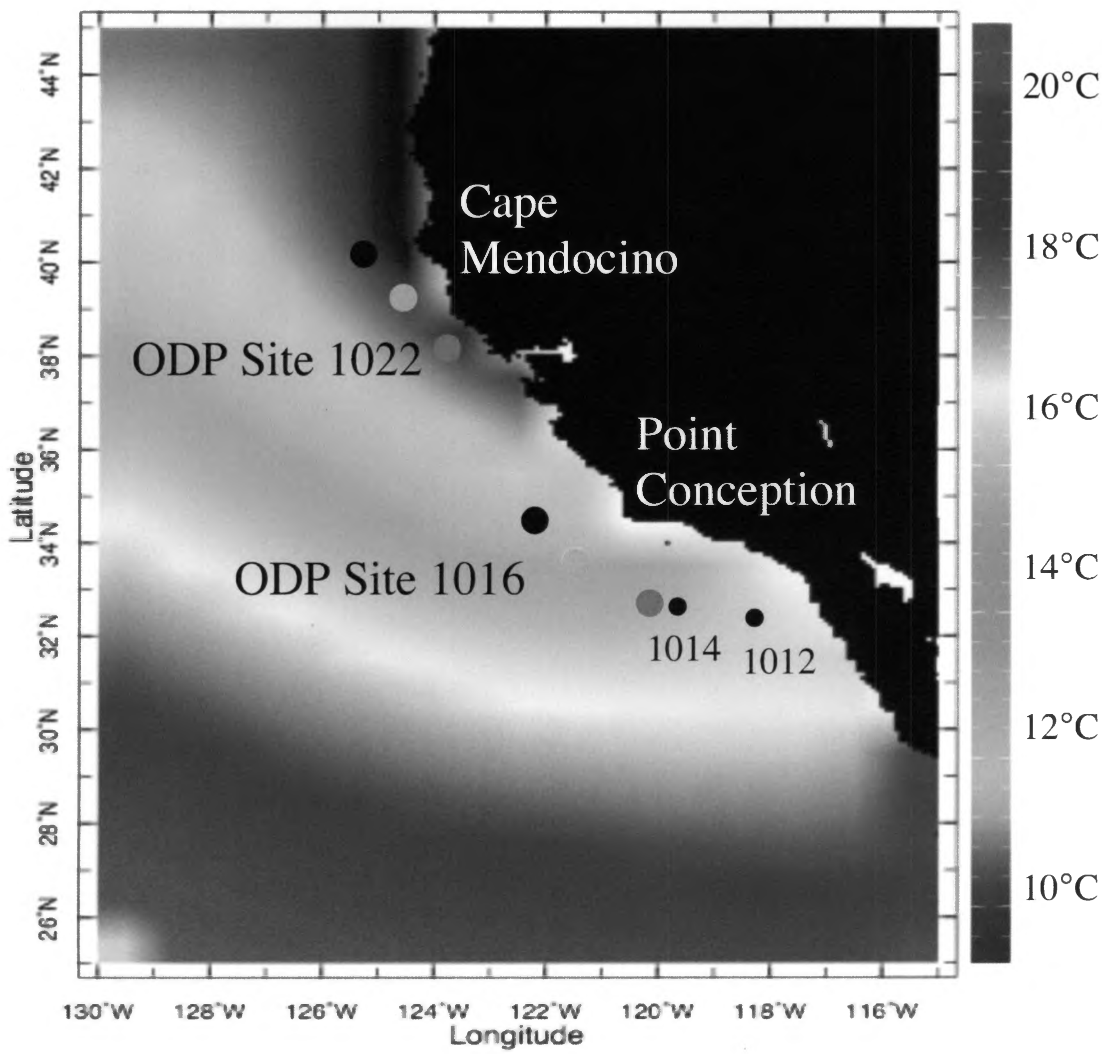

Figure 1: ODP Sites 1016 (34.0°N, 122.0°W, 3835 m water depth) and 1022 (40.0°N, 125.5°W, 1925 m water depth) on a mean annual SST map (NASA GES-DISC). Black dot represents the modern site locations, orange dot represents the 2 Ma site locations, and the purple dot represents the 5 Ma site locations, based on the Lyle et al., 1997 fixed North America reference frame. Mean annual SST at ODP Sites 1016 and 1022 are 14.7 and 12.5°C, respectively. Cape Mendocino and Point Conception marked for reference.

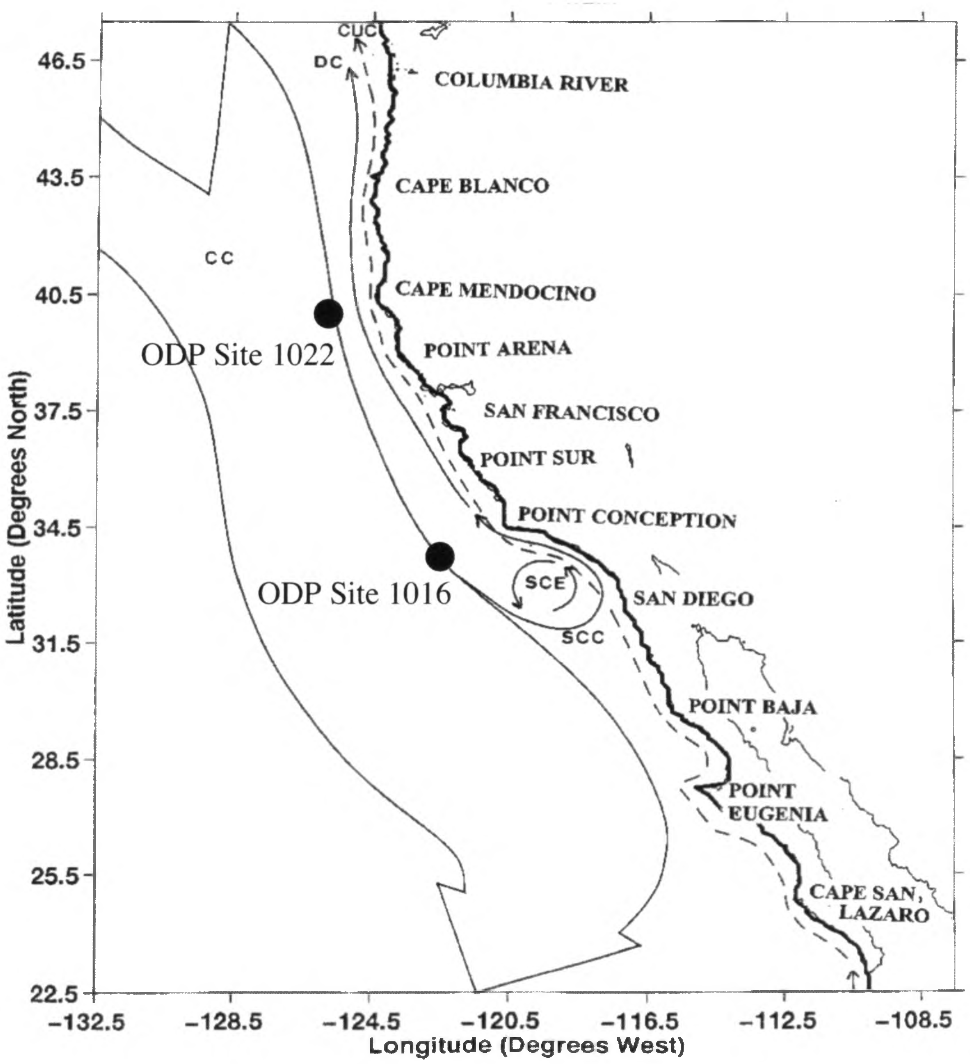

Figure 2: Generalized circulation of the California Current System (CCS) (Batteen et al., 2003) locations of ODP Sites 1016 and 1022 marked for reference. The broad, slow surface southward California Current (CC) overlies the narrow, northward California Undercurrent (CUC). Surface southward flows include the Davidson Current (DC) north of Point Conception, the Southern California Eddy (SCE), and Southern California Countercurrent (SCC) south of Point Conception.

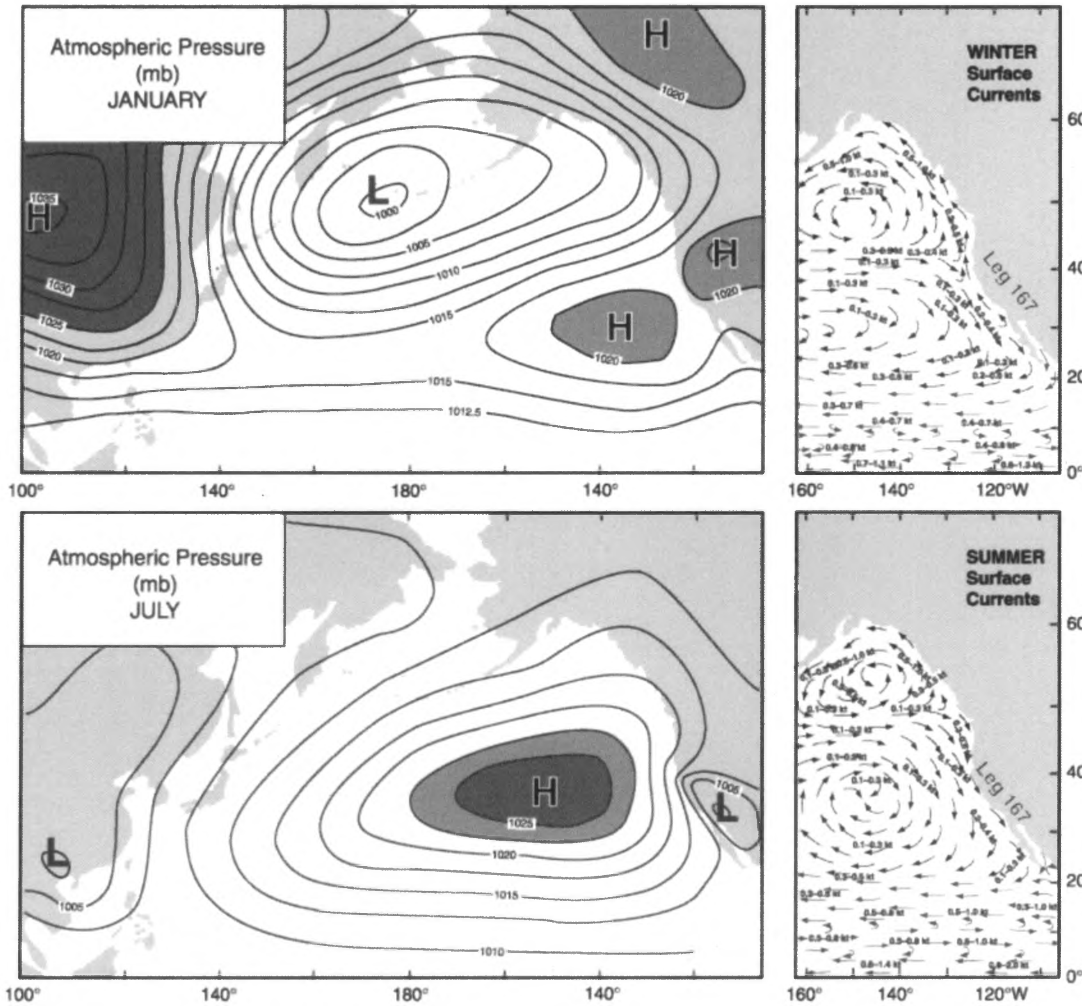

Figure 3: Average atmospheric configuration in winter and summer in the north Pacific, as well as surface currents in winter and summer along the California margin (Lyle et at., 1997). The summer atmospheric configuration leads to intense upwelling along the California margin.

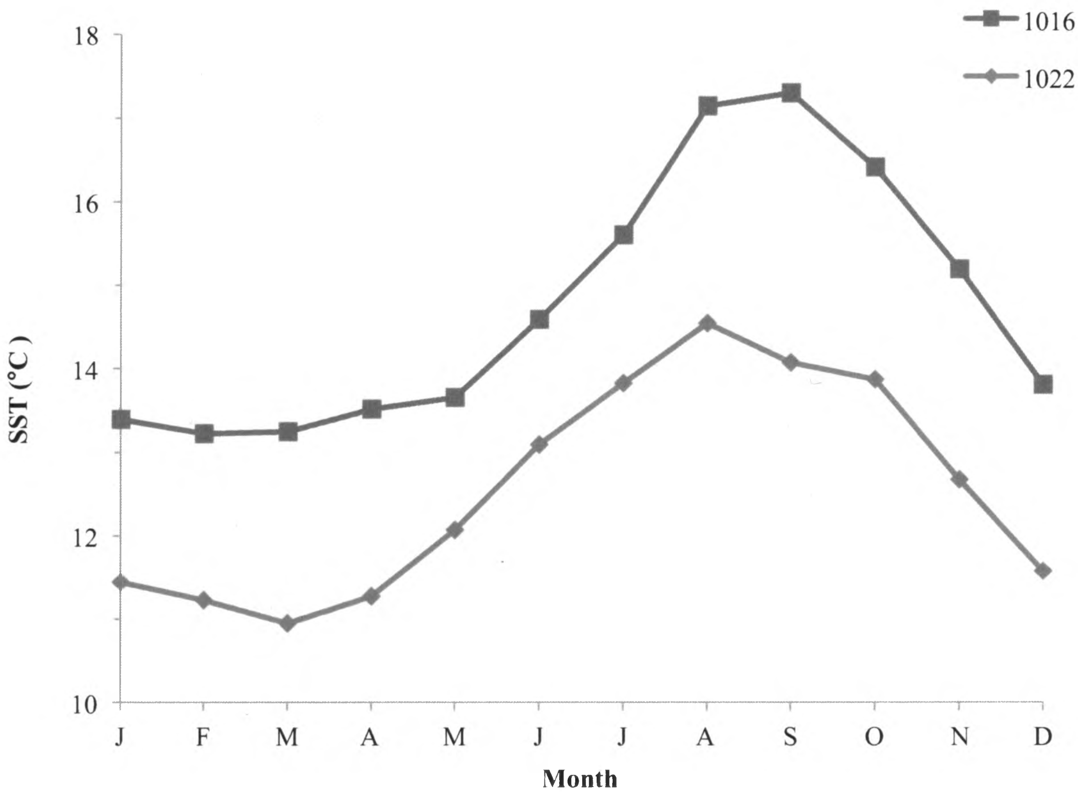

Figure 4: Modern monthly averaged satellite SST's (2003-2011) for ODP Sites 1016 and 1022 (NASA GES-DISC). SST's at ODP site 1022 are slightly cooler then ODP site 1016, but follows a similar trend. The lowest SST's at ODP site 1016 and 1022 are 12 and 9°C, respectively, and occur between January and April. Peak SST's at ODP Site 1016 and 1022 are 18 and 15°C, respectively, and occur between August and September.

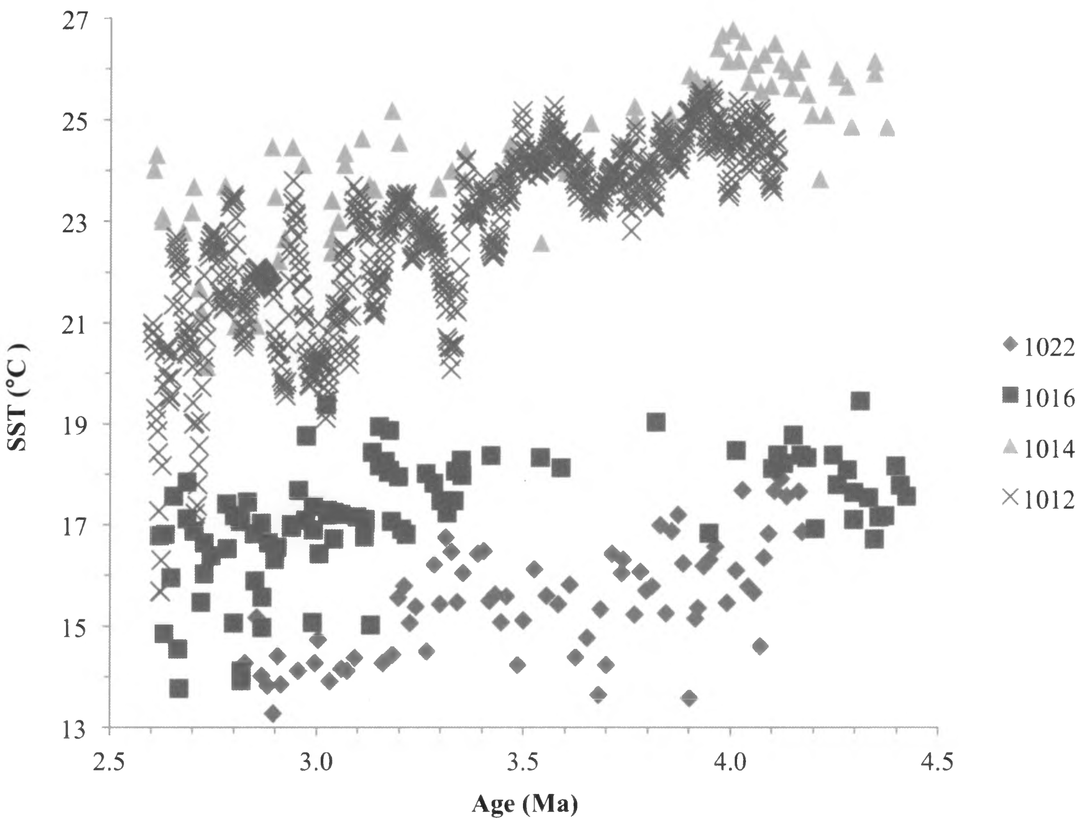

Figure 5: California margin alkenone derived ($U^{K'}_{37}$) SST during the Pliocene at ODP Sites 1012 (Liu et al., 2008), 1014 (Dekens et al., 2007), 1016 (Unpublished), and 1022 (Reed-Sterrett et al., 2010) along the California margin. All SST show a cooling trend out of the Pliocene, the gap in the 1016 record is due to a lack of available samples for that time.

Beckman Coulter LS Particle Size Analyzer

Page

24 Oct 2013 13:3:

File name:	C:\Particle Size Data\Classes\MarSed2013\Valerie\Analyses\16D_13_5_120_5718_01.$l
File ID:	16D_13_5_120
Run number:	5718
Comment 1:	15 sec sonif
Optical model:	Fraunhofer.rfd PIDS included
LS 13 320	Aqueous Liquid Module

Differential Volume

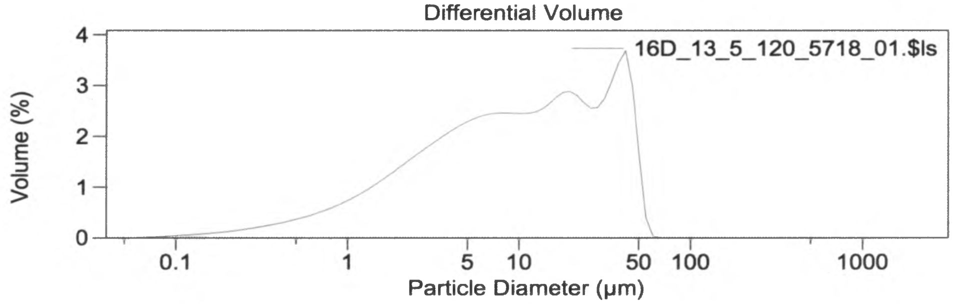

Volume Statistics (Geometric) 16D_13_5_120_5718_01.$ls

Calculations from 0.0400 µm to 2000 µm

Volume:	100%		
Mean:	8.181 µm	S.D.:	3.607
Median:	9.693 µm	Variance:	13.01
D(3,2):	2.950 µm	Skewness:	-0.689 Left skewed
Mean/Median ratio:	0.844	Kurtosis:	0.017 Leptokurtic
Mode:	41.68 µm		
d_{10}:	1.397 µm		
d_{50}:	9.693 µm		
d_{90}:	38.48 µm		
Specific Surf. Area:	20338 cm^2/mL		

% <	10	25	50	75	90
µm	1.397	3.554	9.693	23.39	38.48

Particle Diameter µm	Volume % <
4	27.5874
6	37.428
10	50.8149
32	83.7914
63	99.9969
125	100
250	100
500	100

Figure 6: For each sample run through the Beckman-Coulter laser particle sizer, a PDF is generated showing the grain size distribution, mean, median, and mode grain sizes, and predefined interpolation points. Once the data file for the sample run is saved, the various calculations and interpolation points can be redefined and calculated.

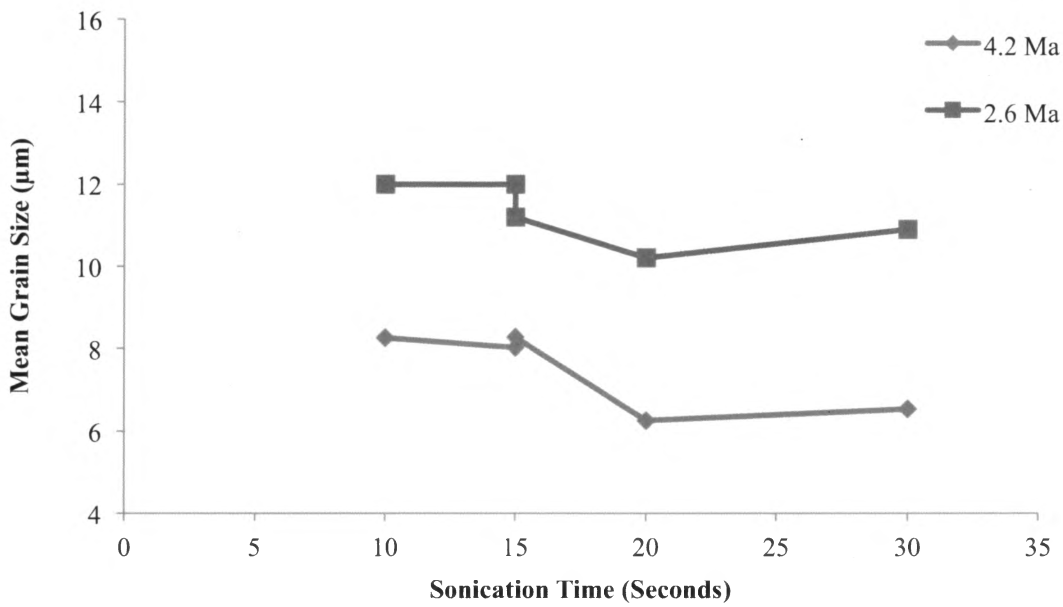

Figure 7: Results from the PSA sonication time experiments, mean grain size observed for the oldest and youngest samples from ODP Site 1016 for various sonication times prior to PSA of the sample. This experimental data was used to determine the appropriate time of sample sonication prior to PSA analysis; the mean grain size curve stabilizes between 15-20 seconds.

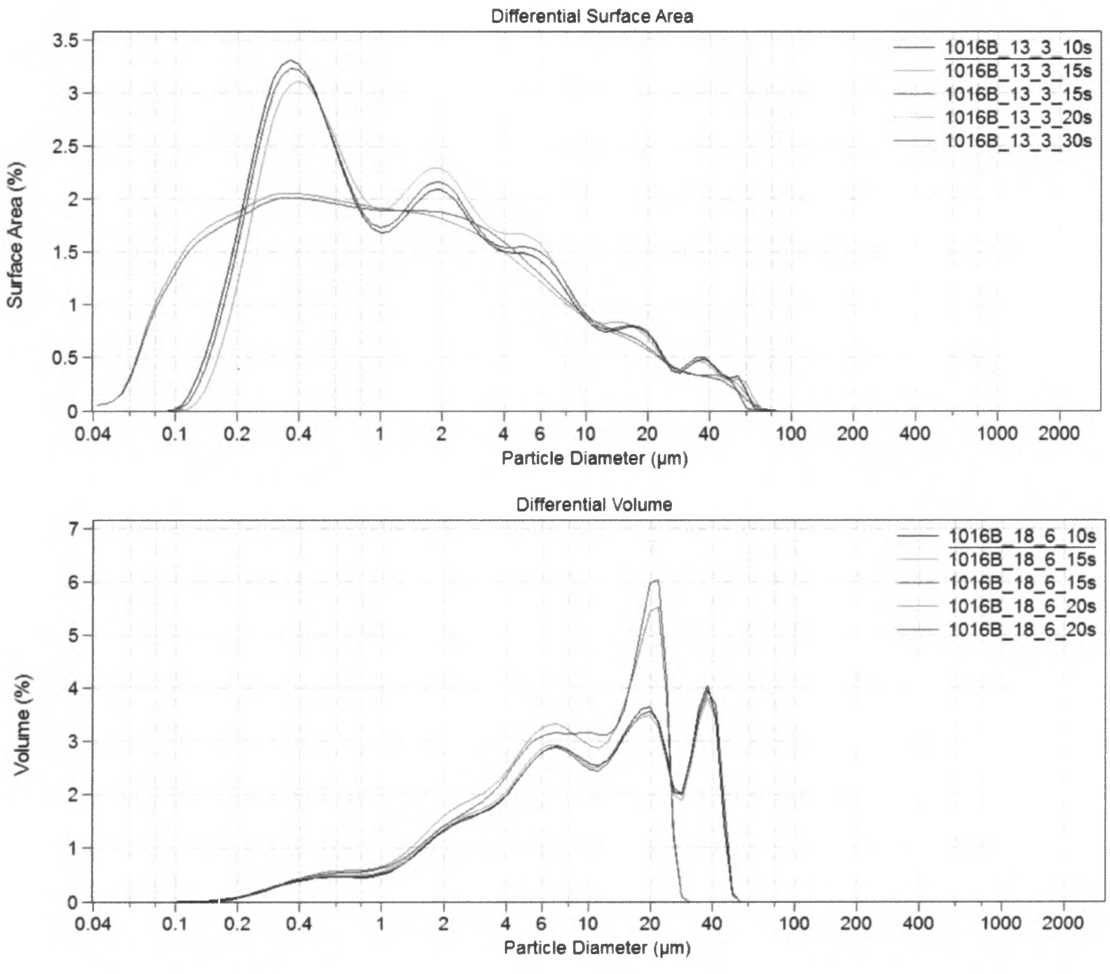

Figure 8: Particle size distributions for the two ODP Site 1016 samples used for the sonication experiment times. The top distribution is of the differential surface area of the youngest (2.6 Ma) sample run after sonication times of 10, 15, 20, and 30 seconds, and for the 20 and 30-second sonication times, the distribution is overly smoothed. The bottom distribution is of the differential volume of the oldest (4.2 Ma) sample run after sonication times of 10, 15, 20, and 30 seconds, and for the 20 and 30-second sonication times, the last peak of larger grain sizes is completely removed and the second to largest peak becomes much larger. The distributions suggest that a sonication time between 15 and 20 seconds is appropriate to break up the aggregates, without overly disrupting the truly larger particle sizes.

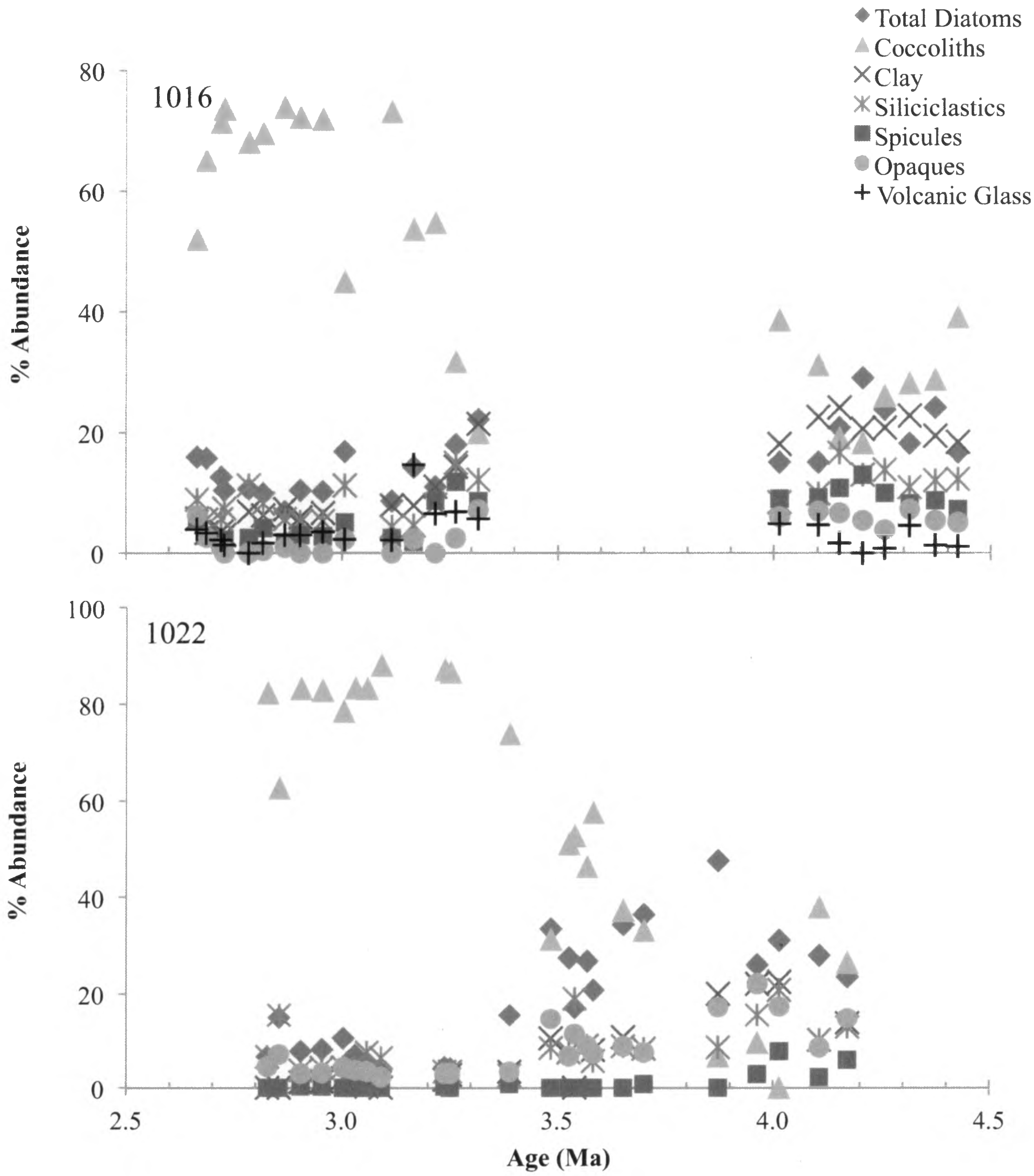

Figure 9: Smear slide percent abundance data of the major and important minor components for both ODP Sites 1016 (top) and 1022 (bottom). This data is also listed in Tables 1 and 2. There is an increase in the abundance of coccoliths in the sediments from the early to late Pliocene. At ODP Site 1016 the abundances of the non-coccolith components decrease from the early to late Pliocene. At ODP Site 1022 the abundances of diatoms, clay and siliciclastics decrease from the early to late Pliocene, and the abundance of spicules is quite low throughout this record.

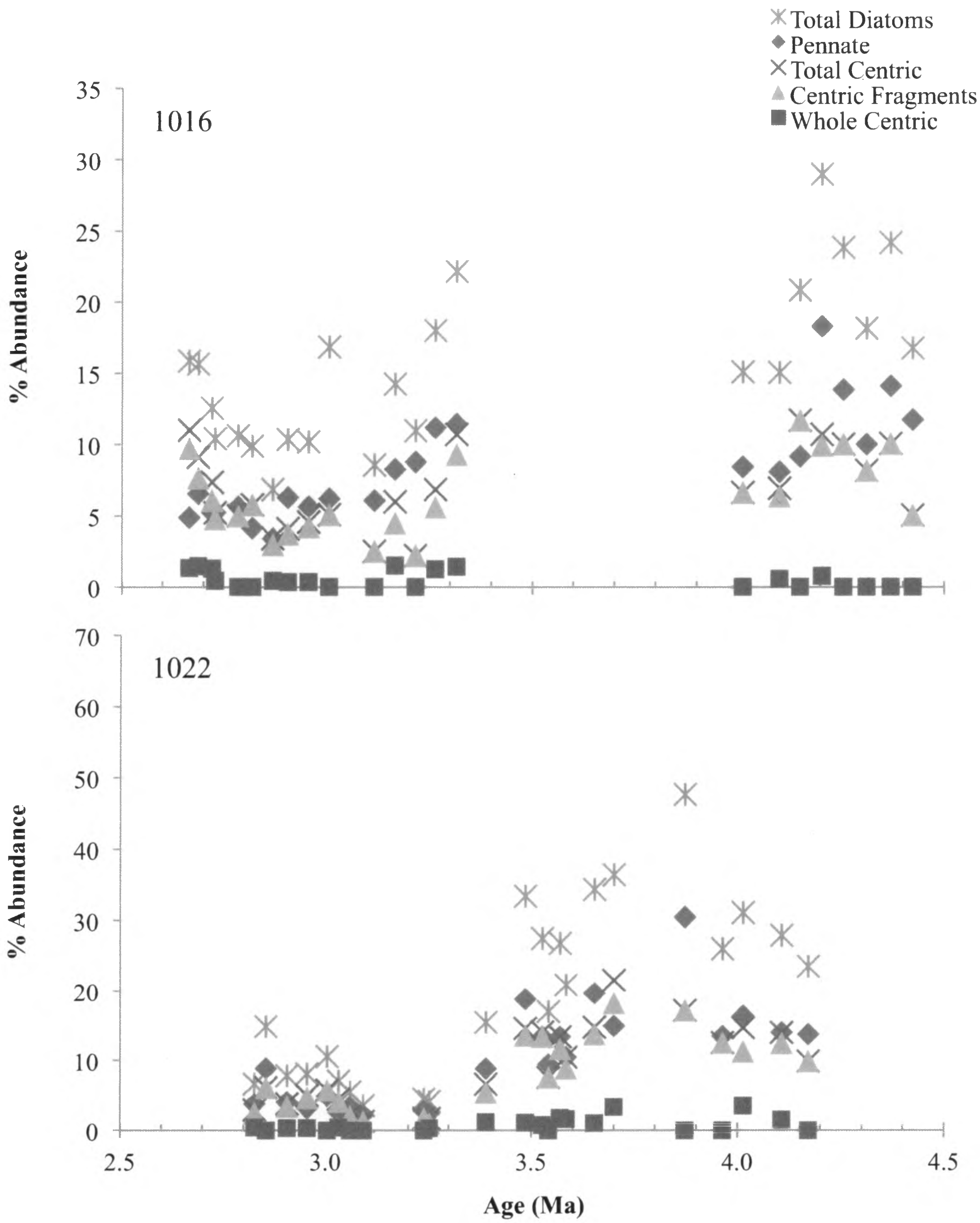

Figure 10: Smear slide percent abundance of the various diatom group components including pennate, centric fragments, whole centric, total centric, and total diatoms, which is the sum of all the diatom components for ODP Sites 1016 (top) and 1022 (bottom). Centric diatom fragments constitute the majority of centric diatoms, pennate diatoms contribute to slightly over half of the total diatoms.

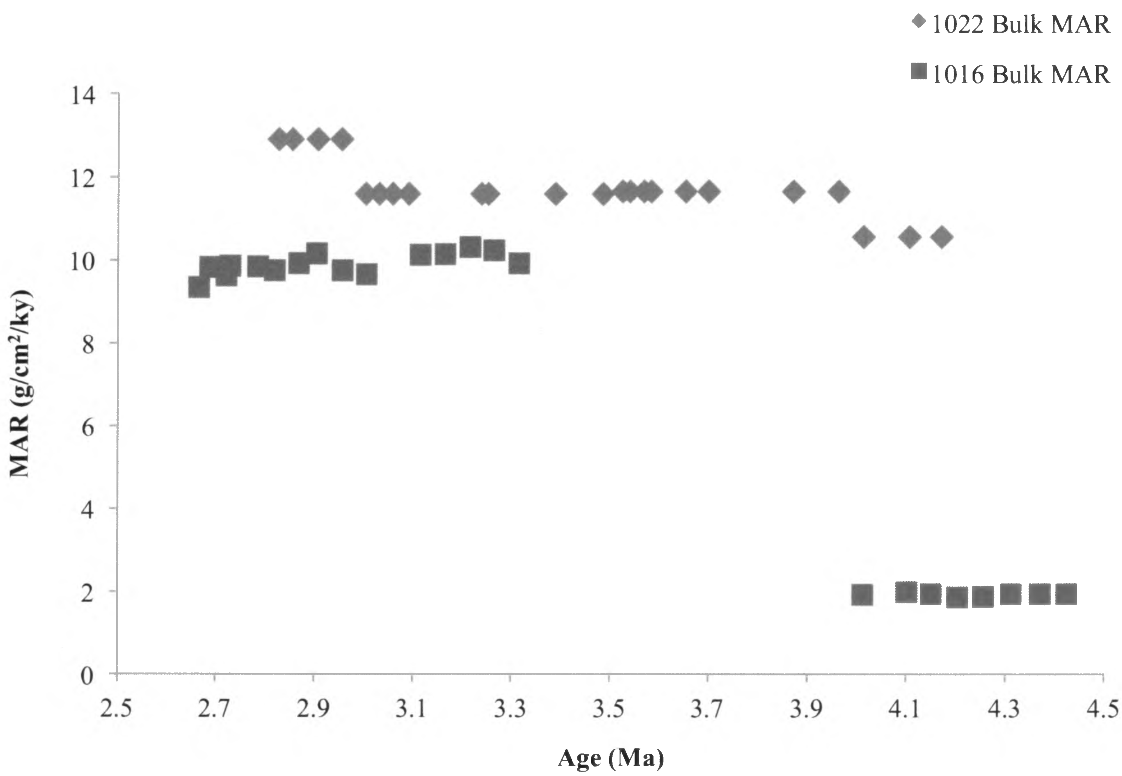

Figure 11: Bulk sediment MAR for ODP Sites 1016 and 1022. The sedimentation rate (Tables 5 and 6) exerts a strong influence over the MAR, as is exhibited by the low sedimentation rate ODP Site 1016 during the early Pliocene resulting in a decreased MAR during that time.

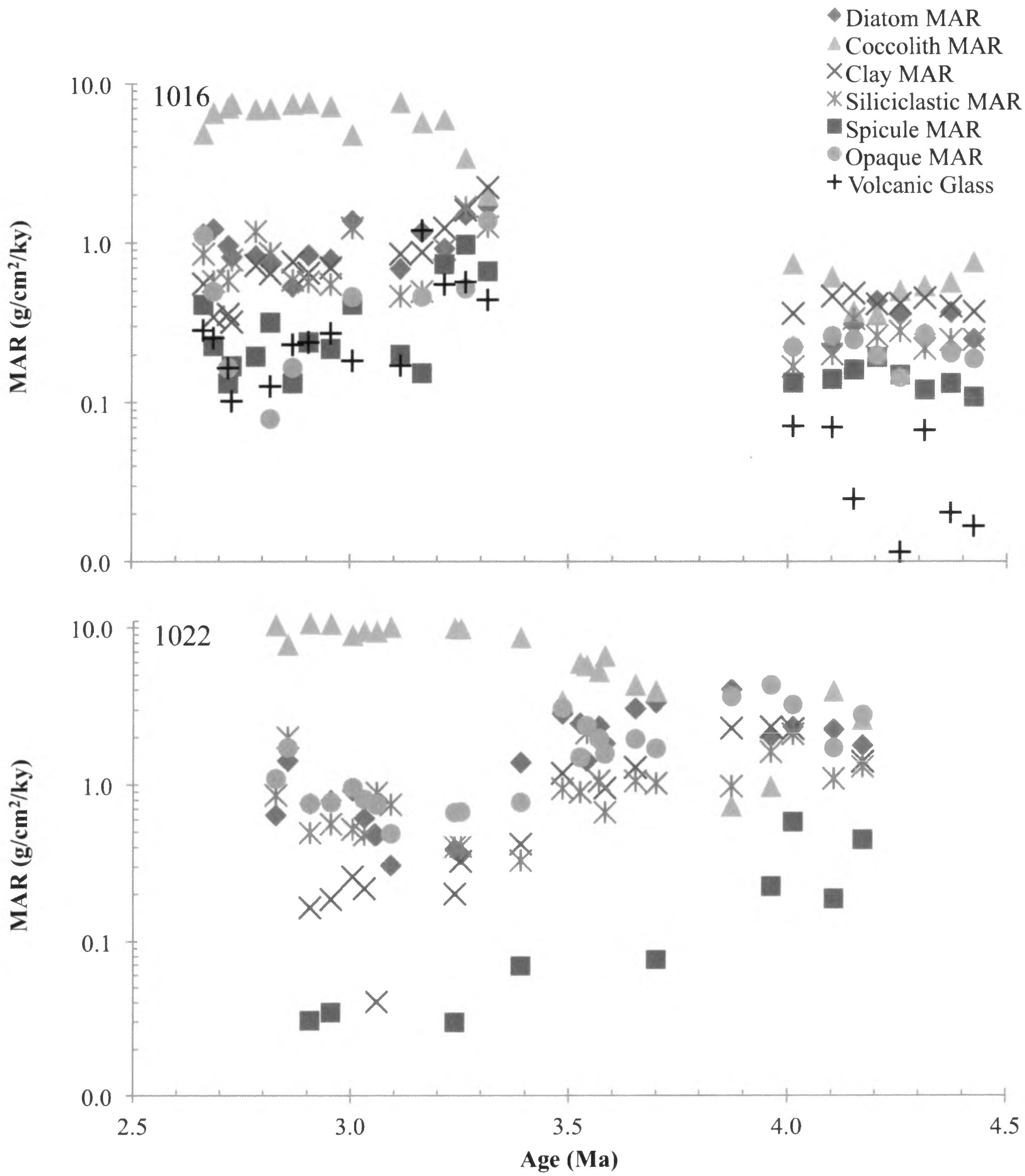

Figure 12: Density specific smear slide component MAR on a log scale for ODP Sites 1016 (top) and 1022 (bottom). Coccolith MAR increases in the late Pliocene at both sites. At ODP Site 1016 the non-coccolith components have slightly higher MAR in the late Pliocene then the early Pliocene. At ODP Site 1022 the non-coccolith components have decreased MAR in the late Pliocene then the early Pliocene. Note that due to the log scale of the y-axis, components that have a zero value (Figure 9) are not included in this figure.

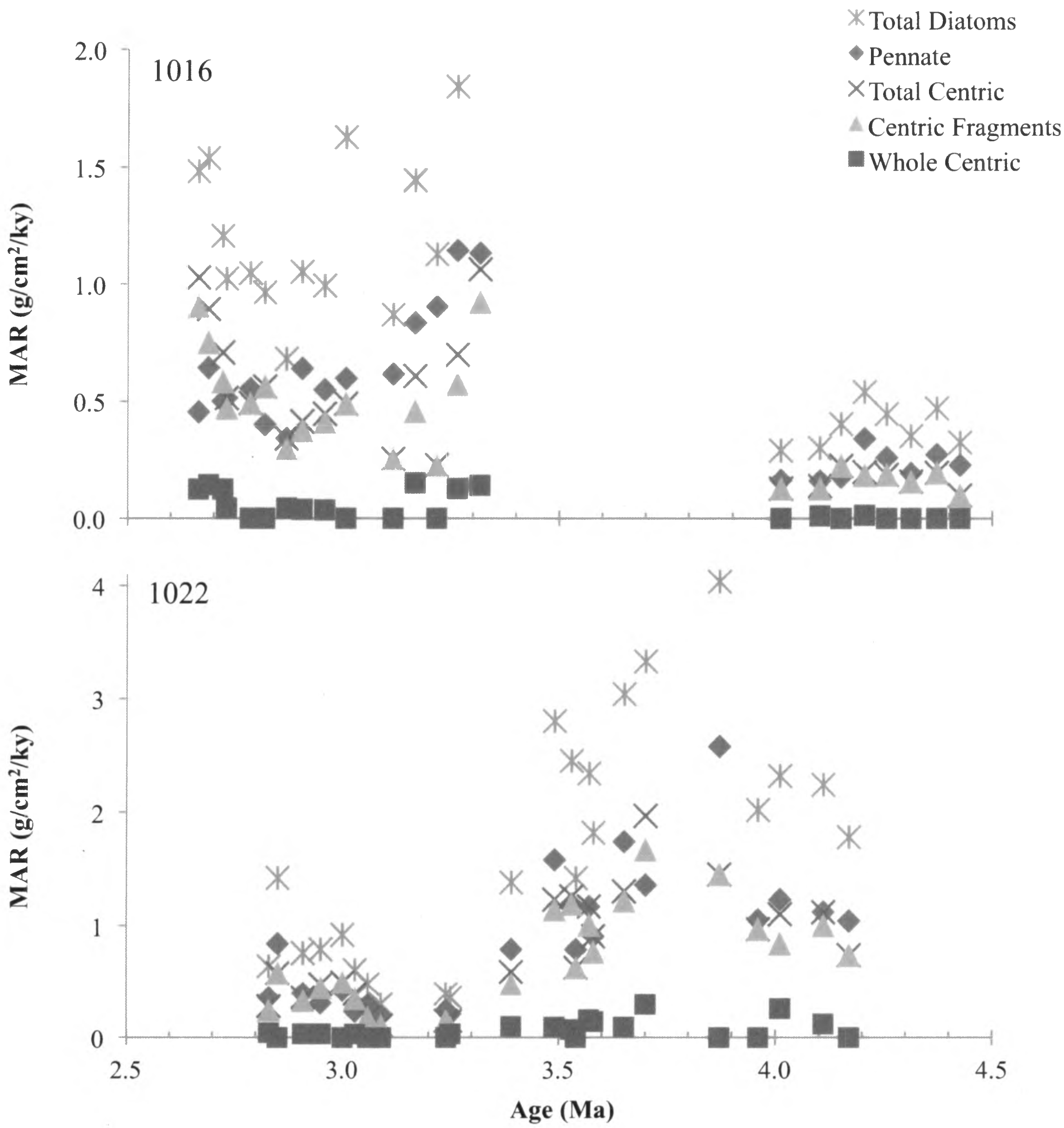

Figure 13: Density specific MAR of the identified diatom groups for ODP Sites 1016 (top) and 1022 (bottom), data listed in Tables 7 and 8. Whole centric diatoms contribute very little at both ODP Sites 1016 and 1022. As in the normalized percent averages, pennate diatoms contribute to roughly more than half of the total diatoms, and centric fragments comprise of the majority of total centric diatoms. At ODP Site 1016 all the diatom groups MAR increase from the early to late Pliocene. At ODP Site 1022 all the diatom groups MAR decrease from the early to late Pliocene.

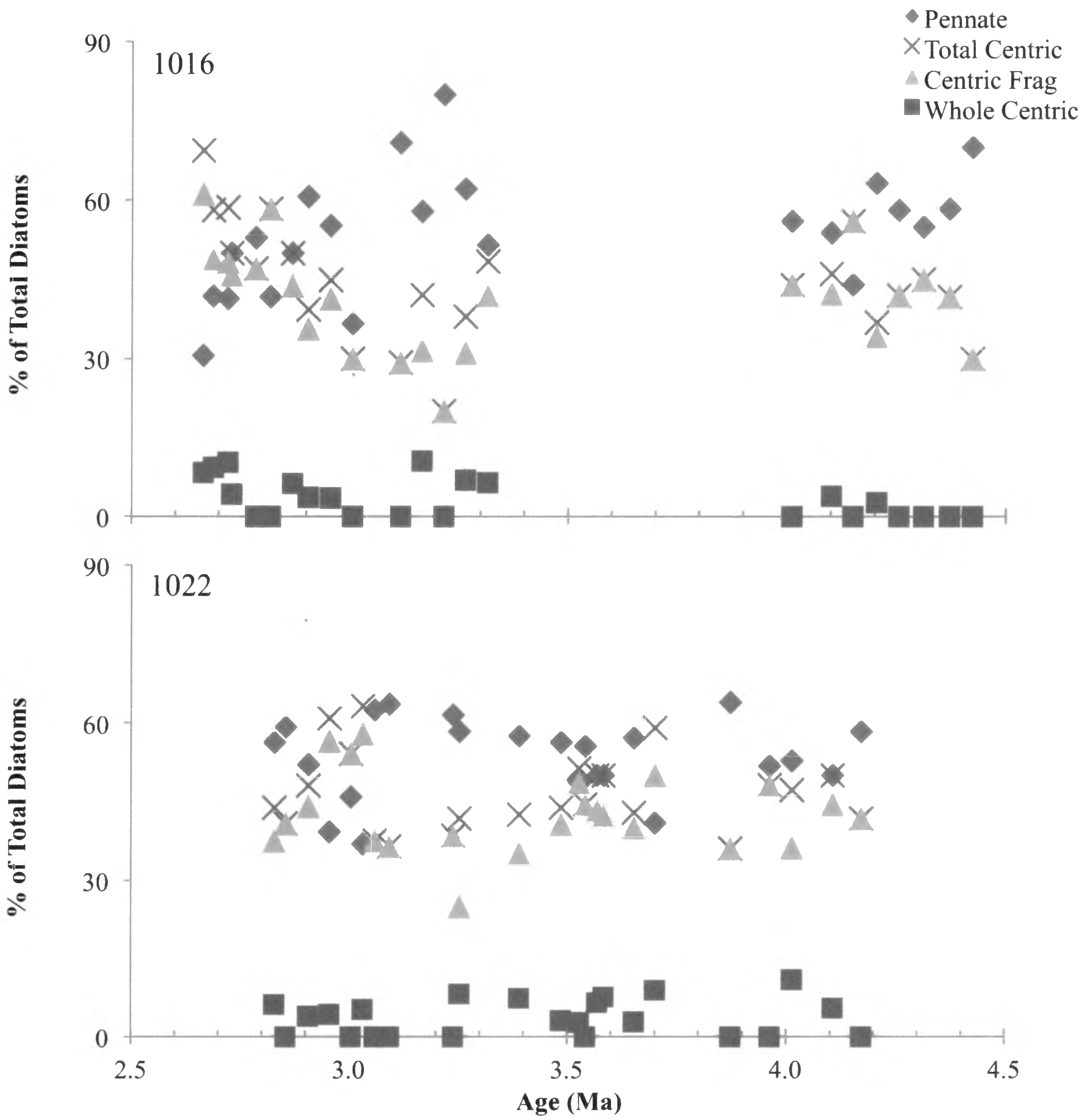

Figure 14: The percent contribution of each diatom group MAR to the total diatom MAR for ODP Sites 1016 (top) and 1022 (bottom). At both Sites 1016 and 1022 pennate diatoms constitute over half of the total diatoms, and total centric diatoms are primarily composed of fragmented pieces.

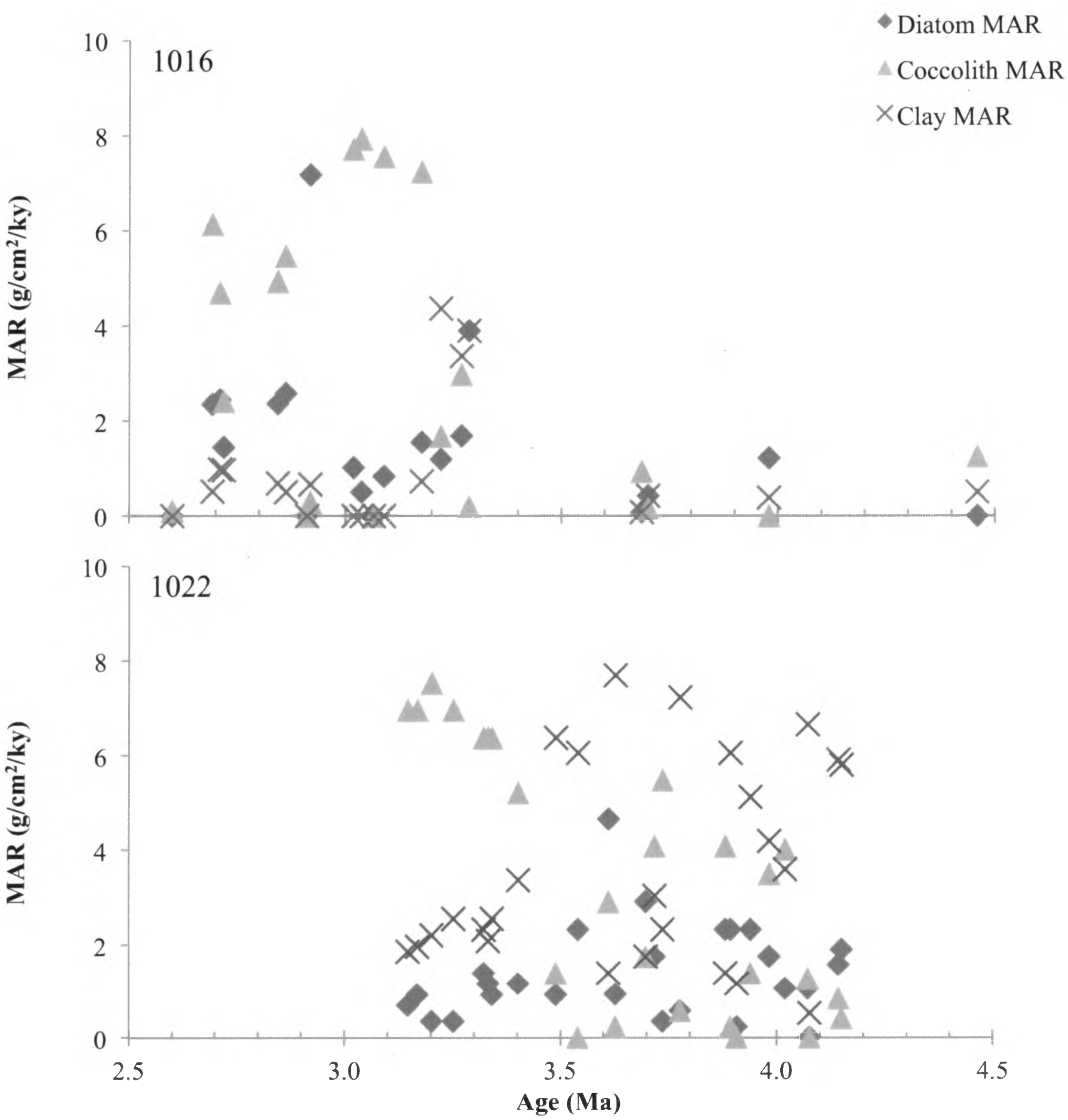

Figure 15: Density specific component MAR calculated for the dominant lithological components from the ODP IR generated smear slide data (coccoliths, diaotms, and clay) for the same core and depth (age) range as this study for ODP Sites 1016 (top) and 1022 (bottom). The ODP IR components MAR are more variable then for this study. At ODP Site 1016 MAR of all the components variability increase in the late Pliocene from the early Pliocene. At ODP Site 1022 coccolith MAR increases in the late Pliocene, diatom MAR fluctuates between ~0.5-4 g/cm^2/kyr, and clay MAR is abundant and fluctuates with slightly lower and constant values in the late Pliocene.

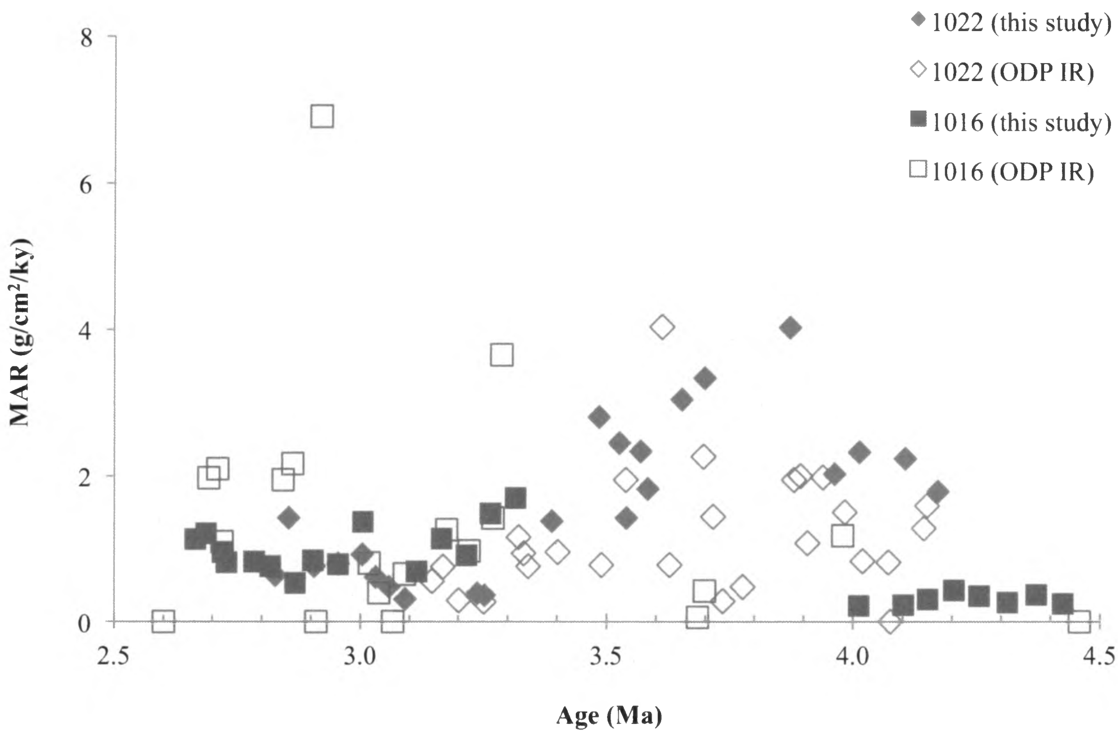

Figure 16: Combined diatom MAR from this study and the ODP IR generated smear slides at both ODP Sites 1016 and 1022. Site 1016 diatom MAR show similar average values for this study and the ODP IR volume, with slightly increased diatom MAR in the late Pliocene then the early Pliocene. ODP Site 1022 diatom MAR in the early Pliocene are slightly larger for this study than for the IR volume, but both this study and the IR volumes have lower diatom MAR in the late Pliocene compared to the early Pliocene. Unlike this study, the ODP IR diatom MAR is more variable at ODP Site 1016 in the late Pliocene and at ODP Site 1022 for the early Pliocene.

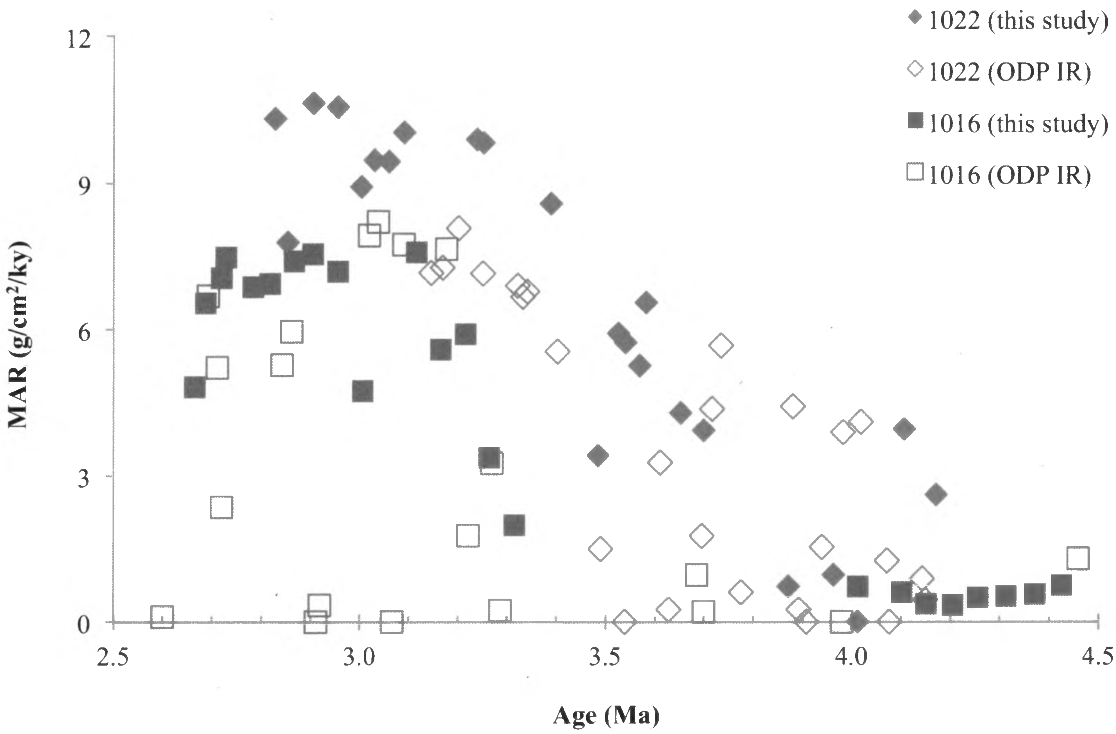

Figure 17: Combined coccolith MAR from this study and the ODP IR generated smear slides at both ODP Sites 1016 and 1022. Site 1016 coccolith MAR show similar values for this study and the IR volume, with increasing MAR from the early Pliocene to the late Pliocene. The site 1016 IR volume coccolith MAR show more variability than for this study. Site 1022 coccolith MAR increase from the early Pliocene toward the late Pliocene in both this study and the IR volume, the MAR values are slightly higher for this study than for the IR volume.

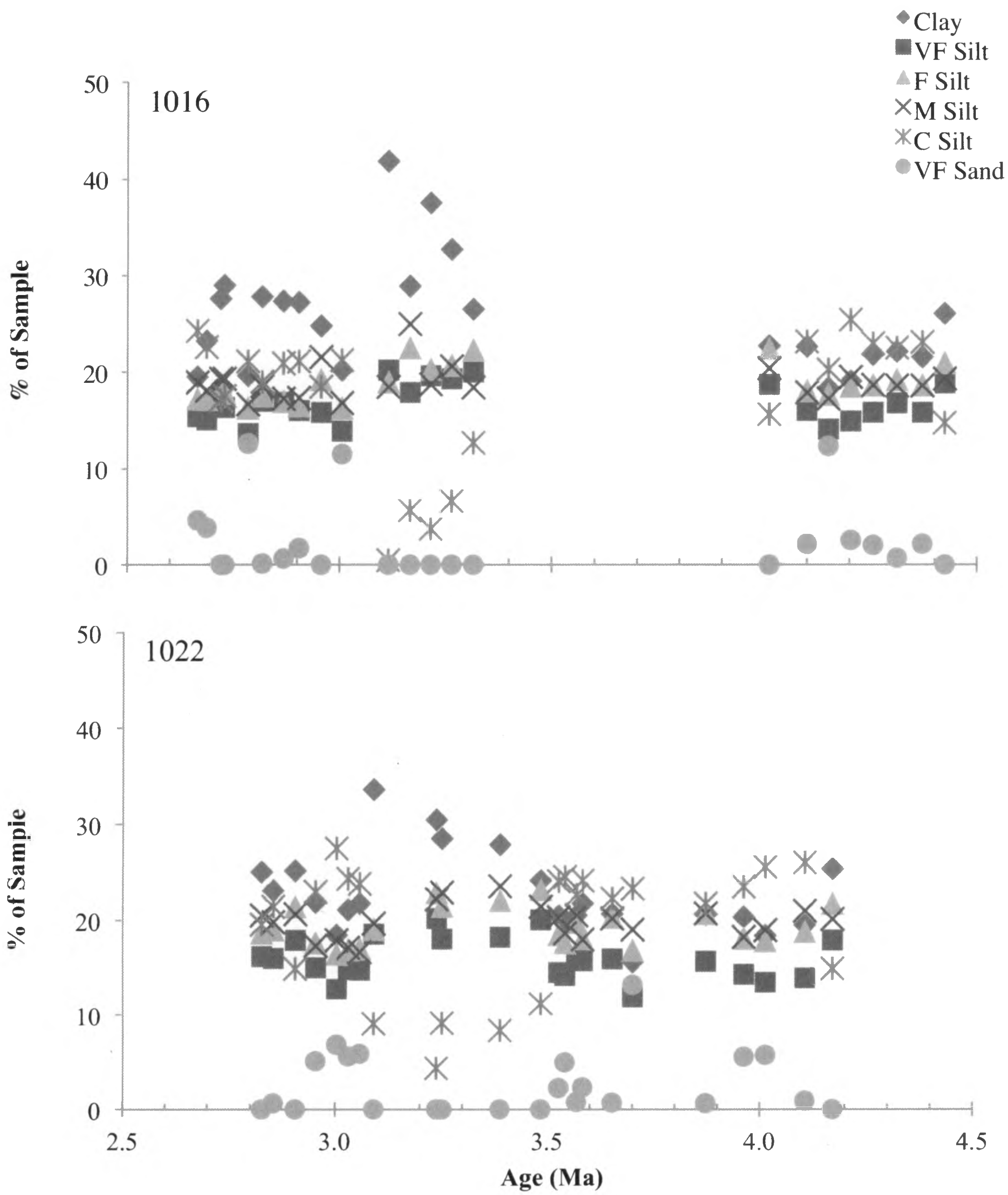

Figure 18: PSA generated standard grain size categories for each sample from ODP Sites 1016 (top) and 1022 (bottom). Categories are defined as clay (<4 μm), very fine silt (4-8 μm), fine silt (8-16 μm), medium silt (16-31 μm), course silt (31-62 μm), and very fine sand (62-125 μm). There are no good trends between age and any of the size categories for both ODP sites 1016 and 1022 (all R^2 values are below 0.10 and 0.13, respectively).

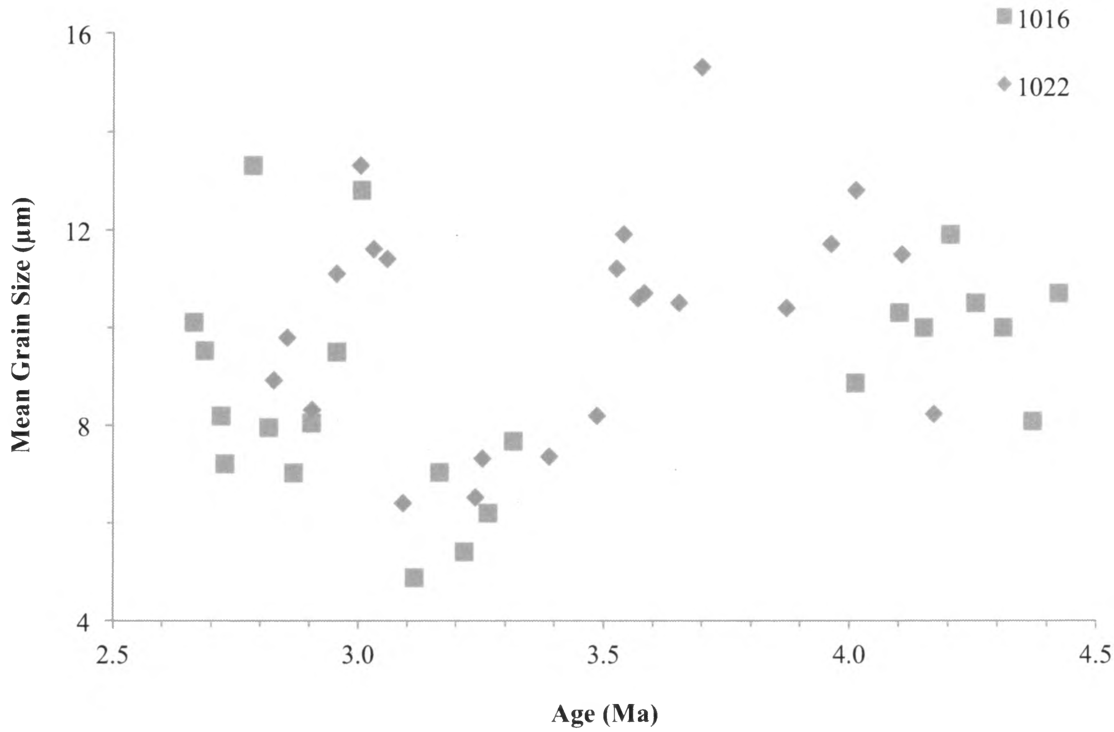

Figure 19: Mean grain size plotted against sample age for both ODP Sites 1016 and 1022. There is no significant trend using linear regression or ANOVA.

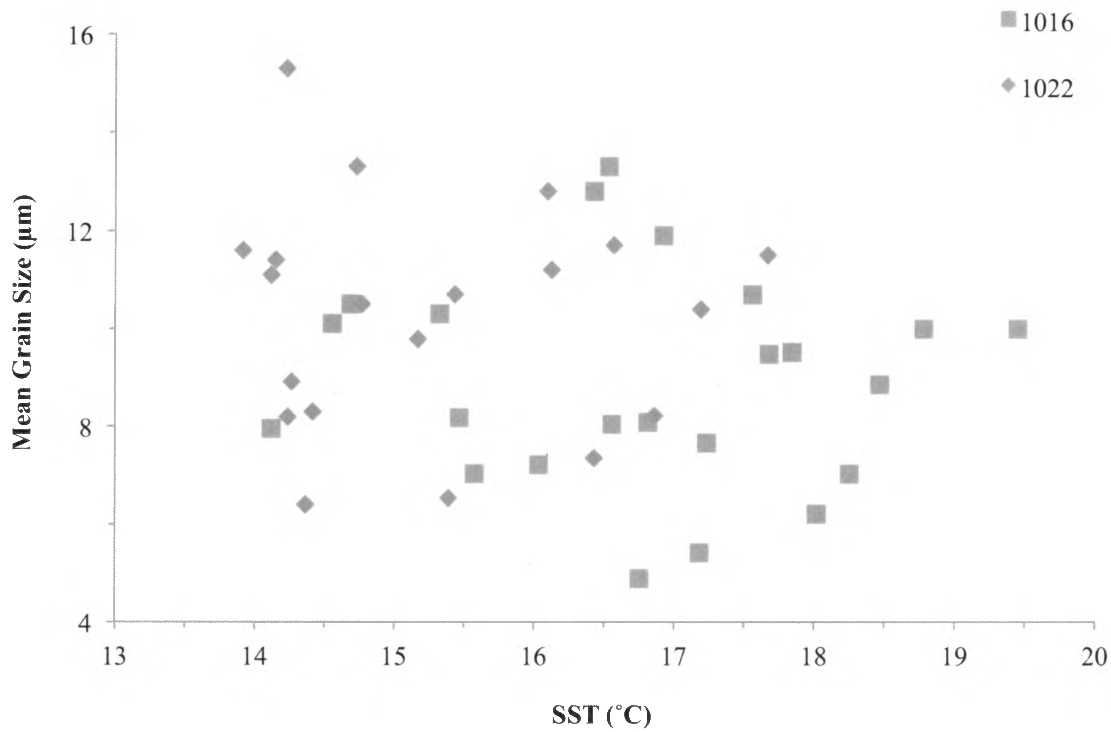

Figure 20: Mean grain size plotted against SST for ODP Sites 1016 and 1022. There is no significant trend using linear regression or ANOVA.

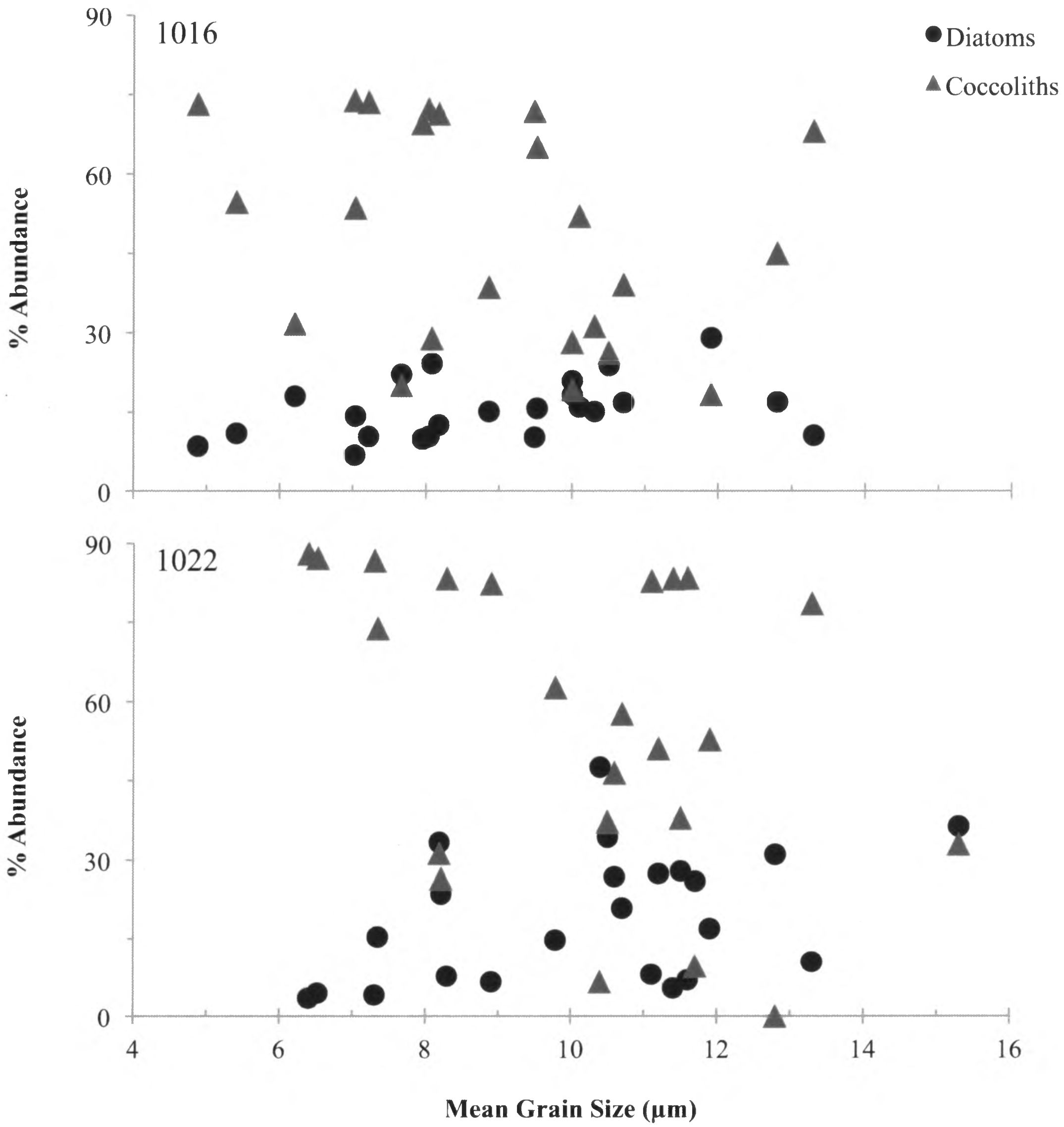

Figure 21: Coccolith and diatom percent abundance smear slide data verses mean grain size at ODP Sites 1016 (top) and 1022 (bottom). There are no significant trends between mean grain size and coccolith and diatom abundance at ODP site 1016. At ODP Site 1022 there is a slight linear trend between mean grain size and coccolith and diatom abundance ($R^2 = 0.16$ and 0.17 respectively), however these trends are outside of the 95% confidence level.

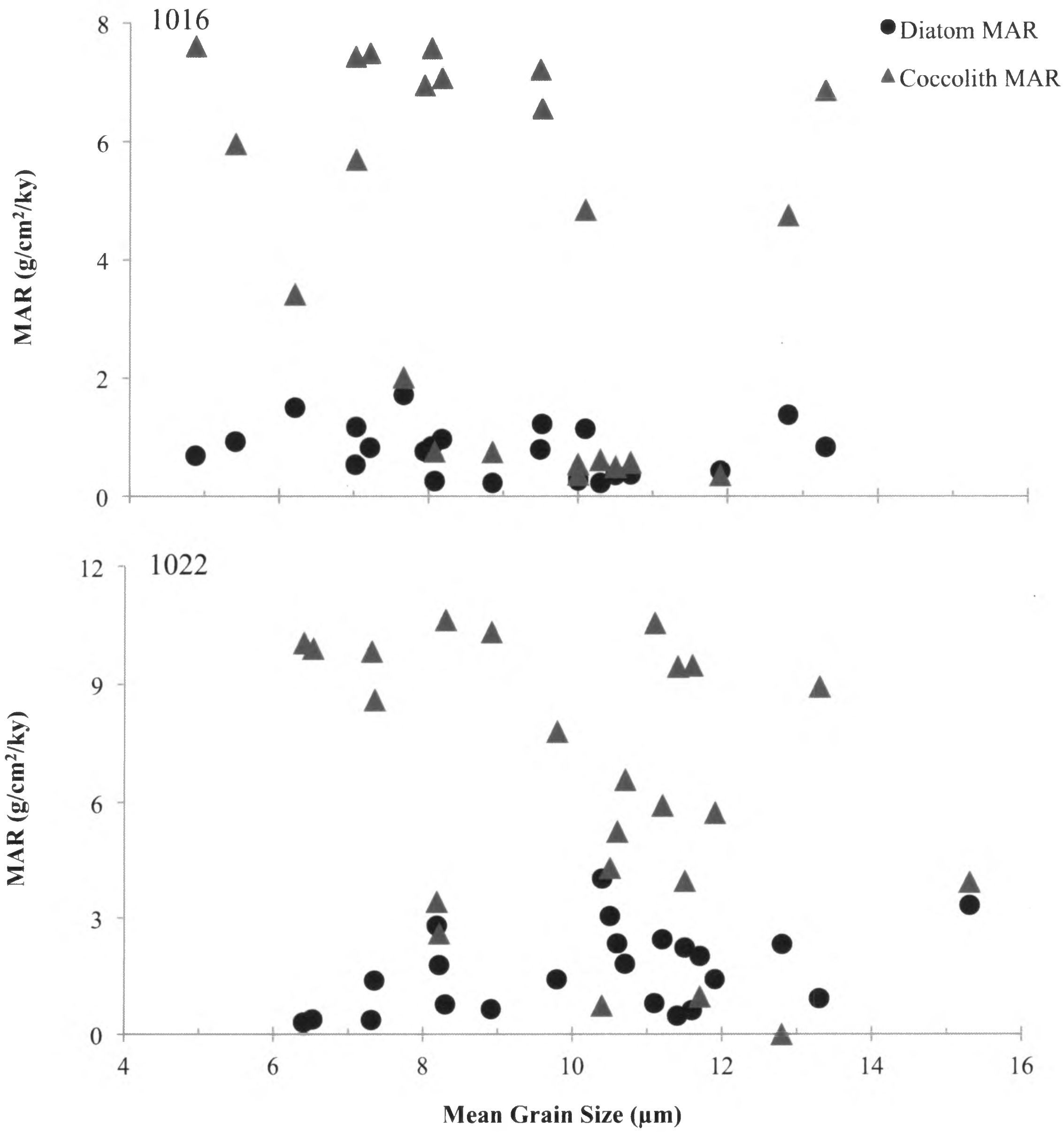

Figure 22: Coccolith and diatom MAR plotted against mean grain size at ODP Sites 1016 (top) and 1022 (bottom). There are no significant trends between mean grain size and coccolith and diatom abundance at ODP Site 1016 or 1022.

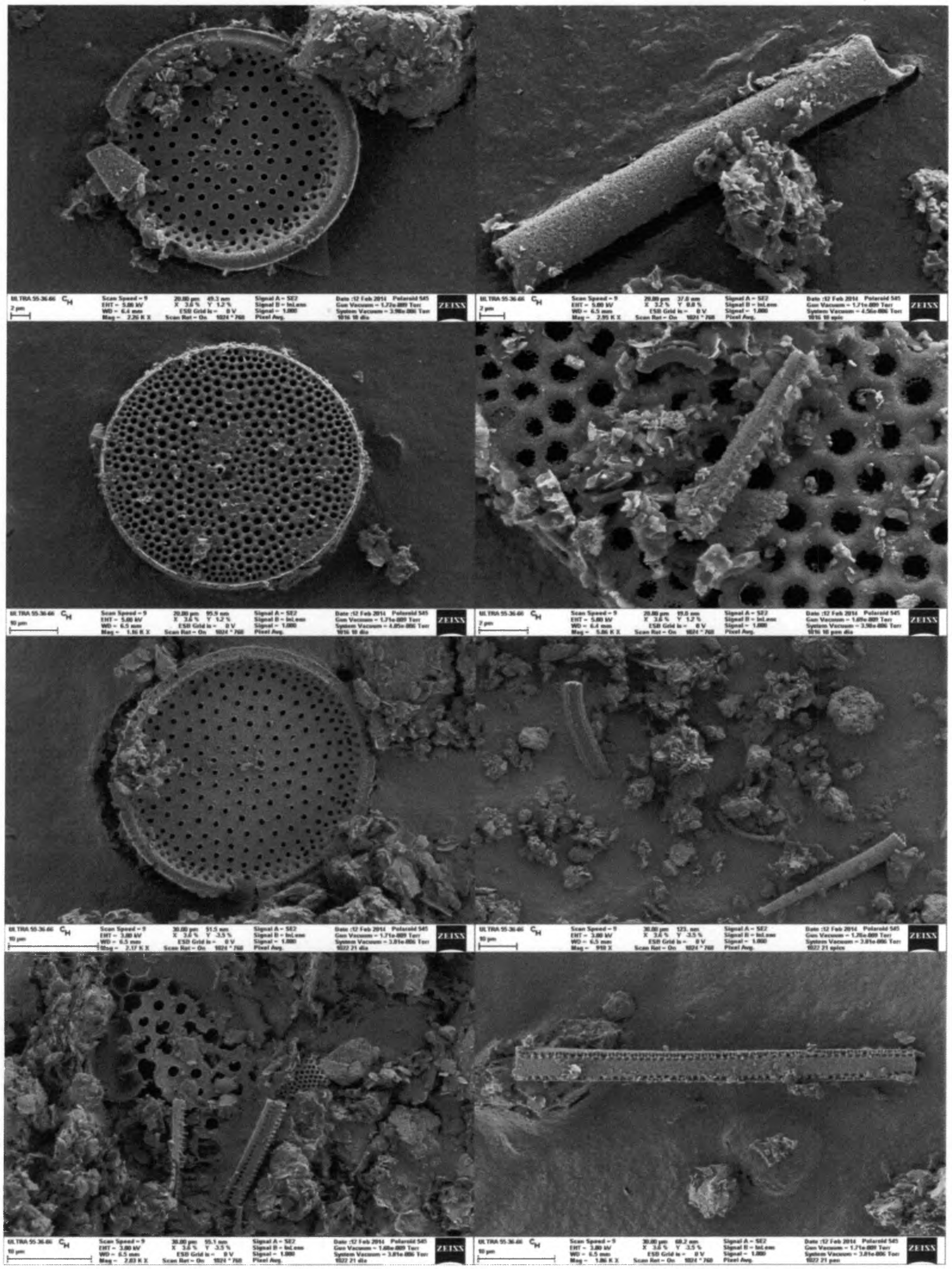

Figure 23: SEM images of samples older then 3.3 Ma for ODP Sites 1016 (top four) and 1022 (bottom four). Images contain centric and pennate diatoms, as well as sponge spicule fragments. These comprise of the main biogenic components in the sediments at both sites before 3.3 Ma.

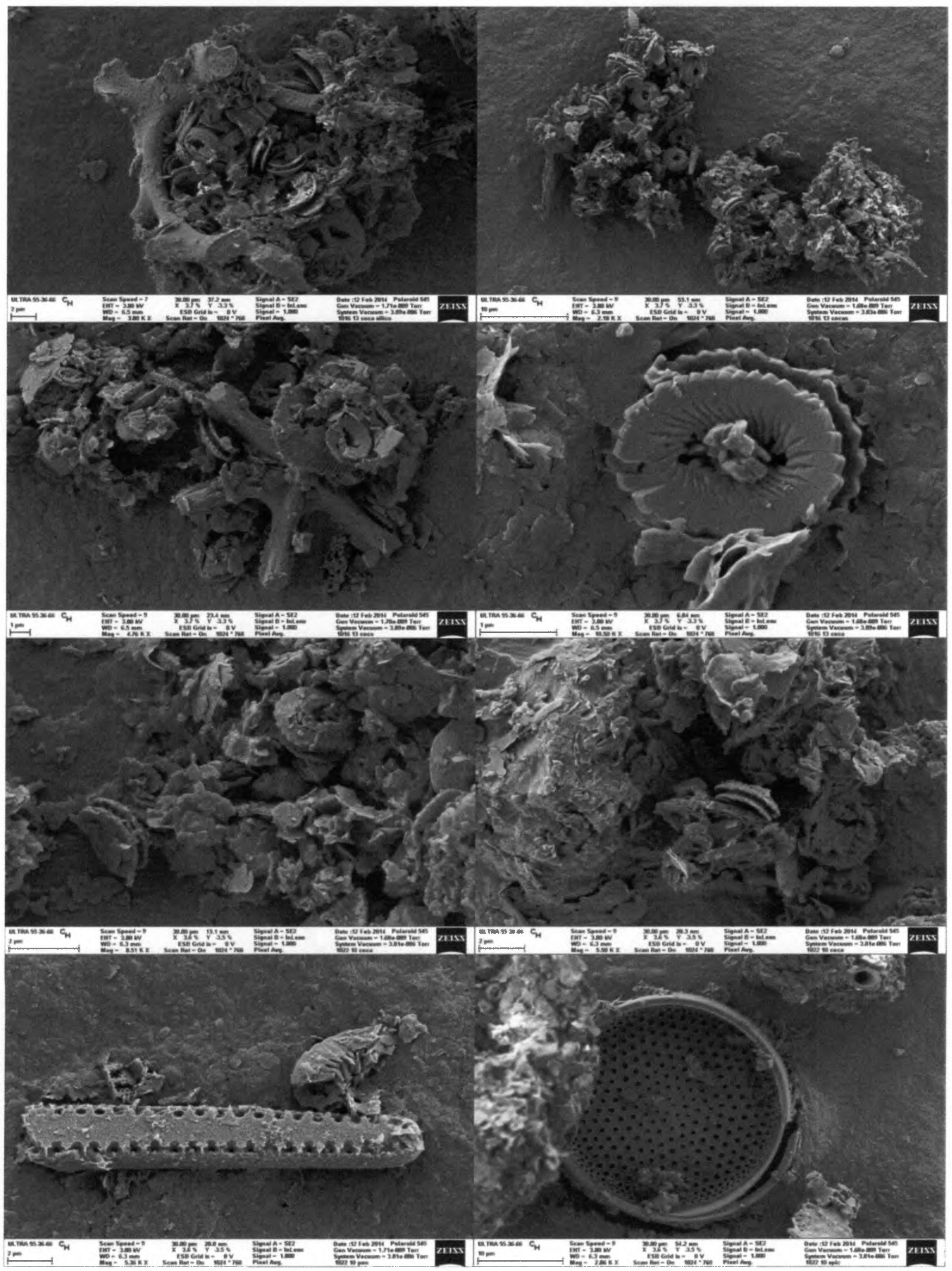

Figure 24: SEM images of samples younger then 3.3 Ma for ODP Sites 1016 (top four) and 1022 (bottom four). Images for ODP site 1016 are all coccolith fragments, and images for ODP site 1022 contain coccolith fragments (top two images) in addition to pennate and centric diatoms (lower two).

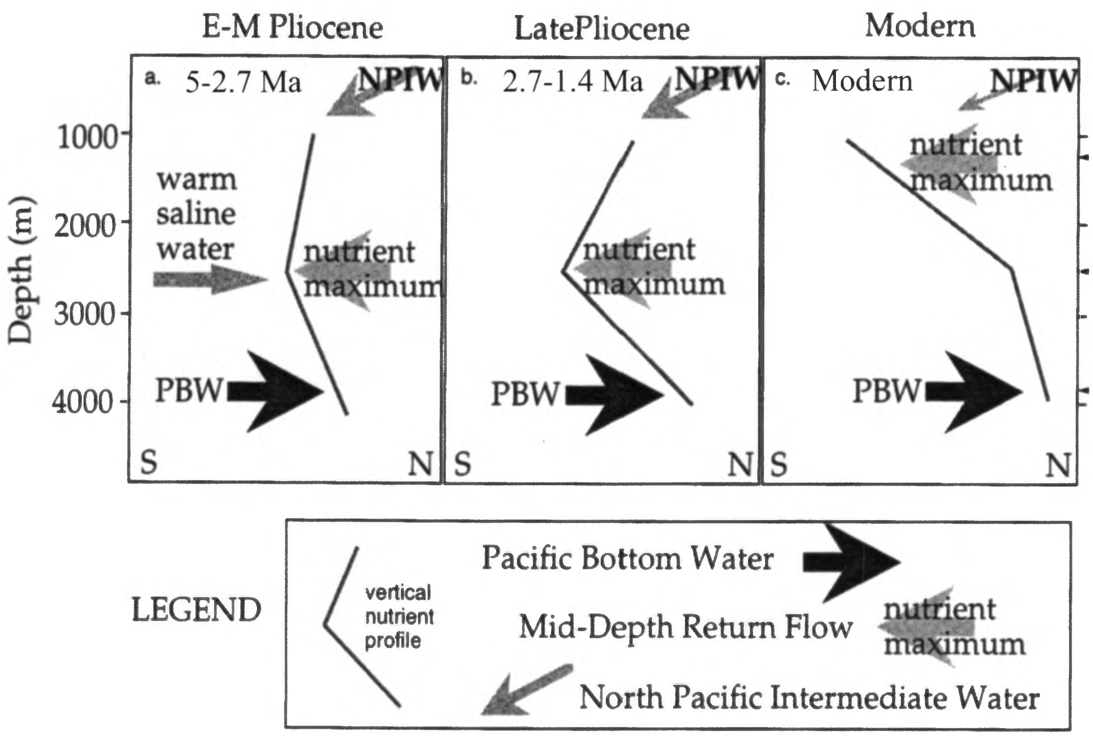

Figure 25: Schematic summary of general water mass circulation changes in the Northeast Pacific at intermediate and mid-depths of the early Pliocene, Late Pliocene, and today (Kwiek & Ravelo, 1999). In both (a) 5-2.7 Ma and (b) 2.7-1.4 Ma North Pacific Intermediate Water (NPIW) is strong and the return flow confined to mid depths. In the modern north Pacific (c) intermediate water ventilation is shallower and weaker and return flow affects intermediate waters.

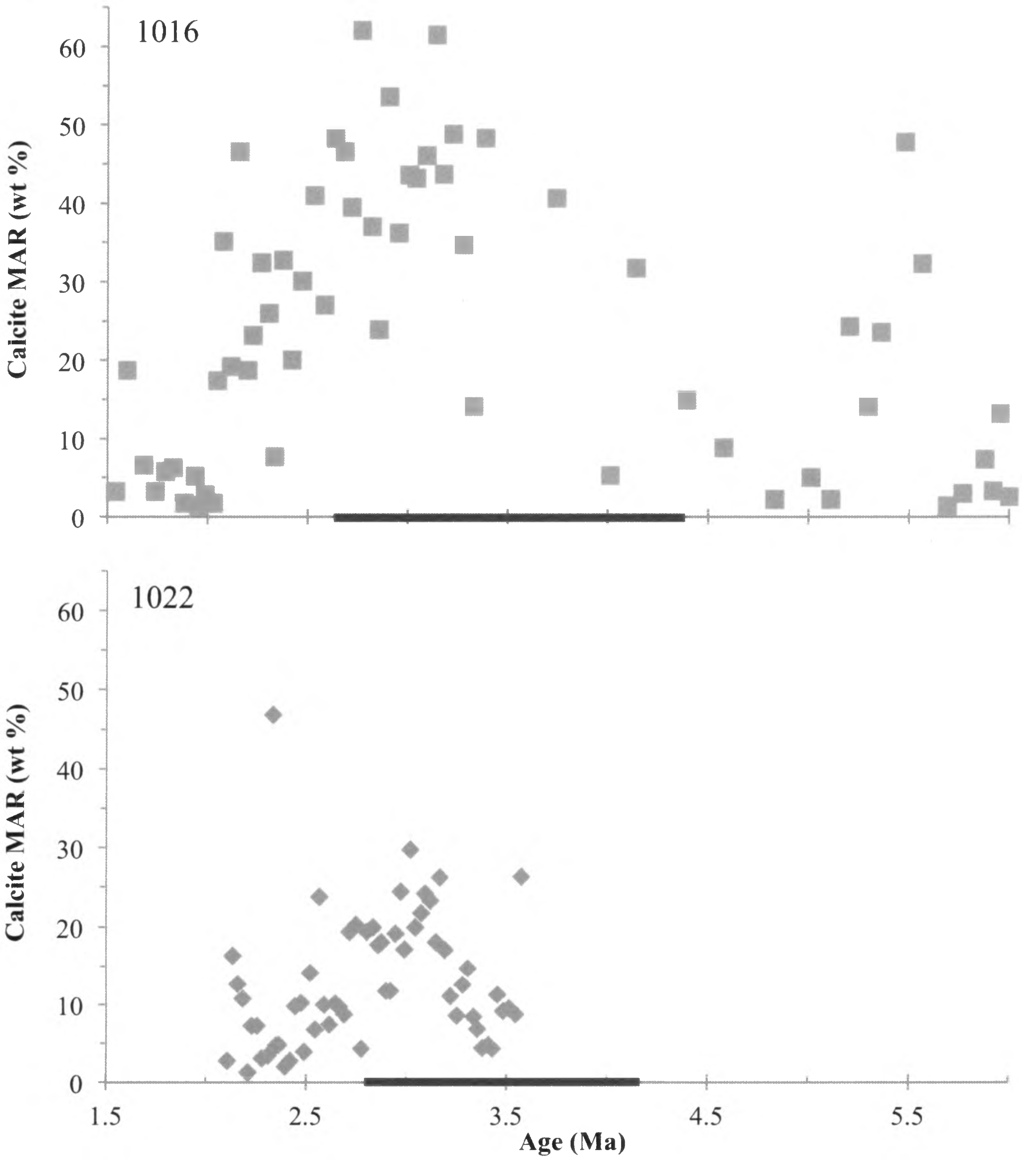

Figure 26: Calcite MAR records available for ODP Sites 1016 (top) and 1022 (bottom) (Lyle, et al., 1997), the red bar indicated the timespan of this study. The middle Pliocene is characterized by a high calcite event along the entire California margin. The onset of increased coccolithophorid abundances in the smear slide data at ~3.5 Ma takes place within the peak of increased calcite values.

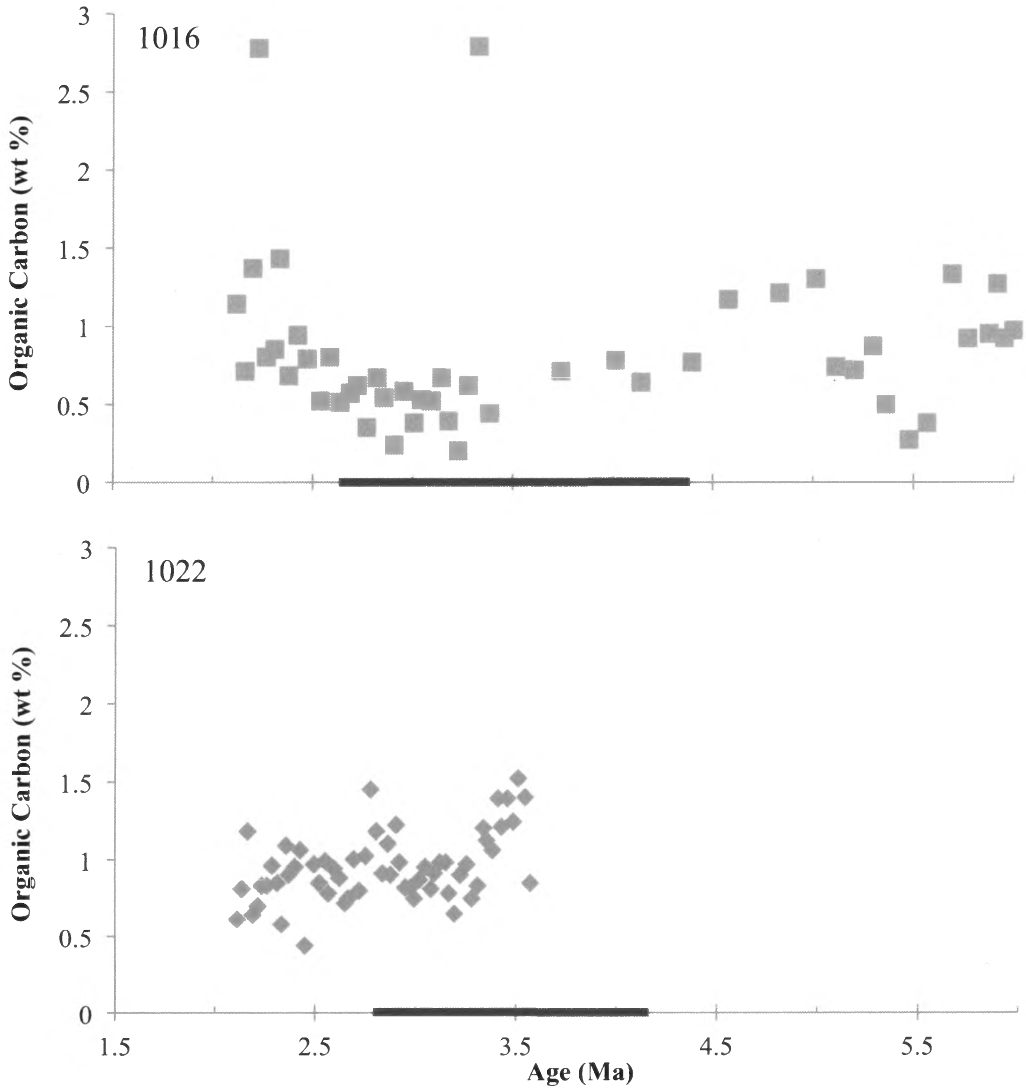

Figure 27: Organic Carbon MAR records available for ODP Sites 1016 (top) and 1022 (bottom) (Lyle, et al., 1997), the red bar indicated the timespan of this study. Organic carbon serves as a rough proxy for overall primary productivity recorded in the sediment. Organic carbon values dip slightly from ~2.5-4.5 Ma at ODP Site 1016 and from ~3.5-2.5 Ma at ODP Site 1022. The timing of decreased organic carbon is similar to the timing of the calcite events (Figure 26).

Table 1: Percent abundance smear slide data, sample age, and SST for ODP site 1016. Values for each category represents the percent contribution of that category relative to all the categories present in the sample, thus the sum of each row totals to 100 percent.

Sample ID	Age	SST	Diatom	Sponge Spicule	Radiolarian	Silicoflagellate	Foraminifera	Coccolith	Volcanic Glass	Clay Mineral	Opaque	Siliciclastic
B 13H3w (125-127)	2.66	14.6	15.9	5.7	0.4	0.4	0.4	52.0	4.0	5.7	6.2	8.8
B 13H4w (70-72)	2.69	17.8	15.6	2.9	1.1	1.1	0.4	65.1	3.3	3.3	2.5	5.5
B 13H5w (120-122)	2.72	15.5	12.6	1.7	1.3	1.3	0.4	71.4	2.2	3.5	0.9	5.6
B 13H6w (20-22)	2.73	16.0	10.4	2.2	1.7	1.7	0.0	73.6	1.3	3.0	0.0	7.4
B 14H2w (2-4)	2.78	16.5	10.6	2.5	0.6	0.6	0.0	68.1	0.0	6.9	0.0	11.3
B 14H3w (51-53)	2.82	14.1	9.9	4.1	0.0	0.0	0.0	69.5	1.6	6.2	0.4	8.2
B 14H5w (50-52)	2.87	15.6	6.8	1.7	0.0	0.0	0.9	73.9	3.0	7.3	0.9	5.6
B 14H6w (120-122)	2.90	16.6	10.4	3.0	0.0	0.0	0.0	72.2	3.0	5.9	0.0	5.2
B 15H2w (75-77)	2.96	17.7	10.2	2.8	0.0	0.0	0.0	71.9	3.5	6.7	0.0	5.3
B 15H4w (75-77)	3.01	16.4	16.9	5.1	0.0	0.0	0.0	44.9	2.2	11.2	2.2	11.2
B 16H2w (78-80)	3.12	16.8	8.6	2.5	0.0	0.0	0.7	73.2	2.1	7.9	0.0	4.3
B16H4w (78-80)	3.17	18.3	14.2	1.9	0.0	0.0	0.4	53.6	14.6	7.9	2.2	4.5
B 16H6w (80-82)	3.22	17.2	10.9	8.8	0.0	0.0	0.0	54.7	6.6	10.9	0.0	8.0
B 17H2w (20-22)	3.26	18.0	18.0	11.8	0.0	0.0	0.0	31.7	6.8	14.3	2.5	14.9
B 17H4w (24-26)	3.32	17.2	22.1	8.6	0.7	0.7	0.7	20.0	5.7	21.4	7.1	12.1
B 18H3w (110-112)	4.01	18.5	15.1	9.0	0.0	0.0	0.0	38.6	4.8	18.1	6.0	8.4
B 18H4w (65-67)	4.10	15.3	15.0	9.2	0.6	0.6	0.0	31.2	4.6	22.5	6.9	9.8
B 18H4w (123-125)	4.15	18.8	20.8	10.8	0.0	0.0	0.0	19.2	1.7	24.2	6.7	16.7
B 18H5w (35-37)	4.20	16.9	29.0	13.0	0.8	0.8	0.0	18.3	0.0	20.6	5.3	13.0
B 18H5w (95-97)	4.26	14.7	23.8	10.0	0.0	0.0	0.8	26.2	0.8	20.8	3.8	13.8
B 18H6w (11-15)	4.31	19.4	18.2	8.2	0.0	0.0	0.0	28.2	4.5	22.7	7.3	10.9
B 18H6w (80-82)	4.37	16.8	24.2	8.7	0.0	0.0	0.0	28.9	1.3	19.5	5.4	12.1
B 18H6w (142-144)	4.42	17.6	16.8	7.3	0.0	0.0	0.0	39.1	1.1	18.4	5.0	12.3

Table 2: Percent abundance smear slide data, sample age, and SST for ODP site 1022. Values for each category represents the percent contribution of that category relative to all the categories present in the sample, thus the sum of each row totals to 100 percent.

Sample ID	Age	SST	Diatom	Sponge Spicule	Radiolarian	Silicoflagellate	Foraminifera	Coccolith	Volcanic Glass	Clay Mineral	Opaque	Siliciclastic
C 9H1w (50-52)	2.83	14.3	6.6	0.0	0.0	0.0	0.0	82.3	0.0	0.0	4.5	6.6
C 9H3w (50-52)	2.85	15.2	14.8	0.0	0.0	0.0	0.0	62.6	0.0	0.0	7.1	15.4
C 9H7w (26-28)	2.91	14.4	7.7	0.3	0.0	0.6	0.0	83.3	0.0	1.2	3.1	3.7
C 10H4w (50-52)	2.95	14.1	8.1	0.4	0.0	0.0	0.0	82.8	0.0	1.4	3.2	4.2
C 11H1w (50-52)	3.00	14.7	10.5	0.0	0.0	0.0	0.0	78.5	0.0	2.2	4.4	4.4
C 11H3w (50-52)	3.03	13.9	7.0	0.0	0.0	0.0	0.0	83.4	0.0	1.8	3.7	4.1
C 11H5w (50-52)	3.06	14.1	5.5	0.0	0.0	0.0	0.0	83.3	0.0	0.3	3.4	7.5
C 12H1w (50-52)	3.09	14.4	3.5	0.0	0.0	0.0	0.0	88.0	0.0	0.0	2.2	6.3
C 13H5w (50-52)	3.24	15.4	4.4	0.3	0.0	0.0	0.0	87.1	0.0	1.7	3.1	3.4
C 13H6w (50-52)	3.25		4.1	0.0	0.0	0.0	0.0	86.6	0.0	2.7	3.1	3.4
C 15H2w (50-52)	3.39	16.4	15.4	0.8	0.0	0.4	0.0	73.8	0.0	3.5	3.5	2.7
C 16H1w (40-42)	3.49	14.2	33.3	0.0	0.0	2.1	0.0	31.3	0.0	10.4	14.6	8.3
C 16H3w (50-52)	3.53	16.1	27.4	0.0	0.0	0.0	0.0	51.1	0.0	7.4	6.7	7.4
C 16H4w (50-52)	3.54		17.0	0.0	0.0	0.0	0.0	52.8	0.0	0.0	11.3	18.9
C 16H6w (50-52)	3.57		26.8	0.0	0.0	0.0	0.0	46.4	0.0	8.9	8.9	8.9
C 16H7w (50-52)	3.58	15.4	20.8	0.0	0.0	0.8	0.0	57.6	0.0	8.0	7.2	5.6
C 17H5w (50-52)	3.65	14.8	34.3	0.0	0.0	0.0	0.0	37.3	0.0	10.8	8.8	8.8
C 18X2w (50-52)	3.70	14.2	36.4	0.8	0.0	5.0	0.8	33.1	0.0	8.3	7.4	8.3
C 20X4w (50-52)	3.87	17.2	47.6	0.0	0.0	0.0	0.0	6.7	0.0	20.0	17.1	8.6
C 21X4w (50-52)	3.96	16.6	26.0	2.9	1.0	0.0	1.0	9.6	0.0	22.1	22.1	15.4
C 22X2w (50-52)	4.01	16.1	31.0	7.8	0.0	0.9	0.0	0.0	0.0	22.4	17.2	20.7
C 23X2w (50-52)	4.11	17.7	27.9	2.3	0.0	2.3	0.8	38.0	0.0	10.1	8.5	10.1
C 23X7w (50-52)	4.17	16.9	23.5	5.9	0.0	2.9	0.0	26.5	0.0	13.7	14.7	12.7

Table 3: Percent abundance of smear slide diatom groups for ODP Site 1016.

Age (Ma)	Pennate Diatoms	Whole Centric Diatoms	Centric Diatom Fragments	Total Centric Diatoms	Total Diatoms
2.66	4.85	1.32	9.69	11.01	15.86
2.69	6.55	1.45	7.64	9.09	15.64
2.72	5.19	1.30	6.06	7.36	12.55
2.73	5.19	0.43	4.76	5.19	10.39
2.78	5.63	0.00	5.00	5.00	10.63
2.82	4.12	0.00	5.76	5.76	9.88
2.87	3.42	0.43	2.99	3.42	6.84
2.90	6.30	0.37	3.70	4.07	10.37
2.96	5.61	0.35	4.21	4.56	10.18
3.01	6.18	0.00	5.06	5.06	16.85
3.12	6.07	0.00	2.50	2.50	8.57
3.17	8.24	1.50	4.49	5.99	14.23
3.22	8.76	0.00	2.19	2.19	10.95
3.26	11.18	1.24	5.59	6.83	18.01
3.32	11.43	1.43	9.29	10.71	22.14
4.01	8.43	0.00	6.63	6.63	15.06
4.10	8.09	0.58	6.36	6.94	15.03
4.15	9.17	0.00	11.67	11.67	20.83
4.20	18.32	0.76	9.92	10.69	29.01
4.26	13.85	0.00	10.00	10.00	23.85
4.31	10.00	0.00	8.18	8.18	18.18
4.37	14.09	0.00	10.07	10.07	24.16
4.42	11.73	0.00	5.03	5.03	16.76

Table 4: Percent abundance of smear slide diatom groups for ODP Site 1022.

Age (Ma)	Pennate Diatoms	Whole Centric Diatoms	Centric Diatom Fragments	Total Centric Diatoms	Total Diatoms
2.83	3.70	0.41	2.47	2.88	6.58
2.85	8.79	0.00	6.04	6.04	14.84
2.91	4.02	0.31	3.41	3.72	7.74
2.95	3.16	0.35	4.56	4.91	8.07
3.00	4.82	0.00	5.70	5.70	10.53
3.03	2.58	0.37	4.06	4.43	7.01
3.06	3.41	0.00	2.05	2.05	5.46
3.09	2.21	0.00	1.26	1.26	3.47
3.24	2.71	0.00	1.69	1.69	4.41
3.25	2.40	0.34	1.03	1.71	4.11
3.39	8.85	1.15	5.38	6.54	15.38
3.49	18.75	1.04	13.54	14.58	33.33
3.53	13.33	0.74	13.33	14.07	27.41
3.54	9.43	0.00	7.55	7.55	16.98
3.57	13.39	1.79	11.61	13.39	26.79
3.58	10.40	1.60	8.80	10.40	20.80
3.65	19.61	0.98	13.73	14.71	34.31
3.70	14.88	3.31	18.18	21.49	36.36
3.87	30.48	0.00	17.14	17.14	47.62
3.96	13.46	0.00	12.50	12.50	25.96
4.01	16.38	3.45	11.21	14.66	31.03
4.11	13.95	1.55	12.40	13.95	27.91
4.17	13.73	0.00	9.80	9.80	23.53

Table 5: Calculated density specific Mass Accumulation Rates (MAR) for ODP Site 1016 of the following smear slide components; total diatoms, sponge spicules, coccoliths, volcanic glass, clay minerals, opaques, and siliciclastics. Each sample is identified by its age. The sedimentation rate is calculated using the biostratigraphic age-depth model from Lyle et al., 1997, and the dry bulk density is from the ODP database.

Age (Ma)	Sed Rate (m/Ma)	GRA Bulk Den (g/cc)	Bulk MAR ($g/cm^2/ky$)	Total Diatom MAR ($g/cm^2/ky$)	Sponge Spicule MAR ($g/cm^2/ky$)	Coccolith MAR ($g/cm^2/ky$)	Volcanic Glass MAR ($g/cm^2/ky$)	Clay Mineral MAR ($g/cm^2/ky$)	Opaque MAR ($g/cm^2/ky$)	Siliciclastic MAR ($g/cm^2/ky$)
2.66	59.66	1.56	9.33	1.13	0.41	4.83	0.28	0.55	1.10	0.85
2.69	59.66	1.65	9.83	1.21	0.23	6.55	0.25	0.34	0.49	0.57
2.72	59.66	1.61	9.61	0.95	0.13	7.06	0.17	0.36	0.16	0.58
2.73	59.66	1.65	9.85	0.81	0.17	7.48	0.10	0.32	0.00	0.78
2.78	59.66	1.65	9.84	0.82	0.19	6.88	0.00	0.72	0.00	1.18
2.82	59.66	1.63	9.74	0.76	0.32	6.94	0.13	0.64	0.08	0.85
2.87	59.66	1.66	9.92	0.53	0.13	7.41	0.23	0.76	0.16	0.58
2.90	59.66	1.70	10.14	0.83	0.24	7.56	0.24	0.64	0.00	0.56
2.96	59.66	1.63	9.74	0.78	0.22	7.19	0.27	0.69	0.00	0.55
3.01	59.66	1.62	9.65	1.37	0.41	4.74	0.18	1.23	0.46	1.23
3.12	59.66	1.70	10.12	0.68	0.20	7.60	0.17	0.85	0.00	0.46
3.17	59.66	1.70	10.13	1.14	0.15	5.59	1.19	0.85	0.45	0.49
3.22	59.66	1.73	10.30	0.91	0.73	5.91	0.55	1.23	0.00	0.90
3.26	59.66	1.72	10.23	1.48	0.97	3.38	0.57	1.59	0.51	1.65
3.32	59.66	1.66	9.92	1.70	0.66	1.99	0.44	2.22	1.37	1.26
4.01	11.68	1.65	1.92	0.22	0.13	0.74	0.07	0.36	0.22	0.17
4.10	11.68	1.70	1.99	0.23	0.14	0.61	0.07	0.46	0.26	0.20
4.15	11.68	1.65	1.93	0.31	0.16	0.37	0.02	0.48	0.25	0.33
4.20	11.68	1.59	1.86	0.43	0.19	0.35	0.00	0.41	0.20	0.26
4.26	11.68	1.60	1.87	0.35	0.15	0.50	0.01	0.42	0.14	0.28
4.31	11.68	1.65	1.93	0.27	0.12	0.54	0.07	0.45	0.27	0.22
4.37	11.68	1.66	1.94	0.37	0.13	0.57	0.02	0.40	0.20	0.25
4.42	11.68	1.66	1.94	0.25	0.11	0.76	0.02	0.37	0.19	0.25

Table 6: Calculated density specific Mass Accumulation Rates (MAR) for ODP Site 1022 of the following smear slide components; total diatoms, sponge spicules, coccoliths, volcanic glass, clay minerals, opaques, and siliciclastics. Each sample is identified by its age. The sedimentation rate is calculated using the biostratigraphic age-depth model from Lyle et al., 1997, and the dry bulk density is from the ODP database.

Age (Ma)	Sed Rate (m/Ma)	GRA Bulk Den (g/cc)	Bulk MAR ($g/cm^2/ky$)	Total Diatom MAR ($g/cm^2/ky$)	Sponge Spicule MAR ($g/cm^2/ky$)	Coccolith MAR ($g/cm^2/ky$)	Volcanic Glass MAR ($g/cm^2/ky$)	Clay Mineral MAR ($g/cm^2/ky$)	Opaque MAR ($g/cm^2/ky$)	Siliciclastic MAR ($g/cm^2/ky$)
2.83	111.29	1.16	12.91	0.64	0.00	10.32	0.00	0.00	1.09	0.86
2.85	111.29	1.16	12.91	1.42	0.00	7.79	0.00	0.00	1.71	1.99
2.91	111.29	1.16	12.91	0.76	0.03	10.64	0.00	0.16	0.76	0.49
2.95	111.29	1.16	12.91	0.79	0.03	10.56	0.00	0.19	0.77	0.56
3.00	108.72	1.07	11.59	0.92	0.00	8.93	0.00	0.26	0.96	0.52
3.03	108.72	1.07	11.59	0.61	0.00	9.47	0.00	0.22	0.81	0.48
3.06	108.72	1.07	11.59	0.48	0.00	9.44	0.00	0.04	0.74	0.88
3.09	108.72	1.07	11.59	0.30	0.00	10.05	0.00	0.00	0.48	0.75
3.24	108.72	1.07	11.59	0.39	0.03	9.91	0.00	0.20	0.67	0.40
3.25	108.72	1.07	11.59	0.36	0.00	9.83	0.00	0.32	0.67	0.40
3.39	108.72	1.07	11.59	1.38	0.07	8.59	0.00	0.42	0.77	0.33
3.49	108.72	1.07	11.59	2.80	0.00	3.42	0.00	1.18	3.07	0.95
3.53	106.15	1.10	11.65	2.45	0.00	5.93	0.00	0.89	1.49	0.89
3.54	106.15	1.10	11.65	1.42	0.00	5.74	0.00	0.00	2.36	2.13
3.57	106.15	1.10	11.65	2.34	0.00	5.26	0.00	1.05	1.95	1.05
3.58	106.15	1.10	11.65	1.82	0.00	6.56	0.00	0.95	1.58	0.66
3.65	106.15	1.10	11.65	3.04	0.00	4.30	0.00	1.29	1.96	1.06
3.70	106.15	1.10	11.65	3.33	0.08	3.94	0.00	1.02	1.70	1.02
3.87	106.15	1.10	11.65	4.03	0.00	0.73	0.00	2.28	3.62	0.98
3.96	106.15	1.10	11.65	2.02	0.22	0.97	0.00	2.33	4.31	1.62
4.01	103.58	1.02	10.55	2.32	0.58	0.00	0.00	2.27	3.23	2.09
4.11	103.58	1.02	10.55	2.24	0.19	3.96	0.00	1.09	1.71	1.09
4.17	103.58	1.02	10.55	1.78	0.45	2.61	0.00	1.40	2.79	1.30

Table 7: Density specific MAR of the various diatom groups for ODP Site 1016.

Age (Ma)	Pennate Diatom MAR ($g/cm^2/ky$)	Whole Centric Diatom MAR ($g/cm^2/ky$)	Centric Diatom Fragment MAR ($g/cm^2/ky$)	Total Centric Diatom MAR ($g/cm^2/ky$)	Total Diatom MAR ($g/cm^2/ky$)
2.66	0.35	0.09	0.69	0.79	1.13
2.69	0.51	0.11	0.59	0.70	1.21
2.72	0.40	0.10	0.46	0.56	0.95
2.73	0.41	0.03	0.37	0.41	0.81
2.78	0.44	0.00	0.39	0.39	0.82
2.82	0.32	0.00	0.44	0.44	0.76
2.87	0.26	0.03	0.23	0.26	0.53
2.90	0.51	0.03	0.30	0.33	0.83
2.96	0.43	0.03	0.32	0.35	0.78
3.01	0.50	0.00	0.41	0.41	1.37
3.12	0.48	0.00	0.20	0.20	0.68
3.17	0.66	0.12	0.36	0.48	1.14
3.22	0.73	0.00	0.18	0.18	0.91
3.26	0.92	0.10	0.46	0.56	1.48
3.32	0.88	0.11	0.71	0.82	1.70
4.01	0.12	0.00	0.10	0.10	0.22
4.10	0.12	0.01	0.10	0.10	0.23
4.15	0.14	0.00	0.17	0.17	0.31
4.20	0.27	0.01	0.15	0.16	0.43
4.26	0.21	0.00	0.15	0.15	0.35
4.31	0.15	0.00	0.12	0.12	0.27
4.37	0.21	0.00	0.15	0.15	0.37
4.42	0.17	0.00	0.07	0.07	0.25

Table 8: Density specific MAR of the various diatom groups for ODP Site 1022.

Age (Ma)	Pennate Diatom MAR ($g/cm^2/ky$)	Whole Centric Diatom MAR ($g/cm^2/ky$)	Centric Diatom Fragment MAR ($g/cm^2/ky$)	Total Centric Diatom MAR ($g/cm^2/ky$)	Total Diatom MAR ($g/cm^2/ky$)
2.83	0.36	0.04	0.24	0.28	0.64
2.85	0.84	0.00	0.58	0.58	1.42
2.91	0.40	0.03	0.33	0.36	0.76
2.95	0.31	0.03	0.45	0.48	0.79
3.00	0.42	0.00	0.50	0.50	0.92
3.03	0.23	0.03	0.35	0.39	0.61
3.06	0.30	0.00	0.18	0.18	0.48
3.09	0.19	0.00	0.11	0.11	0.30
3.24	0.24	0.00	0.15	0.15	0.39
3.25	0.21	0.03	0.09	0.15	0.36
3.39	0.79	0.10	0.48	0.59	1.38
3.49	1.58	0.09	1.14	1.23	2.80
3.53	1.19	0.07	1.19	1.26	2.45
3.54	0.79	0.00	0.63	0.63	1.42
3.57	1.17	0.16	1.01	1.17	2.34
3.58	0.91	0.14	0.77	0.91	1.82
3.65	1.74	0.09	1.22	1.30	3.04
3.70	1.36	0.30	1.67	1.97	3.33
3.87	2.58	0.00	1.45	1.45	4.03
3.96	1.05	0.00	0.97	0.97	2.02
4.01	1.23	0.26	0.84	1.10	2.32
4.11	1.12	0.12	1.00	1.12	2.24
4.17	1.04	0.00	0.74	0.74	1.78

Table 9: Calculated density specific MAR of ODP IR generated smear slide components present and counted for ODP Site 1016. Highlighted rows indicate the sample represents a minor lithology in the core.

Age (Ma)	Sed Rate (m/Ma)	Bulk Den (g/cc)	Bulk MAR (g/cm^2/ky)	Vol Glass MAR (g/cm^2/ky)	Opaque MAR (g/cm^2/ky)	Clay MAR (g/cm^2/ky)	Foram MAR (g/cm^2/ky)	Diatom MAR (g/cm^2/ky)	Sponge MAR (g/cm^2/ky)	Coccolith MAR (g/cm^2/ky)
2.60	59.66	1.64	9.79	8.54	1.00	0.00	0.00	0.00	0.00	0.10
2.69	59.66	1.71	10.23	0.00	0.00	0.58	0.89	1.97	0.09	6.69
2.71	59.66	1.64	9.78	0.17	0.42	1.13	0.54	2.09	0.17	5.23
2.72	59.66	1.62	9.68	0.22	2.73	0.98	1.89	1.09	0.36	2.37
2.84	59.66	1.66	9.87	0.41	0.20	0.77	1.05	1.95	0.16	5.27
2.86	59.66	1.67	9.94	0.00	0.00	0.56	1.08	2.17	0.17	5.96
2.91	59.66	1.70	10.14	9.41	0.64	0.00	0.00	0.00	0.00	0.00
2.92	59.66	1.58	9.44	0.00	0.23	0.86	0.83	6.90	0.27	0.35
3.02	59.66	1.70	10.15	0.00	0.20	0.00	1.05	0.80	0.16	7.94
3.04	59.66	1.66	9.91	0.00	0.20	0.00	1.03	0.40	0.08	8.22
3.07	59.66	1.69	10.05	7.87	1.96	0.00	0.00	0.00	0.00	0.00
3.09	59.66	1.74	10.36	0.00	0.20	0.00	1.59	0.65	0.16	7.75
3.18	59.66	1.73	10.34	0.00	0.00	0.80	0.55	1.26	0.08	7.66
3.22	59.66	1.66	9.91	0.00	0.20	4.79	2.10	0.97	0.08	1.78
3.27	59.66	1.66	9.90	0.00	0.42	3.84	0.87	1.42	0.08	3.26
3.29	59.66	1.63	9.74	0.00	0.23	4.93	0.59	3.66	0.09	0.24
3.69	8.43	1.68	1.41	0.00	0.00	0.08	0.30	0.06	0.01	0.97
3.70	8.43	1.65	1.39	0.00	0.07	0.57	0.09	0.42	0.03	0.22
3.98	11.68	1.61	1.87	0.00	0.09	0.49	0.05	1.19	0.05	0.00
4.46	11.68	1.72	2.00	0.00	0.04	0.53	0.10	0.00	0.03	1.30

Table 10: Calculated density specific MAR of ODP IR generated smear slide components present and counted for ODP Site 1022. Highlighted rows indicate the sample represents a minor lithology in the core.

Age (Ma)	Sed Rate (m/Ma)	Bulk Den (g/cc)	Bulk MAR ($g/cm^2/ky$)	Quartz MAR ($g/cm^2/ky$)	Pyrite MAR ($g/cm^2/ky$)	Dolomite MAR ($g/cm^2/ky$)	Clay MAR ($g/cm^2/ky$)	Foram MAR ($g/cm^2/ky$)	Diatom MAR ($g/cm^2/ky$)	Coccolith MAR ($g/cm^2/ky$)
3.15	108.72	1.07	11.59	0.49	0.46	0.00	1.97	0.71	0.55	7.13
3.17	108.72	1.07	11.59	0.50	0.23	0.00	2.13	0.48	0.75	7.23
3.20	108.72	1.07	11.59	0.39	0.00	0.00	2.44	0.25	0.29	8.04
3.25	108.72	1.07	11.59	0.37	0.46	0.00	2.71	0.47	0.28	7.12
3.32	108.72	1.07	11.59	0.26	0.00	0.00	2.60	0.50	1.16	6.88
3.33	108.72	1.07	11.59	0.38	0.23	0.00	2.26	0.97	0.93	6.64
3.34	108.72	1.07	11.59	0.51	0.00	0.00	2.80	0.49	0.76	6.75
3.40	108.72	1.07	11.59	0.51	0.24	0.00	3.70	0.49	0.95	5.52
3.49	108.72	1.07	11.59	1.28	0.48	0.00	7.06	0.25	0.77	1.48
3.54	106.14	1.10	11.64	1.29	1.20	0.00	6.73	0.12	1.95	0.00
3.61	106.14	1.10	11.64	0.41	1.00	0.42	1.62	0.52	4.04	3.26
3.63	106.14	1.10	11.64	1.54	0.24	0.00	8.46	0.12	0.77	0.25
3.70	106.14	1.10	11.64	0.48	0.89	4.11	1.80	0.23	2.27	1.73
3.72	106.14	1.10	11.64	0.64	0.72	0.13	3.35	0.74	1.44	4.34
3.74	106.14	1.10	11.64	0.74	0.69	0.39	2.48	1.19	0.28	5.61
3.78	106.14	1.10	11.64	1.87	0.46	0.00	7.73	0.24	0.47	0.60
3.88	106.14	1.10	11.64	0.78	0.96	0.40	1.56	1.25	1.95	4.38
3.89	106.14	1.10	11.64	1.33	0.74	0.00	6.90	0.26	2.00	0.26
3.91	106.14	1.10	11.64	2.13	0.00	0.00	7.10	1.37	1.08	0.00
3.94	106.14	1.10	11.64	1.57	0.48	0.00	5.75	0.00	1.98	1.51
3.98	106.14	1.10	11.64	0.80	0.25	0.00	4.80	0.26	1.50	3.86
4.02	103.58	1.02	10.55	0.67	0.62	0.00	3.78	0.43	0.83	4.07
4.07	103.58	1.02	10.55	0.65	0.80	0.00	6.81	0.00	0.81	1.25
4.08	103.58	1.02	10.55	0.20	0.19	9.66	0.51	0.00	0.00	0.00
4.14	103.58	1.02	10.55	0.91	0.85	0.00	6.39	0.00	1.29	0.88
4.15	103.58	1.02	10.55	1.17	0.65	0.00	6.44	0.11	1.59	0.45

Table 11: ODP Site 1016 smear slide diatom and coccolith MAR age separated averages for this study and ODP IR data, using the ODP lithological unit age divisions (Table A) and visually identified changes in the combined data (Table B). Analysis of variance (ANOVA) was compared between the averages for both the ODP lithological age units and the age of visually identified changes in the data. The diatom MAR populations only significantly differ statistically for the data from this study using only the observed age grouping. The coccolith MAR populations only significantly differ statistically for the data from this study using both the ODP lithological unit and observed age grouping.

A Site and Data Source	**2.6-2.8 (Ma)**	**2.8-4.5 (Ma)**	ANOVA (significance)
1016 Diatom MAR (this study)	0.98± 0.19	0.70± 0.09	Not Significant
1016 Diatom MAR (ODP IR)	1.42± 0.74	1.32± 0.42	Not Significant
1016 Coccolith MAR (this study)	6.55± 1.24	3.48± 0.65	Significant
1016 Coccolith MAR (ODP IR)	3.93± 1.45	3.04± 0.84	Not Significant

B Site and Data Source	**2.6-3.5 (Ma)**	**3.5-4.5 (Ma)**	ANOVA (significance)
1016 Diatom MAR (this study)	1.00± 0.07	0.30± 0.09	Significant
1016 Diatom MAR (ODP IR)	1.44± 0.42	1.06± 0.74	Not Significant
1016 Coccolith MAR (this study)	6.07± 0.35	0.55± 0.48	Significant
1016 Coccolith MAR (ODP IR)	4.17± 0.73	0.54± 1.26	Significant

Table 12: ODP Site 1022 smear slide diatom and coccolith MAR age separated averages for this study and ODP IR data, using the ODP lithological age divisions (Table A) and visually identified changes in the combined data (Table B). Analysis of variance (ANOVA) was compared between the averages for both the ODP lithological age units and the age of visually identified changes in the data. The diatom MAR populations only significantly differ statistically using the data from this study using both the ODP lithological unit and observed age grouping. The coccolith MAR populations significantly differ statistically for the data from this study and the ODP IR using both the ODP lithological unit and observed age grouping.

A Site and Data Source	**2.3-3.58 (Ma)**	**3.58-4.2 (Ma)**	ANOVA (significance)
1022 Diatom MAR (this study)	1.13± 0.21	2.57± 0.28	Significant
1022 Diatom MAR (ODP IR)	0.84± 0.26	1.39± 0.20	Not Significant
1022 Coccolith MAR (this study)	8.39± 0.57	2.88± 0.79	Significant
1022 Coccolith MAR (ODP IR)	5.71± 0.71	2.05± 0.56	Significant

B Site and Data Source	**2.3-3.5 (Ma)**	**3.5-4.2 (Ma)**	ANOVA (significance)
1022 Diatom MAR (this study)	0.90± 0.21	2.43± 0.22	Significant
1022 Diatom MAR (ODP IR)	0.71± 0.26	1.42± 0.19	Significant
1022 Coccolith MAR (this study)	9.07± 0.61	3.63± 0.64	Significant
1022 Coccolith MAR (ODP IR)	6.35± 0.64	1.93± 0.46	Significant

Table 13: ANOVA comparing this study and the ODP IR coccolith and diatom MAR averages at ODP Sites 1016 and 1022 for both the ODP IR lithologic unit and visually identified age divisions. Not Significant indicates that the identified populations between this study and the ODP IR data are not statistically distinguishable from each other, below a 95% confidence level. Significant indicates that the identified populations between this study and the ODP IR are statistically distinguishable from each other, within a 95% confidence level. At ODP Site 1016 the only populations statistically distinguishable between this study and the ODP IR data are the coccolith MAR of the late Pliocene for both the lithologic unit and visually identified age divisions. At ODP Site 1022 the diatom MAR are only statistically distinguishable between this study and the ODP IR data in the early Pliocene for both the lithologic unit and visually identified age divisions. At ODP Site 1022 the only coccolith MAR populations not statistically distinguishable between this study and the ODP IR data is for the ODP IR lithologic age unit of the early Pliocene.

Site and Data Type	**2.6-2.8 (Ma)**	**2.8-4.5 (Ma)**	**2.6-3.5 (Ma)**	**3.5-4.5 (Ma)**
1016 Diatoms	Not Significant	Not Significant	Not Significant	Not Significant
1016 Coccoliths	Not Significant	Not Significant	Significant	Not Significant
	2.3-3.58 (Ma)	**3.58-4.2 (Ma)**	**2.3-3.5 (Ma)**	**3.5-4.2 (Ma)**
1022 Diatoms	Not Significant	Significant	Not Significant	Significant
1022 Coccoliths	Significant	Not Significant	Significant	Significant

APPENDIX I: **Productivity verses Preservation**

There are two essential factors governing what is in marine sediment; productivity in the overlying water column and preservation of the material into the sediment. Only 0.5% of global primary productivity makes it to the sediment water interface due to remineralization in the water column (Hedges & Keil, 1995). The biogenic organic matter that does reach the sediment water interface is then subjected to alteration by various biological, physical, and chemical processes (Zonneveld et al., 2010). Sediment alteration can even take place after relatively deep burial (Henrichs, 1992), and changes in the relative abundance and preservation can also be the result of dilution by other sediment types (Hedges & Keil, 1995). In addition different taxa have various degrees of fragility and robustness. The world's oceans are undersaturated in biosilica, on a global scale only 3% of biosilica produced in the surface ocean is preserved in the sediment record, whereas in coastal upwelling regions 15-25% of surface production is preserved (Nelson et al., 1995). Calcium carbonate (coccolithophorid) tests are also highly susceptible to dissolution in acidic deeper waters below the lysocline and calcite compensation depth (CCD).

At ODP site 1016 calcareous nannofossil preservation ranges from good to moderate, and diatom preservation ranges from poor to moderate during the time period of this study ~2.6-4.4 Ma (Lyle et al., 1997). Dissolved silicate concentrations, indicative of the dissolution of biogenic opal, including diatoms, reach near their maximum values before the youngest sediments that are used in this study and values only very slightly increase with depth (Lyle et al., 1997). Strontium concentrations, consistent with the influence of dissolution and/or recrystallization of calcium carbonate is relatively high (160 μM), but remains consistent during the time period of this study (Lyle et al., 1997). These data suggest that all the ODP site 1016 samples used in this study have been subjected to roughly the same degree of dissolution and should be able to be compared to each other.

In addition to the ODP IR for site 1022 there is also a diatom assemblage study during the Pliocene, in part because it is the most diatomaceous of all the California margin drill sites (Lyle et al., 1997). At ODP Site 1022 the calcareous nannofossil preservation is good from the start of this study until ~3.6 Ma, and alternates between poor, moderate, and good through ~4.2 Ma (Lyle et al., 1997). The diatom preservation alternates between poor and moderate during the time period of this study ~2.8-4.2 Ma (Lyle et al., 1997). Geochemical data is only available to a depth that corresponds to ~3.6 Ma, dissolved silicate concentrations reach their maximum values before the youngest sediments used in this study and remain consistent with depth until at least ~3.6 Ma, and strontium values increase (~150-190 μM) from ~2.8-3.6 Ma (Lyle et al., 1997). The diatom assemblage study of Pliocene aged sediment at ODP site 1022 used *Coscinodiscus marginatus* as an indicator of dissolution to ensure that preferential dissolution has not altered the proportions of the diatom assemblages (Reed-Sterrett et al., 2010). The *C. marginatus* species is robust and preferentially preserved, becoming more concentrated in the sediment as opal dissolution increases (White & Alexandrovich, 1992). No trend in the dissolution indicator was found at ODP site 1022 through the Pliocene, suggesting it is unlikely that any trends in the diatom abundances are the result of preferential dissolution.

Clearly, the preservation potential serves as an essential control on the relative abundance of diatoms and coccolithophorids in marine sediments. Based on the ODP IR chapters and the diatom assemblage study at ODP site 1022, it appears that the majority of the sediment used in this study have all been similarly subjected to various alteration processes, and there is evidence that there was not much selective dissolution of the diatom and coccolithophorid groups. The ODO IR reports do not indicate that there was selective dissolution of certain species within phytoplankton groups, and that the preservation listed appeared to apply to all the species they identified (Lyle et al., 1997). Phytoplankton fossil distributions preserved in surface sediments generally have geographical distributions in relation to their ecological preferences particularly in areas of high surface productivity and sedimentation/rain rates (Crosta & Koc, 2007; Giraudeau & Beaufort, 2007). The different requirements for growth of the diatoms and coccolithophorids means that the relative abundances of these two groups of phytoplankton found in these deep marine sediments can be carefully used as a proxy for paleoproductivity, where dissolution and preservation should always be considered when interpreting the records. (Crosta & Koc, 2007; Giraudeau & Beaufort, 2007). A limitation in using smear slide analysis as a method to determine productivity, is that the sediment contents is a reflection of both productivity and preservation. It is however one of the oldest and widely used ways to examine marine sediment lithology down-core.

APPENDIX II: Visual estimation counts and averages of smear slides for ODP Site 1016

B 13H3w (125-127)

Sample Age (Ma)	Estimated Total % Cover	Pennate Diatom	Total Centric Diatom	Whole Centric Diatom	Centric Diatom Fragment	Sponge Spicule	Radiolarian	Silicoflagellate	Foram	Coccolith	Volcanic Glass	Clay Mineral	Opaque	Siliciclastic	Calculated Total % Cover
2.66	20	2	5	1	4	1	0	0	0	10	0	1	2	1	22
2.66	22	1	5	0	5	1	0	0	1	10	1	2	2	2	25
2.66	18	1	2	0	2	1	1	0	0	13	1	1	1	1	22
2.66	22	1	2	1	1	1	0	0	0	12	1	1	1	2	21
2.66	23	1	1	0	1	2	0	0	0	12	1	1	1	2	21
2.66	24	0	2	1	1	2	0	0	0	13	1	2	2	2	24
2.66	20	2	1	0	1	1	1	0	0	9	1	2	1	3	21
2.66	22	1	2	0	2	2	0	0	0	14	1	1	1	2	24
2.66	25	1	2	0	2	1	0	0	0	14	1	1	2	2	24
2.66	20	1	3	0	3	1	0	1	0	11	1	1	1	3	23
Average	21.6	1.1	2.5	0.3	2.2	1.3	0.2	0.1	0.1	11.8	0.9	1.3	1.4	2	22.7

B 13H4w (70-72)

2.69	28	1	3	0	3	1	0	0	0	18	1	1	1	2	28
2.69	26	2	2	0	2	0	0	0	1	18	1	1	1	1	27
2.69	26	3	2	0	2	0	0	1	0	18	1	1	1	1	28
2.69	28	2	3	0	3	1	0	1	0	18	1	1	1	1	29
2.69	28	2	3	1	2	0	0	0	0	18	1	1	1	1	27
2.69	22	1	1	0	1	1	0	0	0	16	0	0	0	2	21
2.69	26	2	3	1	2	2	0	1	0	18	1	1	1	2	31
2.69	25	2	2	0	2	1	1	0	0	17	1	1	0	1	26
2.69	26	1	3	0	3	1	0	0	0	18	1	1	0	2	27
2.69	30	2	3	2	1	1	0	0	0	20	1	1	1	2	31
Average	26.5	1.8	2.5	0.4	2.1	0.8	0.1	0.3	0.1	17.9	0.9	0.9	0.7	1.5	27.5

B 13H5w (120-122)

2.72	24	2	2	0	2	0	0	1	0	17	0	0	1	2	25
2.72	22	2	2	1	1	1	0	0	0	17	1	1	0	1	25
2.72	20	1	1	0	1	0	0	0	1	16	0	1	0	1	21
2.72	22	1	2	0	2	0	0	1	0	17	1	1	0	1	24
2.72	20	1	1	0	1	0	0	1	0	15	1	0	0	1	20
2.72	20	1	2	0	2	0	0	0	0	16	0	1	0	1	21
2.72	22	1	2	1	1	1	0	0	0	16	0	1	0	1	22
2.72	24	1	1	0	1	0	0	0	0	17	1	1	0	2	23
2.72	25	1	2	0	2	1	1	0	0	16	0	1	0	2	24
2.72	25	1	2	1	1	1	0	0	0	18	1	1	1	1	26
Average	22.4	1.2	1.7	0.3	1.4	0.4	0.1	0.3	0.1	16.5	0.5	0.8	0.2	1.3	23.1

APPENDIX II: Visual estimation counts and averages of smear slides for ODP Site 1016 continued

B 13H6w (20-22)

Sample Age (Ma)	Estimated Total % Cover	Pennate Diatom	Total Centric Diatom	Whole Centric Diatom	Centric Diatom Fragment	Sponge Spicule	Radiolarian	Silicoflagellate	Foram	Coccolith	Volcanic Glass	Clay Mineral	Opaque	Siliciclastic	Calculated Total % Cover
2.73	20	1	1	0	1	0	0	0	0	17	0	0	0	1	20
2.73	22	1	2	0	2	0	0	0	0	18	0	0	0	2	23
2.73	25	1	2	1	1	0	0	1	0	18	1	1	0	1	25
2.73	24	2	2	0	2	1	0	0	0	16	1	1	0	2	25
2.73	22	1	1	0	1	1	0	1	0	16	0	1	0	2	23
2.73	25	1	0	0	0	1	1	0	0	19	1	1	0	2	26
2.73	22	1	1	0	1	0	0	0	0	17	0	1	0	2	22
2.73	20	1	1	0	1	1	0	2	0	15	0	1	0	1	22
2.73	24	1	1	0	1	1	0	0	0	16	0	0	0	2	21
2.73	22	2	1	0	1	0	0	0	0	18	0	1	0	2	24
Average	22.6	1.2	1.2	0.1	1.1	0.5	0.1	0.4	0	17	0.3	0.7	0	1.7	23.1

B 14H2w (2-4)

2.78	20	1	1	0	1	0	0	0	0	14	0	1	0	2	19
2.78	18	1	1	0	1	1	0	0	0	12	0	2	0	2	19
2.78	20	1	0	0	0	0	0	1	0	13	0	1	0	2	18
2.78	15	0	1	0	1	0	0	0	0	10	0	1	0	2	14
2.78	16	2	1	0	1	0	0	0	0	10	0	1	0	1	15
2.78	13	1	1	0	1	1	0	0	0	8	0	1	0	2	14
2.78	14	0	1	0	1	0	0	0	0	9	0	1	0	1	12
2.78	18	1	1	0	1	1	0	0	0	11	0	1	0	2	17
2.78	16	1	0	0	0	1	0	0	0	10	0	1	0	2	15
2.78	16	1	1	0	1	0	0	0	0	12	0	1	0	2	17
Average	16.6	0.9	0.8	0	0.8	0.4	0	0.1	0	10.9	0	1.1	0	1.8	16

B 14H3w (51-53)

2.82	22	0	1	0	1	1	0	0	0	17	0	1	0	2	22
2.82	24	1	2	0	2	1	0	0	0	16	0	1	1	2	24
2.82	22	0	1	0	1	2	0	0	0	16	0	1	0	2	22
2.82	25	1	2	0	2	1	0	0	0	17	1	1	0	2	25
2.82	24	1	1	0	1	2	0	0	0	17	0	1	0	2	24
2.82	24	2	1	0	1	0	0	0	0	17	1	2	0	2	25
2.82	25	1	2	0	2	1	0	0	0	17	0	2	0	2	25
2.82	26	1	2	0	2	1	0	0	0	18	1	2	0	2	27
2.82	26	2	1	0	1	0	0	0	0	18	1	2	0	2	26
2.82	24	1	1	0	1	1	0	0	0	16	0	2	0	2	23
Average	24.2	1	1.4	0	1.4	1	0	0	0	16.9	0.4	1.5	0.1	2	24.3

APPENDIX II: Visual estimation counts and averages of smear slides for ODP Site 1016 continued

B 14H5w (50-52)

Sample Age (Ma)	Estimated Total % Cover	Pennate Diatom	Total Centric Diatom	Whole Centric Diatom	Centric Diatom Fragment	Sponge Spicule	Radiolarian	Silicoflagellate	Foram	Coccolith	Volcanic Glass	Clay Mineral	Opaque	Siliciclastic	Calculated Total % Cover
2.86	22	1	1	0	1	1	0	0	0	16	1	2	0	2	24
2.86	23	1	1	0	1	0	0	0	0	17	1	2	1	1	24
2.86	20	1	1	0	1	1	0	0	0	16	1	2	0	1	23
2.86	22	1	1	0	1	0	0	0	0	17	0	2	0	2	23
2.86	22	1	0	0	0	0	0	0	0	19	1	1	0	1	23
2.86	20	1	0	0	0	0	0	0	0	17	0	1	0	1	20
2.86	20	1	1	0	1	0	0	0	0	16	1	1	0	1	21
2.86	28	0	0	0	0	1	0	0	1	22	0	2	1	1	28
2.86	25	0	2	1	1	1	0	0	0	16	1	2	0	1	23
2.86	24	1	1	0	1	0	0	0	1	17	1	2	0	2	25
Average	22.6	0.8	0.8	0.1	0.7	0.4	0	0	0.2	17.3	0.7	1.7	0.2	1.3	23.4

B 14H6w (120-122)

2.90	26	1	1	0	1	1	0	0	0	20	1	2	0	1	27
2.90	25	1	1	0	1	1	0	0	0	19	1	1	0	1	25
2.90	30	1	0	0	0	2	0	0	0	23	1	2	0	2	31
2.90	22	2	1	0	1	1	0	0	0	16	1	1	0	1	23
2.90	26	2	1	0	1	0	0	0	0	20	0	2	0	2	27
2.90	30	2	1	0	1	0	1		0	21	1	2	0	2	30
2.90	30	1	2	1	1	1	0	0	0	21	1	2	0	2	30
2.90	26	2	1	0	1	1	0	0	0	18	1	1	0	1	25
2.90	26	2	1	0	1	0	0	0	0	18	0	2	0	1	24
2.90	26	3	2	0	2	1	0	0	0	19	1	1	0	1	28
Average	26.7	1.7	1.1	0.1	1	0.8	0.1	0	0	19.5	0.8	1.6	0	1.4	27

B 15H2w (75-77)

2.95	30	3	1	0	1	2	0	0	0	20	1	2	0	1	30
2.95	30	1	1	0	1	0	0	0	0	22	1	2	0	1	28
2.95	30	1	1	0	1	0	0	0	0	21	1	2	0	2	28
2.95	30	1	1	0	1	2	0	0	0	22	1	2	0	2	31
2.95	28	3	1	1	0	0	0	0	0	19	1	2	0	2	28
2.95	30	2	2	0	2	0	0	0	0	22	1	2	0	2	31
2.95	28	2	2	0	2	1	0	0	0	20	1	2	0	1	29
2.95	25	1	1	0	1	1	0	0	0	17	1	2	0	1	24
2.95	28	1	2	0	2	1	0	0	0	22	1	1	0	1	29
2.95	28	1	1	0	1	1	0	0	0	20		2	0	2	27
Average	28.7	1.6	1.3	0.1	1.2	0.8	0	0	0	20.5	1	1.9	0	1.5	28.5

APPENDIX II: Visual estimation counts and averages of smear slides for ODP Site 1016 continued

B 15H4w (75-77)

Sample Age (Ma)	Estimated Total % Cover	Pennate Diatom	Total Centric Diatom	Whole Centric Diatom	Centric Diatom Fragment	Sponge Spicule	Radiolarian	Silicoflagellate	Foram	Coccolith	Volcanic Glass	Clay Mineral	Opaque	Siliciclastic	Calculated Total % Cover
3.00	18	2	1	0	1	0	0	0	0	10	0	2	0	2	17
3.00	20	1	1	0	1	2	0	0	0	9	1	2	1	2	19
3.00	18	1	1	0	1	1	0	0	0	10	1	2	1	2	19
3.00	20	1	2	0	2	1	0	0	0	10	1	2	0	2	19
3.00	22	1	1	0	1	0	0	0	0	15	1	2	1	2	23
3.00	18	1	1	0	1	3	0	0	0	10	0	2	0	2	19
3.00	16	1	1	0	1	0	0	0	0	9	0	2	0	2	15
3.00	14	1	0	0	0	0	0	0	0	8	0	2	0	2	13
3.00	18	1	1	0	1	1	0	0	0	10	0	2	0	2	17
3.00	18	1	0	0	0	1	0	0	0	10	0	2	1	2	17
Average	18.2	1.1	0.9	0	0.9	0.9	0	0	0	10.1	0.4	2	0.4	2	17.8

B 16H2w (78-80)

3.11	26	2	1	0	1	0	0	0	0	20	0	2	0	1	26
3.11	28	2	0	0	0	0	1	0	0	20	2	2	0	1	28
3.11	26	1	1	0	1	0	0	0	0	20	1	2	0	1	26
3.11	26	2	0	0	0	1	0	0	0	20	0	2	0	2	27
3.11	26	1	1	0	1	0	0	0	1	20	0	2	0	2	27
3.11	28	2	1	0	1	0	0	0	0	22	1	2	0	1	29
3.11	28	2	1	0	1	1	0	0	0	20	0	3	0	1	28
3.11	26	1	0	0	0	1	0	0	0	21	0	3	0	1	27
3.11	30	2	1	0	1	2	1	0	1	20	1	2	0	1	31
3.11	30	2	1	0	1	2	0	0	0	22	1	2	0	1	31
Average	27.4	1.7	0.7	0	0.7	0.7	0.2	0	0.2	20.5	0.6	2.2	0	1.2	28

B16H4w (78-80)

3.16	20	1	0	0	0	0	0	0	0	12	4	2	0	2	21
3.16	20	1	2	0	2	0	0	0	0	10	4	2	1	2	22
3.16	28	3	2	0	2	1	1	0	1	14	5	2	0	1	30
3.16	24	3	3	2	1	0	1	0	0	11	4	2	1	1	26
3.16	28	3	2	0	2	0	0	0	0	18	4	2	0	1	30
3.16	26	1	2	1	1	0	0	0	0	15	4	2	1	1	26
3.16	26	2	0	0	0	0	0	0	0	16	4	2	1	1	26
3.16	28	2	2	0	2	1	0	0	0	15	3	2	1	1	27
3.16	28	2	2	1	1	2	0	0	0	15	4	2	1	1	29
3.16	30	4	1	0	1	1	0	0	0	17	3	3	0	1	30
Average	25.8	2.2	1.6	0.4	1.2	0.5	0.2	0	0.1	14.3	3.9	2.1	0.6	1.2	26.7

APPENDIX II: Visual estimation counts and averages of smear slides for ODP Site 1016 continued

B 16H6w (80-82)

Sample Age (Ma)	Estimated Total % Cover	Pennate Diatom	Total Centric Diatom	Whole Centric Diatom	Centric Diatom Fragment	Sponge Spicule	Radiolarian	Silicoflagellate	Foram	Coccolith	Volcanic Glass	Clay Mineral	Opaque	Siliciclastic	Calculated Total % Cover
3.21	12	2	0	0	0	2	0	0	0	6	1	2	0	1	14
3.21	14	2	0	0	0	1	0	0	0	8	1	2	0	1	15
3.21	12	1	1	0	1	2	0	0	0	7	1	1	0	1	14
3.21	14	1	1	0	1	2	0	0	0	7	1	2	0	1	15
3.21	12	1	0	0	0	1	0	0	0	7	0	1	0	1	11
3.21	14	1	1	0	1	0	0	0	0	8	1	2	0	1	14
3.21	13	1	0	0	0	0	0	0	0	9	1	2	0	1	14
3.21	12	1	0	0	0	1	0	0	0	8	1	1	0	1	13
3.21	14	1	0	0	0	2	0	0	0	8	1	1	0	1	14
3.21	12	1	0	0	0	1	0	0	0	7	1	1	0	2	13
Average	12.9	1.2	0.3	0	0.3	1.2	0	0	0	7.5	0.9	1.5	0	1.1	13.7

B 17H2w (20-22)

3.26	16	2	1	0	1	2	0	0	0	4	1	2	1	3	16
3.26	16	2	1	0	1	2	0	0	0	4	1	2	1	3	16
3.26	15	1	2	1	1	2	0	0	0	4	1	2	0	2	14
3.26	20	3	1	0	1	2	0	0	0	5	1	3	1	3	19
3.26	14	2	0	0	0	2	0	0	0	5	1	3	0	2	15
3.26	20	1	2	1	1	2	0	0	0	6	2	3	0	3	19
3.26	15	1	1	0	1	2	0	0	0	5	1	2	0	2	14
3.26	16	2	1	0	1	1	0	0	0	7	1	2	0	2	16
3.26	16	2	1	0	1	1	0	0	0	6	1	2	0	2	15
3.26	16	2	1	0	1	3	0	0	0	5	1	2	1	2	17
Average	16.4	1.8	1.1	0.2	0.9	1.9	0	0	0	5.1	1.1	2.3	0.4	2.4	16.1

B 17H4w (24-26)

3.31	14	2	1	0	1	1	0	0	1	3	1	3	1	2	15
3.31	14	2	2	1	1	1	0	1	0	3	0	3	1	2	15
3.31	15	1	2	0	2	2	0	0	0	3	1	3	1	1	14
3.31	15	2	2	0	2	0	1	0	0	4	1	3	1	1	15
3.31	14	2	2	1	1	1	0	0	0	2	1	3	1	2	14
3.31	14	1	1	0	1	1	0	0	0	2	1	3	1	2	12
3.31	15	2	1	0	1	2	0	0	0	3	1	3	1	2	15
3.31	14	2	1	0	1	1	0	0	0	3	0	3	1	2	13
3.31	14	1	2	0	2	1	0	0	0	2	1	4	1	2	14
3.31	14	1	1	0	1	2	1	0	0	3	1	2	1	1	13
Average	14.3	1.6	1.5	0.2	1.3	1.2	0.2	0.1	0.1	2.8	0.8	3	1	1.7	14

APPENDIX II: Visual estimation counts and averages of smear slides for ODP Site 1016 continued

B 18H3w (110-112)

Sample Age (Ma)	Estimated Total % Cover	Pennate Diatom	Total Centric Diatom	Whole Centric Diatom	Centric Diatom Fragment	Sponge Spicule	Radiolarian	Silicoflagellate	Foram	Coccolith	Volcanic Glass	Clay Mineral	Opaque	Siliciclastic	Calculated Total % Cover
4.01	16	1	1	0	1	2	0	0	0	7	1	3	1	1	17
4.01	16	1	1	0	1	2	0	0	0	6	1	3	1	1	16
4.01	18	2	1	0	1	2	0	0	0	6	0	3	1	2	17
4.01	16	1	1	0	1	1	0	0	0	7	1	3	1	2	17
4.01	16	2	1	0	1	1	0	0	0	6	1	3	1	1	16
4.01	16	2	1	0	1	2	0	0	0	6	1	3	1	1	17
4.01	15	1	0	0	0	1	0	0	0	7	0	3	1	2	15
4.01	15	2	1	0	1	0	0	0	0	6	1	3	1	2	16
4.01	18	1	2	0	2	2	0	0	0	7	1	3	1	1	18
4.01	16	1	2	0	2	2	0	0	0	6	1	3	1	1	17
Average	16.2	1.4	1.1	0	1.1	1.5	0	0	0	6.4	0.8	3	1	1.4	16.6

B 18H4w (65-67)

4.10	15	1	1	0	1	1	0	0	0	5	1	3	1	2	15
4.10	16	1	1	0	1	2	0	0	0	5	1	4	1	2	17
4.10	16	1	2	0	2	2	0	0	0	5	0	4	1	2	17
4.10	16	2	1	0	1	1	0	0	0	6	1	4	1	1	17
4.10	17	1	1	0	1	2	0	0	0	6	0	4	1	2	17
4.10	17	2	1	0	1	1	0	0	0	5	1	4	1	2	17
4.10	18	1	2	0	2	1	0	0	0	5	1	4	2	2	18
4.10	18	2	1	0	1	3	0	0	0	5	1	4	1	2	19
4.10	15	1	1	0	1	1	0	0	0	6	1	4	1	1	16
4.10	18	2	1	1	0	2	0	1	0	6	1	4	2	1	20
Average	16.6	1.4	1.2	0.1	1.1	1.6	0	0.1	0	5.4	0.8	3.9	1.2	1.7	17.3

B 18H4w (123-125)

4.15	14	2	1	0	1	2	0	0	0	2	0	3	1	2	13
4.15	12	1	1	0	1	2	0	0	0	2	0	3	1	2	12
4.15	12	2	1	0	1	0	0	0	0	2	0	3	1	2	11
4.15	12	1	1	0	1	2	0	0	0	2	0	3	1	2	12
4.15	12	0	2	0	2	0	0	0	0	2	1	3	1	2	11
4.15	14	1	1	0	1	1	0	0	0	3	0	3	1	3	13
4.15	12	1	2	0	2	2	0	0	0	3	0	3	0	1	12
4.15	12	0	2	0	2	0	0	0	0	3	0	3	1	2	11
4.15	12	1	1	0	1	2	0	0	0	2	0	3	0	2	11
4.15	14	2	2	0	2	2	0	0	0	2	1	2	1	2	14
Average	12.6	1.1	1.4	0	1.4	1.3	0	0	0	2.3	0.2	2.9	0.8	2	12

APPENDIX II: Visual estimation counts and averages of smear slides for ODP Site 1016 continued

B 18H5w (35-37)

Sample Age (Ma)	Estimated Total % Cover	Pennate Diatom	Total Centric Diatom	Whole Centric Diatom	Centric Diatom Fragment	Sponge Spicule	Radiolarian	Silicoflagellate	Foram	Coccolith	Volcanic Glass	Clay Mineral	Opaque	Siliciclastic	Calculated Total % Cover
4.20	15	3	2	0	2	1	0	0	0	2	0	3	0	2	13
4.20	14	3	2	0	2	1	0	0	0	2	0	2	0	2	12
4.20	15	3	2	0	2	2	0	0	0	2	0	2	1	1	13
4.20	14	3	1	0	1	1	0	0	0	2	0	3	0	2	12
4.20	15	2	1	0	1	2	0	0	0	3	0	3	1	2	14
4.20	14	2	0	0	0	3	0	0	0	2	0	2	1	2	12
4.20	15	2	2	1	1	2	0	0	0	3	0	3	1	1	14
4.20	15	2	2	0	2	2	0	1	0	3	0	3	1	2	16
4.20	14	2	1	0	1	1	0	0	0	3	0	3	1	2	13
4.20	14	2	1	0	1	2	0	0	0	2	0	3	1	1	12
Average	14.5	2.4	1.4	0.1	1.3	1.7	0	0.1	0	2.4	0	2.7	0.7	1.7	13.1

B 18H5w (95-97)

4.25	14	2	1	0	1	2	0	0	0	4	0	3	1	2	15
4.25	12	2	1	0	1	1	0	0	0	3	1	3	0	2	13
4.25	12	1	1	0	1	2	0	0	0	3	0	3	0	2	12
4.25	12	2	1	0	1	1	0	0	0	3	0	3	1	2	13
4.25	14	3	2	0	2	0	0	0	0	4	0	3	1	1	14
4.25	13	1	2	0	2	2	0	0	1	3	0	2	1	1	13
4.25	14	2	2	0	2	1	0	0	0	3	0	3	0	2	13
4.25	12	1	1	0	1	2	0	0	0	3	0	2	1	2	12
4.25	12	2	1	0	1	1	0	0	0	4	0	2	0	2	12
4.25	12	2	1	0	1	1	0	0	0	4	0	3	0	2	13
Average	12.7	1.8	1.3	0	1.3	1.3	0	0	0.1	3.4	0.1	2.7	0.5	1.8	13

B 18H6w (11-15)·

4.31	12	1	1	0	1	1	0	0	0	4	0	2	1	1	11
4.31	12	1	1	0	1	1	0	0	0	3	1	2	1	1	11
4.31	12	1	1	0	1	0	0	0	0	3	0	3	1	2	11
4.31	12	1	0	0	0	1	0	0	0	3	0	3	1	1	10
4.31	12	2	1	0	1	0	0	0	0	3	0	2	1	2	11
4.31	12	1	2	0	2	0	0	0	0	2	1	2	1	1	10
4.31	12	1	1	0	1	2	0	0	0	3	0	3	0	1	11
4.31	12	1	1	0	1	1	0	0	0	3	1	2	1	1	11
4.31	12	1	1	0	1	0	0	0	0	4	1	3	1	1	12
4.31	12	1	0	0	0	3	0	0	0	3	1	3	0	1	12
Average	12	1.1	0.9	0	0.9	0.9	0	0	0	3.1	0.5	2.5	0.8	1.2	11

APPENDIX II: Visual estimation counts and averages of smear slides for ODP Site 1016 continued

B 18H6w (80-82)

Sample Age (Ma)	Estimated Total % Cover	Pennate Diatom	Total Centric Diatom	Whole Centric Diatom	Centric Diatom Fragment	Sponge Spicule	Radiolarian	Silicoflagellate	Foram	Coccolith	Volcanic Glass	Clay Mineral	Opaque	Siliciclastic	Calculated Total % Cover
4.37	15	2	1	0	1	2	0	0	0	4	0	3	1	1	14
4.37	15	2	1	0	1	0	0	0	0	4	0	3	1	2	13
4.37	15	2	2	0	2	1	0	0	0	5	0	3	1	2	16
4.37	16	3	1	0	1	0	0	0	0	4	1	3	1	2	15
4.37	16	2	2	0	2	1	0	0	0	5	0	3	0	2	15
4.37	15	2	2	0	2	2	0	0	0	4	0	3	0	2	15
4.37	15	2	2	0	2	0	0	0	0	4	0	3	1	2	14
4.37	15	2	2	0	2	2	0	0	0	4	0	3	1	1	15
4.37	15	2	1	0	1	2	0	0	0	4	1	2	1	2	15
4.37	16	2	1	0	1	3	0	0	0	5	0	3	1	2	17
Average	15.3	2.1	1.5	0	1.5	1.3	0	0	0	4.3	0.2	2.9	0.8	1.8	14.9

B 18H6w (142-144)

4.42	20	3	1	0	1	2	0	0	0	10	0	2	0	3	21
4.42	20	2	1	0	1	1	0	0	0	9	1	3	1	2	20
4.42	18	2	1	0	1	0	0	0	0	7	0	3	1	3	17
4.42	20	3	1	0	1	2	0	0	0	7	0	4	1	2	20
4.42	18	3	1	0	1	0	0	0	0	7	0	3	1	2	17
4.42	18	1	1	0	1	2	0	0	0	6	1	3	1	2	17
4.42	20	2	1	0	1	3	0	0	0	7	0	4	1	2	20
4.42	18	2	1	0	1	1	0	0	0	7	0	3	1	2	17
4.42	15	2	0	0	0	0	0	0	0	5	0	4	1	2	14
4.42	18	1	1	0	1	2	0	0	0	5	0	4	1	2	16
Average	18.5	2.1	0.9	0	0.9	1.3	0	0	0	7	0.2	3.3	0.9	2.2	17.9

APPENDIX III: Visual estimation counts and averages of smear slides for ODP Site 1022

C 9H1w (50-52)

Sample Age (Ma)	Estimated Total % Cover	Pennate Diatom	Total Centric Diatom	Whole Centric Diatom	Centric Diatom Fragment	Sponge Spicule	Radiolarian	Silicoflagellate	Foram	Coccolith	Volcanic Glass	Clay Mineral	Opaque	Siliciclastic	Calculated Total % Cover
2.82	25	1	0	0	0	0	0	0	0	20	0	0	2	1	24
2.82	25	2	1	0	1	0	0	0	0	20	0	0	1	1	25
2.82	25	1	1	0	1	0	0	0	0	22	0	0	1	3	28
2.82	25	1	1	0	1	0	0	0	0	20	0	0	1	2	25
2.82	28	1	1	0	1	0	0	0	0	23	0	0	1	2	28
2.82	23	1	0	0	0	0	0	0	0	20	0	0	1	1	23
2.82	26	0	1	0	1	0	0	0	0	22	0	0	1	2	26
2.82	20	1	1	1	0	0	0	0	0	15	0	0	1	1	19
2.82	25	1	1	0	1	0	0	0	0	20	0	0	1	2	25
2.82	20	0	0	0	0	0	0	0	0	18	0	0	1	1	20
Average	24.2	0.9	0.7	0.1	0.6	0	0	0	0	20	0	0	1.1	1.6	24.3

C 9H3w (50-52)

2.85	22	2	1	0	1	0	0	0	0	18	0	0	1	1	23
2.85	20	1	1	0	1	0	0	0	0	15	0	0	1	1	19
2.85	20	2	1	0	1	0	0	0	0	13	0	0	2	2	20
2.85	18	1	1	0	1	0	0	0	0	10	0	0	1	2	15
2.85	18	1	1	0	1	0	0	0	0	10	0	0	1	4	17
2.85	16	2	2	0	2	0	0	0	0	7	0	0	2	4	17
2.85	17	2	1	0	1	0	0	0	0	7	0	0	2	4	16
2.85	18	2	0	0	0	0	0	0	0	10	0	0	1	3	16
2.85	22	2	2	0	2	0	0	0	0	14	0	0	1	3	22
2.85	20	1	1	0	1	0	0	0	0	10	0	0	1	4	17
Average	19.1	1.6	1.1	0	1.1	0	0	0	0	11.4	0	0	1.3	2.8	18.2

C 9H7w (26-28)

2.90	28	2	0	0	0	0	0	0	0	25	0	0	1	1	29
2.90	30	2	1	0	1	0	0	0	0	27	0	0	1	1	32
2.90	30	2	1	0	1	1	0	0	0	28	0	0	1	1	34
2.90	30	1	1	0	1	0	0	0	0	27	0	0	1	2	32
2.90	30	1	2	1	1	0	0	1	0	27	0	0	1	2	34
2.90	30	1	2	0	2	0	0	1	0	27	0	0	1	1	33
2.90	30	1	2	0	2	0	0	0	0	27	0	1	1	1	33
2.90	30	1	1	0	1	0	0	0	0	27	0	1	1	1	32
2.90	30	1	1	0	1	0	0	0	0	27	0	1	1	1	32
2.90	30	1	1	0	1	0	0	0	0	27	0	1	1	1	32
Average	29.8	1.3	1.2	0.1	1.1	0.1	0	0.2	0	26.9	0	0.4	1	1.2	32.3

APPENDIX III: Visual estimation counts and averages of smear slides for ODP Site 1022 continued

C 10H4w (50-52)

Sample Age (Ma)	Estimated Total % Cover	Pennate Diatom	Total Centric Diatom	Whole Centric Diatom	Centric Diatom Fragment	Sponge Spicule	Radiolarian	Silicoflagellate	Foram	Coccolith	Volcanic Glass	Clay Mineral	Opaque	Siliciclastic	Calculated Total % Cover
2.95	28	1	1	0	1	0	0	0	0	23	0	0	1	2	28
2.95	28	1	1	0	1	0	0	0	0	25	0	1	1	2	31
2.95	26	1	1	0	1	0	0	0	0	23	0	1	0	1	27
2.95	28	1	2	0	2	0	0	0	0	25	0	0	1	1	30
2.95	22	0	1	0	1	0	0	0	0	20	0	0	1	1	23
2.95	28	1	2	0	2	0	0	0	0	23	0	1	1	1	29
2.95	28	1	3	0	3	0	0	0	0	24	0	1	1	1	31
2.95	30	1	1	0	1	0	0	0	0	26	0	0	1	1	30
2.95	28	1	1	0	1	1	0	0	0	25	0	0	1	1	30
2.95	25	1	1	1	0	0	0	0	0	22	0	0	1	1	26
Average	27.1	0.9	1.4	0.1	1.3	0.1	0	0	0	23.6	0	0.4	0.9	1.2	28.5

C 11H1w (50-52)

3.00	20	1	1	0	1	0	0	0	0	16	0	1	1	1	21
3.00	20	0	1	0	1	0	0	0	0	15	0	0	1	1	18
3.00	25	2	2	0	2	0	0	0	0	18	0	1	1	1	25
3.00	23	1	1	0	1	0	0	0	0	16	0	1	1	1	21
3.00	18	1	1	0	1	0	0	0	0	15	0	0	1	1	19
3.00	20	1	2	0	2	0	0	0	0	17	0	0	1	1	22
3.00	28	1	2	0	2	0	0	0	0	23	0	1	1	1	29
3.00	20	1	1	0	1	0	0	0	0	15	0	0	1	1	19
3.00	26	2	1	0	1	0	0	0	0	22	0	0	1	1	27
3.00	28	1	1	0	1	0	0	0	0	22	0	1	1	1	27
Average	22.8	1.1	1.3	0	1.3	0	0	0	0	17.9	0	0.5	1	1	22.8

C 11H3w (50-52)

3.03	28	1	2	0	2	0	0	0	0	18	0	1	2	1	25
3.03	28	1	2	0	2	0	0	0	0	25	0	1	1	2	32
3.03	28	1	2	0	2	0	0	0	0	25	0	0	1	1	30
3.03	26	1	1	1	0	0	0	0	0	23	0	0	0	1	26
3.03	20	0	0	0	0	0	0	0	0	18	0	0	1	1	20
3.03	24	0	0	0	0	0	0	0	0	22	0	1	1	1	25
3.03	28	1	1	0	1	0	0	0	0	23	0	0	1	1	27
3.03	30	0	1	0	1	0	0	0	0	27	0	0	1	1	30
3.03	30	2	2	0	2	0	0	0	0	25	0	1	1	1	32
3.03	25	0	1	0	1	0	0	0	0	20	0	1	1	1	24
Average	26.7	0.7	1.2	0.1	1.1	0	0	0	0	22.6	0	0.5	1	1.1	27.1

APPENDIX III: Visual estimation counts and averages of smear slides for ODP Site 1022 continued

C 11H5w (50-52)

Sample Age (Ma)	Estimated Total % Cover	Pennate Diatom	Total Centric Diatom	Whole Centric Diatom	Centric Diatom Fragment	Sponge Spicule	Radiolarian	Silicoflagellate	Foram	Coccolith	Volcanic Glass	Clay Mineral	Opaque	Siliciclastic	Calculated Total % Cover
3.06	30	2	1	0	1	0	0	0	0	27	0	0	1	1	32
3.06	26	1	0	0	0	0	0	0	0	25	0	0	1	1	28
3.06	25	1	1	0	1	0	0	0	0	25	0	0	1	1	29
3.06	25	2	0	0	0	0	0	0	0	23	0	0	1	1	27
3.06	26	1	1	0	1	0	0	0	0	22	0	0	1	1	26
3.06	26	1	1	0	1	0	0	0	0	23	0	1	1	1	28
3.06	30	1	0	0	0	0	0	0	0	26	0	0	1	1	29
3.06	26	0	0	0	0	0	0	0	0	23	0	0	1	1	25
3.06	26	0	1	0	1	0	0	0	0	24	0	0	1	14	40
3.06	30	1	1	0	1	0	0	0	0	26	0	0	1	0	29
Average	27	1	0.6	0	0.6	0	0	0	0	24.4	0	0.1	1	2.2	29.3

C 12H1w (50-52)

3.09	30	0	2	0	2	0	0	0	0	27	0	0	1	2	32
3.09	30	0	0	0	0	0	0	0	0	29	0	0	0	2	31
3.09	30	1	0	0	0	0	0	0	0	29	0	0	1	2	33
3.09	30	1	0	0	0	0	0	0	0	29	0	0	0	2	32
3.09	30	1	0	0	0	0	0	0	0	28	0	0	1	2	32
3.09	30	1	1	0	1	0	0	0	0	27	0	0	1	2	32
3.09	30	1	0	0	0	0	0	0	0	27	0	0	1	2	31
3.09	30	0	1	0	1	0	0	0	0	28	0	0	1	2	32
3.09	30	1	0	0	0	0	0	0	0	27	0	0	1	2	31
3.09	30	1	0	0	0	0	0	0	0	28	0	0	0	2	31
Average	30	0.7	0.4	0	0.4	0	0	0	0	27.9	0	0	0.7	2	31.7

C 13H5w (50-52)

3.23	30	1	1	0	1	0	0	0	0	26	0	1	1	1	31
3.23	30	1	1	0	1	1	0	0	0	26	0	1	1	1	32
3.23	28	1	0	0	0	0	0	0	0	25	0	0	0	1	27
3.23	30	1	1	0	1	0	0	0	0	26	0	1	1	1	31
3.23	30	1	1	0	1	0	0	0	0	28	0	1	1	1	33
3.23	26	0	0	0	0	0	0	0	0	24	0	0	1	1	26
3.23	30	1	0	0	0	0	0	0	0	26	0	0	1	1	29
3.23	30	1	1	0	1	0	0	0	0	26	0	1	1	1	31
3.23	28	1	0	0	0	0	0	0	0	25	0	0	1	1	28
3.23	28	0	0	0	0	0	0	0	0	25	0	0	1	1	27
Average	29	0.8	0.5	0	0.5	0.1	0	0	0	25.7	0	0.5	0.9	1	29.5

APPENDIX III: Visual estimation counts and averages of smear slides for ODP Site 1022 continued

C 13H6w (50-52)

Sample Age (Ma)	Estimated Total % Cover	Pennate Diatom	Total Centric Diatom	Whole Centric Diatom	Centric Diatom Fragment	Sponge Spicule	Radiolarian	Silicoflagellate	Foram	Coccolith	Volcanic Glass	Clay Mineral	Opaque	Siliciclastic	Calculated Total % Cover
3.25	30	1	1	0	1	0	0	0	0	27	0	1	1	1	32
3.25	30	1	0	0	0	0	0	0	0	27	0	1	1	1	31
3.25	30	1	0	0	0	0	0	0	0	26	0	1	1	1	30
3.25	30	1	2	1	1	0	0	0	0	26	0	1	1	1	32
3.25	30	1	1	0	1	0	0	0	0	27	0	1	1	1	32
3.25	30	1	0	0	0	0	0	0	0	27	0	1	1	1	31
3.25	26	0	0	0	0	0	0	0	0	24	0	1	0	1	26
3.25	26	0	0	0	0	0	0	0	0	24	0	0	2	1	27
3.25	28	1	1	0	0	0	0	0	0	23	0	0	1	1	27
3.25	25	0	0	0	0	0	0	0	0	22		1	0	1	24
Average	28.5	0.7	0.5	0.1	0.3	0	0	0	0	25.3	0	0.8	0.9	1	29.2

C 15H2w (50-52)

3.39	26	3	1	0	1	0	0	0	0	20	0	1	1	1	27
3.39	26	2	1	0	1	0	0	0	0	20	0	1	1	1	26
3.39	20	1	0	0	0	0	0	0	0	16	0	1	1	1	20
3.39	28	2	2	1	1	2	0	0	0	20	0	1	1	1	29
3.39	28	3	2	1	1	0	0	0	0	19	0	0	1	1	26
3.39	30	3	3	0	3	0	0	0	0	23	0	1	1	0	31
3.39	28	2	2	1	1	0	0	0	0	19	0	1	0	1	25
3.39	25	2	2	0	2	0	0	0	0	20	0	1	1	0	26
3.39	26	2	2	0	2	0	0	1	0	16	0	1	1	1	24
3.39	26	3	2	0	2	0	0	0	0	19	0	1	1	0	26
Average	26.3	2.3	1.7	0.3	1.4	0.2	0	0.1	0	19.2	0	0.9	0.9	0.7	26

C 16H1w (40-42)

3.48	12	2	1	0	1	0	0	1	0	4	0	1	1	1	11
3.48	10	2	2	0	2	0	0	0	0	3	0	1	2	1	11
3.48	10	2	2	0	2	0	0	0	0	3	0	1	1	0	9
3.48	10	2	1	0	1	0	0	0	0	2	0	1	1	1	8
3.48	10	1	1	0	1	0	0	0	0	3	0	1	1	1	8
3.48	10	2	1	0	1	0	0	0	0	3	0	1	2	1	10
3.48	10	2	2	0	2	0	0	0	0	3	0	0	2	1	10
3.48	10	1	1	0	1	0	0	0	0	3	0	2	1	1	9
3.48	10	2	2	0	2	0	0	1	0	3	0	1	2	0	11
3.48	10	2	1	1	0	0	0	0	0	3	0	1	1	1	9
Average	10.2	1.8	1.4	0.1	1.3	0	0	0.2	0	3	0	1	1.4	0.8	9.6

APPENDIX III: Visual estimation counts and averages of smear slides for ODP Site 1022 continued

C 16H3w (50-52)

Sample Age (Ma)	Estimated Total % Cover	Pennate Diatom	Total Centric Diatom	Whole Centric Diatom	Centric Diatom Fragment	Sponge Spicule	Radiolarian	Silicoflagellate	Foram	Coccolith	Volcanic Glass	Clay Mineral	Opaque	Siliciclastic	Calculated Total % Cover
3.52	18	3	2	0	2	0	0	0	0	7	0	1	1	1	15
3.52	15	1	1	0	1	0	0	0	0	9	0	1	1	1	14
3.52	15	1	2	0	2	0	0	0	0	7	0	1	1	1	13
3.52	15	2	2	0	2	0	0	0	0	8	0	1	1	1	15
3.52	10	1	1	0	1	0	0	0	0	6	0	0	1	1	10
3.52	10	1	2	0	2	0	0	0	0	5	0	1	1	1	11
3.52	15	3	2	0	2	0	0	0	0	8	0	2	1	1	17
3.52	15	2	3	1	2	0	0	0	0	6	0	1	0	1	13
3.52	15	3	3	0	3	0	0	0	0	8	0	1	1	1	17
3.52	10	1	1	0	1	0	0	0	0	5	0	1	1	1	10
Average	13.8	1.8	1.9	0.1	1.8		0	0	0	6.9	0	1	0.9	1	13.5

C 16H4w (50-52)

3.54	12	1	1	0	1	0	0	0	0	5	0	0	1	3	11
3.54	10	1	0	0	0	0	0	0	0	6	0	0	2	2	11
3.54	10	1	0	0	0	0	0	0	0	6	0	0	1	2	10
3.54	10	1	1	0	1	0	0	0	0	5	0	0	1	2	10
3.54	10	1	1	0	1	0	0	0	0	5	0	0	1	2	10
3.54	12	1	1	0	1	0	0	0	0	7	0	0	1	2	12
3.54	10	1	0	0	0	0	0	0	0	5	0	0	1	2	9
3.54	10	1	1	0	1	0	0	0	0	5	0	0	1	2	10
3.54	15	1	3	0	3	0	0	0	0	7	0	0	1	2	14
3.54	10	1	0	0	0	0	0	0	0	5	0	0	2	1	9
Average	10.9	1	0.8	0	0.8		0	0	0	5.6	0	0	1.2	2	10.6

C 16H6w (50-52)

3.56	10	2	1	0	1	0	0	0	0	6	0	1	1	1	12
3.56	10	1	1	0	1	0	0	0	0	5	0	1	1	1	10
3.56	10	1	1	0	1	0	0	0	0	6	0	1	1	1	11
3.56	10	1	2	0	2	0	0	0	0	5	0	1	1	1	11
3.56	12	2	2	0	2	0	0	0	0	6	0	1	1	1	13
3.56	12	2	2	1	1	0	0	0	0	6	0	1	1	1	13
3.56	10	1	1	0	1	0	0	0	0	5	0	1	1	2	11
3.56	10	2	1	0	1	0	0	0	0	5	0	1	1	1	11
3.56	10	1	2	1	1	0	0	0	0	4	0	1	1	1	10
3.56	10	2	2	0	2	0	0	0	0	4	0	1	1	0	10
Average	10.4	1.5	1.5	0.2	1.3	0	0	0	0	5.2	0	1	1	1	11.2

APPENDIX III: Visual estimation counts and averages of smear slides for ODP Site 1022 continued

C 16H7w (50-52)

Sample Age (Ma)	Estimated Total % Cover	Pennate Diatom	Total Centric Diatom	Whole Centric Diatom	Centric Diatom Fragment	Sponge Spicule	Radiolarian	Silicoflagellate	Foram	Coccolith	Volcanic Glass	Clay Mineral	Opaque	Siliciclastic	Calculated Total % Cover
3.58	11	3	1	0	1	0	0	0	0	4	0	1	1	1	11
3.58	10	2	2	0	2	0	0	0	0	4	0	1	1	1	11
3.58	10	2	1	0	1	0	0	0	0	4	0	1	1	0	9
3.58	10	2	2	0	2	0	0	0	0	4	0	1	0	1	10
3.58	10	1	1	0	1	0	0	0	0	4	0	1	1	1	9
3.58	10	3	1	0	1	0	0	0	0	3	0	1	1	1	10
3.58	10	1	2	1	1	0	0	0	0	3	0	1	1	1	9
3.58	12	2	2	0	2	0	0	0	0	4	0	1	1	1	11
3.58	10	2	1	0	1	0	0	0	0	4	0	2	1	1	11
3.58	10	2	2	0	2	0	0	0	0	4	0	1	1	1	11
Average	10.3	2	1.5	0.1	1.4	0	0	0	0	3.8	0	1.1	0.9	0.9	10.2

C 17H5w (50-52)

3.65	12	1	2	0	2	0	0	1	0	7	0	1	1	1	14
3.65	12	1	1	0	1	0	0	0	0	7	0	0	1	1	11
3.65	10	1	1	0	1	0	0	0	0	7	0	1	0	1	11
3.65	10	1	1	0	1	0	0	0	0	7	0	1	1	0	11
3.65	10	1	0	0	0	0	0	0	0	7	0	1	1	1	11
3.65	12	2	1	0	1	0	0	0	0	7	0	1	1	1	13
3.65	11	1	1	0	1	0	0	0	0	8	0	1	1	0	12
3.65	12	2	2	0	2	0	0	0	0	7	0	1	1	1	14
3.65	12	2	1	0	1	0	0	0	0	7	0	2	1	1	14
3.65	14	1	3	2	1	0	0	0	0	8	0	1	1	0	14
Average	11.5	1.3	1.3	0.2	1.1	0	0	0.1	0	7.2	0	1	0.9	0.7	12.5

C 18X2w (50-52)

3.70	13	2	3	0	3	0	0	1	0	4	0	1	1	1	13
3.70	10	1	1	0	1	0	0	0	0	4	0	1	1	1	9
3.70	12	2	3	0	3	0	0	0	0	6	0	1	0	1	13
3.70	13	2	4	2	2	0	0	1	0	3	0	1	1	1	13
3.70	11	1	3	0	3	1	0	0	0	4	0	1	1	1	12
3.70	10	2	4	1	3	0	0	0	0	3	0	1	1	1	12
3.70	12	2	1	0	1	0	0	2	0	5	0	1	1	1	13
3.70	11	2	2	1	1	0	0	0	0	4	0	1	1	1	11
3.70	12	2	2	0	2	0	0	2	0	4	0	1	1	1	13
3.70	11	2	3	0	3	0	0	0	1	3	0	1	1	1	12
Average	11.5	1.8	2.6	0.4	2.2	0.1	0	0.6	0.1	4	0	1	0.9	1	12.1

APPENDIX III: Visual estimation counts and averages of smear slides for ODP Site 1022 continued

C 20X4w (50-52)

Sample Age (Ma)	Estimated Total % Cover	Pennate Diatom	Total Centric Diatom	Whole Centric Diatom	Centric Diatom Fragment	Sponge Spicule	Radiolarian	Silicoflagellate	Foram	Coccolith	Volcanic Glass	Clay Mineral	Opaque	Siliciclastic	Calculated Total % Cover
3.87	10	3	1	0	1	0	0	0	0	1	0	3	1	1	10
3.87	10	3	2	0	2	0	0	0	0	1	0	2	2	0	10
3.87	12	5	2	0	2	0	0	0	0	0	0	2	2	1	12
3.87	10	2	1	0	1	0	0	0	0	1	0	2	2	1	9
3.87	12	4	3	0	3	0	0	0	0	1	0	2	2	1	13
3.87	10	3	3	0	3	0	0	0	0	0	0	2	1	1	10
3.87	10	3	2	0	2	0	0	0	0	1	0	1	2	1	10
3.87	10	3	1	0	1	0	0	0	0	0	0	2	2	1	9
3.87	10	2	1	0	1	0	0	0	0	1	0	3	2	1	10
3.87	11	4	2	0	2	0	0	0	0	1	0	2	2	1	12
Average	10.5	3.2	1.8	0	1.8	0	0	0	0	0.7	0	2.1	1.8	0.9	10.5

C 21X4w (50-52)

3.96	12	1	1	0	1	1	0	0	0	1	0	3	2	2	11
3.96	10	1	1	0	1	0	0	0	1	1	0	2	3	1	10
3.96	10	1	2	0	2	0	0	0	0	1	0	3	2	1	10
3.96	10	1	2	0	2	0	0	0	0	1	0	2	2	1	9
3.96	10	2	1	0	1	0	1	0	0	1	0	2	2	2	11
3.96	10	2	1	0	1	1	0	0	0	1	0	2	2	1	10
3.96	12	2	2	0	2	0	0	0	0	1	0	2	3	2	12
3.96	10	1	1	0	1	0	0	0	0	1	0	3	2	2	10
3.96	10	1	1	0	1	1	0	0	0	1	0	2	2	2	10
3.96	11	2	1	0	1	0	0	0	0	1	0	2	3	2	11
Average	10.5	1.4	1.3	0	1.3	0.3	0.1	0	0.1	1	0	2.3	2.3	1.6	10.4

C 22X2w (50-52)

4.01	11	1	2	1	1	0	0	0	0	0	0	3	2	2	10
4.01	10	2	1	0	1	0	0	0	0	0	0	3	2	2	10
4.01	11	3	2	1	1	0	0	0	0	0	0	2	2	2	11
4.01	11	2	2	0	2	1	0	0	0	0	0	3	2	2	12
4.01	12	2	2	0	2	1	0	1	0	0	0	2	2	2	12
4.01	11	2	2	0	2	1	0	0	0	0	0	3	2	3	13
4.01	11	2	1	0	1	2	0	0	0	0	0	3	2	3	13
4.01	11	2	1	0	1	2	0	0	0	0	0	2	2	3	12
4.01	10	1	2	1	1	1	0	0	0	0	0	2	2	3	11
4.01	10	2	2	1	1	1	0	0	0	0	0	3	2	2	12
Average	10.8	1.9	1.7	0.4	1.3	0.9	0	0.1	0	0	0	2.6	2	2.4	11.6

APPENDIX III: Visual estimation counts and averages of smear slides for ODP Site 1022 continued

C 23X2w (50-52)

Sample Age (Ma)	Estimated Total % Cover	Pennate Diatom	Total Centric Diatom	Whole Centric Diatom	Centric Diatom Fragment	Sponge Spicule	Radiolarian	Silicoflagellate	Foram	Coccolith	Volcanic Glass	Clay Mineral	Opaque	Siliciclastic	Calculated Total % Cover
4.10	15	3	3	0	3	1	0	0	0	4	0	2	2	2	17
4.10	14	2	2	1	1	0	0	0	1	4	0	1	1	2	13
4.10	12	1	1	0	1	0	0	0	0	6	0	1	1	1	11
4.10	12	2	2	0	2	0	0	0	0	5	0	2	1	2	14
4.10	11	1	1	0	1	0	0	2	0	5	0	1	1	1	12
4.10	11	1	2	1	1	1	0	0	0	4	0	1	1	1	11
4.10	10	1	1	0	1	1	0	0	0	4	0	1	1	1	10
4.10	12	2	3	0	3	0	0	0	0	6		1	1	1	14
4.10	12	3	2	0	2	0	0	1	0	5	0	1	1	1	14
4.10	11	2	1	0	1	0	0	0	0	6	0	2	1	1	13
Average	12	1.8	1.8	0.2	1.6	0.3	0	0.3	0.1	4.9	0	1.3	1.1	1.3	12.9

C 23X7w (50-52)

4.17	10	1	1	0	1	1	0	0	0	3	0	2	1	1	10
4.17	10	1	1	0	1	1	0	0	0	3	0	1	1	1	9
4.17	10	2	1	0	1	0	0	2	0	3	0	1	1	1	11
4.17	10	1	1	0	1	0	0	0	0	3	0	2	1	1	9
4.17	10	1	1	0	1	1	0	0	0	2	0	2	1	2	10
4.17	11	2	1	0	1	1	0	0	0	3	0	1	2	1	11
4.17	10	1	1	0	1	0	0	0	0	2	0	2	2	2	10
4.17	10	1	1	0	1	2	0	0	0	3	0	1	2	1	11
4.17	10	2	1	0	1	0	0	1	0	3	0	1	2	1	11
4.17	10	2	1	0	1	0	0	0	0	2	0	1	2	2	10
Average	10.1	1.4	1	0	1	0.6	0	0.3	0	2.7	0	1.4	1.5	1.3	10.2

APPENDIX IV: Smear slide visual estimation consistency experiment

Sample ID	Estimated Total % Cover	Pennate Diatoms	Total Centric Diatoms	Whole Centric Diatoms	Centric Diatom Fragments	Silicoflagellates	Coccoliths	Clay Minerals	Opaques	Siliciclastics	Calculated Total % Cover
C 12H1W (50-52)	30	1	1	0	1	0	28	1	0	2	33
C 12H1W (50-52)	30	1	1	0	1	0	27	0	0	2	31
C 12H1W (50-52)	30	0	1	0	1	0	29	1	0	2	33
C 12H1W (50-52)	30	2	1	0	1	0	29	1	0	2	35
C 12H1W (50-52)	30	0	1	0	1	0	29	0	0	2	32
C 12H1W (50-52)	30	1	1	0	1	0	27	0	0	2	31
C 12H1W (50-52)	30	1	1	0	1	0	28	0	0	2	32
C 12H1W (50-52)	30	0	1	0	1	0	29	0	0	2	32
C 12H1W (50-52)	30	1	0	0	0	1	29	0	0	2	33
C 12H1W (50-52)	30	0	0	0	0	0	29	0	0	2	31
C 12H1W (50-52)	30	0	2	0	2	0	27	0	1	2	32
C 12H1W (50-52)	30	0	0	0	0	0	29	0	0	2	31
C 12H1W (50-52)	30	1	0	0	0	0	29	0	1	2	33
C 12H1W (50-52)	30	1	0	0	0	0	29	0	0	2	32
C 12H1W (50-52)	30	1	0	0	0	0	28	0	1	2	32
C 12H1W (50-52)	30	1	1	0	1	0	27	0	1	2	32
C 12H1W (50-52)	30	1	0	0	0	0	27	0	1	2	31
C 12H1W (50-52)	30	0	1	0	1	0	28	0	1	2	32
C 12H1W (50-52)	30	1	0	0	0	0	27	0	1	2	31
C 12H1W (50-52)	30	1	0	0	0	0	28	0	0	2	31
C 12H1W (50-52)	30	1	0	0	0	0	28	0	1	1	31
C 12H1W (50-52)	30	1	1	0	1	0	28	0	1	1	32
C 12H1W (50-52)	30	0	0	0	0	0	29	0	0	1	30
C 12H1W (50-52)	30	0	1	0	1	0	29	0	0	1	31
C 12H1W (50-52)	30	1	0	0	0	0	29	0	1	1	32
C 12H1W (50-52)	30	1	0	0	0	0	29	0	1	1	32
C 12H1W (50-52)	30	1	1	0	1	0	28	0	1	1	32
C 12H1W (50-52)	30	1	0	0	0	0	29	0	1	1	32
C 12H1W (50-52)	30	0	0	0	0	0	28	0	1	1	30
C 12H1W (50-52)	30	0	0	0	0	0	28	0	1	1	30
Total Average	30	0.67	0.50	0.00	0.50	0.03	28.27	0.10	0.50	1.67	31.73
Total Standard Deviation	0	0.55	0.57	0.00	0.57	0.18	0.78	0.31	0.51	0.48	1.05
Total Average %		2.10	1.57	0.00	1.57	0.10	89.07	0.32	1.57	5.25	100
Standard Deviation of %		0.20	0.91	0.00	0.76	0.22	4.33	0.44	1.40	2.01	1.05